Syntheses and Characterization

of

Polyimidosulfate Complexes

Dissertation

zur Erlangung des mathematisch-naturwissenschaftlichen Doktorgrades

„Doctor rerum naturalium“

der Georg-August Universität Göttingen

im Promotionsprogramm

der Georg-August University School of Science (GAUSS)

vorgelegt von

Julia Matussek

aus Bremen

Göttingen, 2014

Betreuungsausschuss

Prof. Dr. D. Stalke, Institut für Anorganische Chemie

Prof. Dr. L. Ackermann, Institut für Organische und Biomolekulare Chemie

Mitglieder der Prüfungskommission

Referent Prof. Dr. D. Stalke, Institut für Anorganische Chemie

Korreferent Prof. Dr. L. Ackermann, Institut für Organische und Biomolekulare Chemie

Weitere Mitglieder

Dr. I. Siewert, Institut für Anorganische Chemie

Prof. G. M. Sheldrick, Institut für Anorganische Chemie

Dr. H. Sowa, GZG, Abt. Kristallographie

Prof. Dr. K. Koszinowski, Institut für Organische und Biomolekulare Chemie

Tag der mündlichen Prüfung: 09. Mai 2014

“Es gibt keine gescheiterten Experimente,
sondern nur Experimente mit unerwartetem Ergebnis“

Richard Buckminster Fuller

Table of Contents

List of compounds

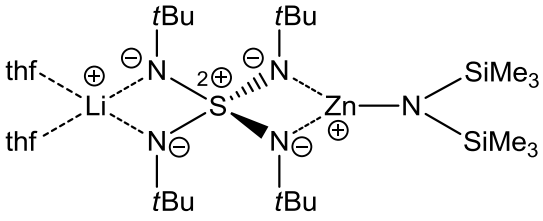

2

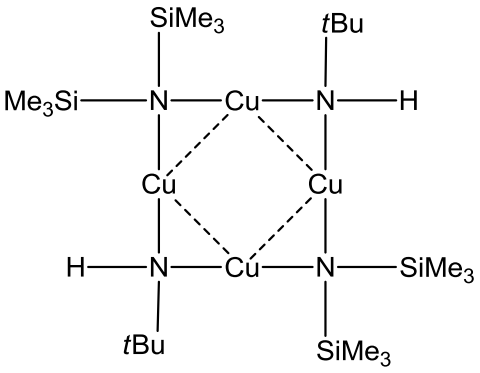

3

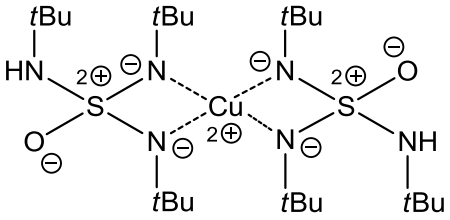

4

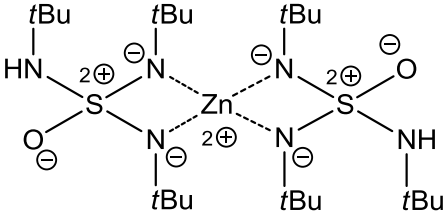

5

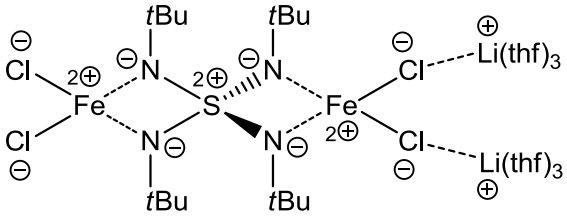

6

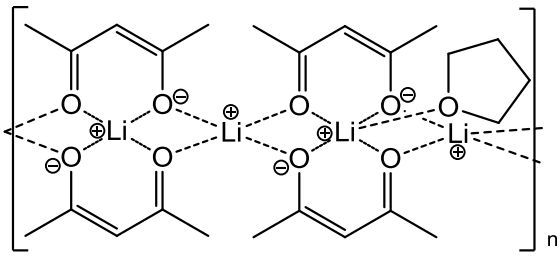

7

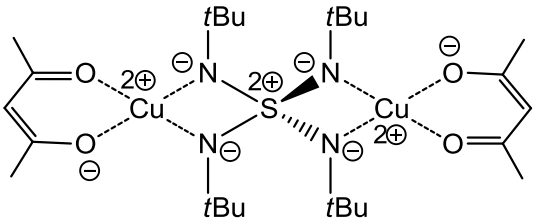

8

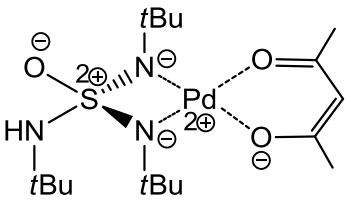

9

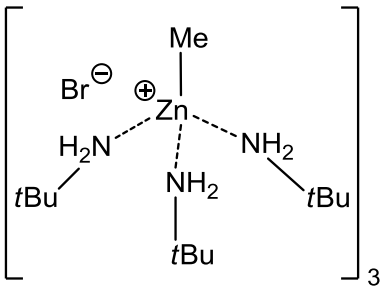

10

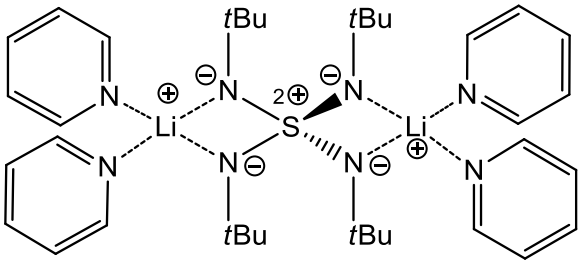

11

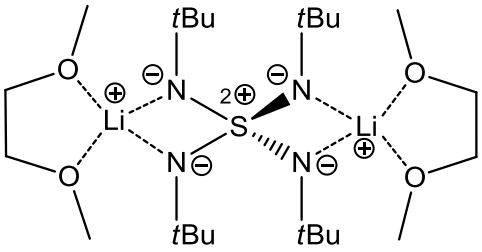

12

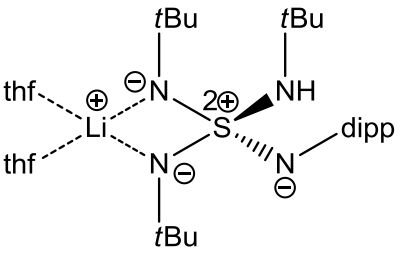

14

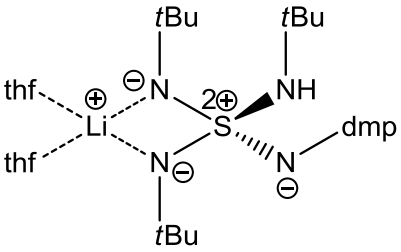

15

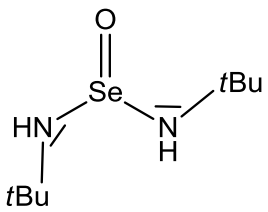

16

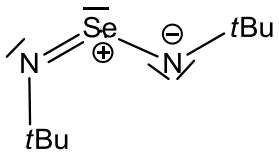

17

1. Introduction

1.1. Polyimido analogs of the sulfur-oxygen species (SO_n^{m-})

Isovalent electronic replacement of the oxygen atoms in the classic SO_n^{m-} molecules and ions by NR imido groups yields the polyimido sulfur species $S(NR)_n^{m-}$ (n = 2, 3, 4 and m = 0, 2).[1] These compounds are equal in their valence- and overall electron number. According to *Langmuir* isovalent species are supposed to be similar in their chemical and physical properties.[2] However, this is only an estimate as, e.g. the sulfate anion SO_4^{2-} is stable under ambient conditions and water while the tetrakis(*tert*butyl)imido-sulfate $S(N\textit{t}Bu)_4^{2-}$ readily decomposes. Table 1.1 shows all known sulfur-oxygen compounds and their sulfur-nitrogen analogs.

Table 1.1: Sulfur-oxygen compounds and their sulfur-nitrogen analogs.

S–O	*S–N*	*examples*	*S–O*	*S–N*	*examples*
SO_2	$S(NR)_2$	$S(N\textit{t}Bu)_2$	SO_4^{2-}	$S(NR)_4^{2-}$	$S(N\textit{t}Bu)_4^{2-}$
SO_3^{2-}	$S(NR)_3^{2-}$	$S(N(SiMe_3))_3^{2-}$	RSO_3^-	$RS(NR)_3^-$	$(N\textit{t}Bu)_3SMe^-$
RSO_2^-	$RS(NR)_2^-$	$\{(N(SiMe_3))_2SPh\}^-$	R_2SO_2	$R_2S(NR)_2$	$O_2S(NH\textit{t}Bu)_2$
SO_3	$S(NR)_3$	$S(N\textit{t}Bu)_3$			

In these sulfur-nitrogen compounds, sulfur mostly exhibits the oxidation states +IV or +VI. Oxidation state +IV is represented in the *S*-alkyl-iminosulfinamides, $RS(NR')_2^-$ (**A**)[3] (Figure 1.1), which results from the addition of lithium organyls to the formal double bond of the sulfurdiimides (Figure 1.1). With R being an alkyl- or aryl group and R' an alkyl-, aryl-, or trimethylsilyl group many main group[3-13] and transition metal[11, 14, 15] complexes are known. Furthermore, iminosulfindiamides can be obtained (**B**, **C** and **D**). On the one hand, there is the dianionic compound $S(NR)_3^{2-}$ (**B**),[16] on the other hand the monoanionic $R_2NS(NR')_2^-$ (**C**),[17, 18] and additionally the neutral compound $(R_2N)_2SNR'$ (**D**)[19, 20] are known. Sulfur atoms with the oxidation state +VI are found in the compounds diiminosulfuramides $RS(NR')_3^-$ (**E**)[21] and tetrakis(*tert*butyl)imidosulfate $S(N\textit{t}Bu)_4^{2-}$ (**F**).[22] **F** could be obtained in the reaction of $S(NtBu)_3$ with *tert*butylamine

and *n*butyllithium.[22] **E** was formed in the reaction of $Ba(N(SiMe_3)_2)_2$ and $H(NtBu)_3SMe$.[21] Summarizing, many compounds with sulfur being coordinated by four nitrogen atoms, $SO_x(NR)_4^{2-}$ are known.[23-25]

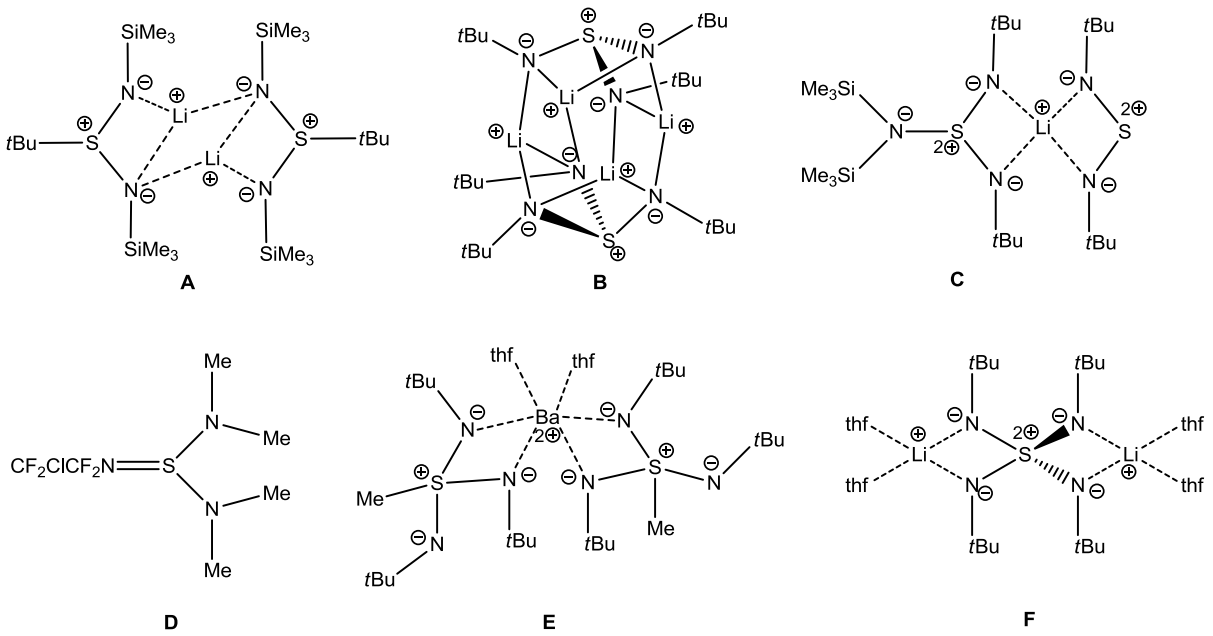

Figure 1.1: Examples for $RS(NR')_2^-$ (**A**),[3] $S(NR)_3^{2-}$ (**B**),[16] $R_2NS(NR')_2^-$ (**C**),[18] $(R_2N)_2SNR'$ (**D**),[19] $RS(NR')_3^-$ (**E**),[21] and $S(NtBu)_4^{2-}$ (**F**)[22].

Because of their nitrogen donor centers, polyimdo ligands are perfectly suitable for the coordination of metal atoms. Furthermore, the sulfur-nitrogen ligands can either delocalize (e.g. $[(thf)_4Li_2(NtBu)_4S]$)[22] or localize (e.g. $[H(NtBu)_3SMe]$)[21] their charge to open a broad field of diversely coordinated metal ion complexes.[16, 18, 26, 27] Some examples for transmetalation reactions are given in Scheme 1.1: Sulfurtriimide reacts with elemental lithium in THF to the dimeric product $[(thf)Li_4\{(NtBu)_3S\}_2]$, which can be transmetalated with two equivalents of metal *tert*butanolate to a hetero bimetallic compound. Additionally, a reaction of the dimeric structure with metal hexamethyldisilazanes (M-HMDS) can be executed. This illustrates that the $S(NR)_n^{m-}$ compounds open a broad field of new ligand designs and transmetalation reactions.

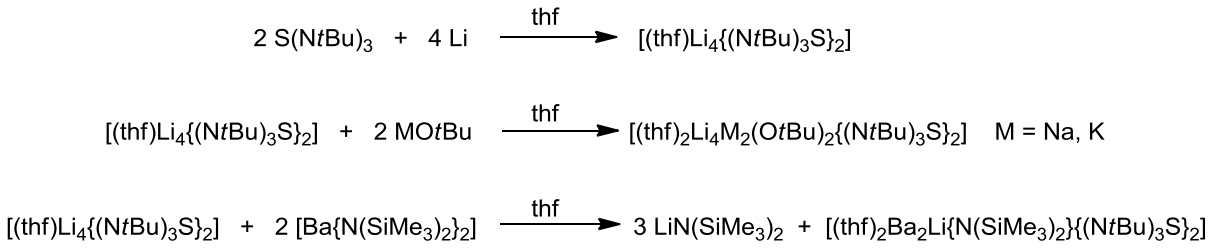

Scheme 1.1: Examples for transmetalation reactions of polyimido compounds.[16, 18, 26, 27]

This thesis focuses on the tetrakis(*tert*butyl)imidosulfate $S(NtBu)_4^{2-}$ and the corresponding protonated compound $OS(NtBu)_2(NHtBu)$.

In the seventies *Glemser* and *Wegener* obtained the first sulfur-nitrogen compound with sulfur in the oxidation state of +VI.[28] $S(NSiMe_3)_3$ was synthesized in the reaction of sulfur nitride trifluoride and lithium bis(trimethylsilyl)amide (Scheme 1.2, (I)). As a side product, bis(*N*-trimethylsilylimido)sulfur difluoride could be isolated.[28] In addition, *Glemser et al.* reported the synthesis of $S(NtBu)_3$ *via* addition of NSF_3 (II).[29] Alternatively, *Verbeek et al.* utilized OSF_4 instead of NSF_3 for the reaction of a sulfate anion analog (III).[30]

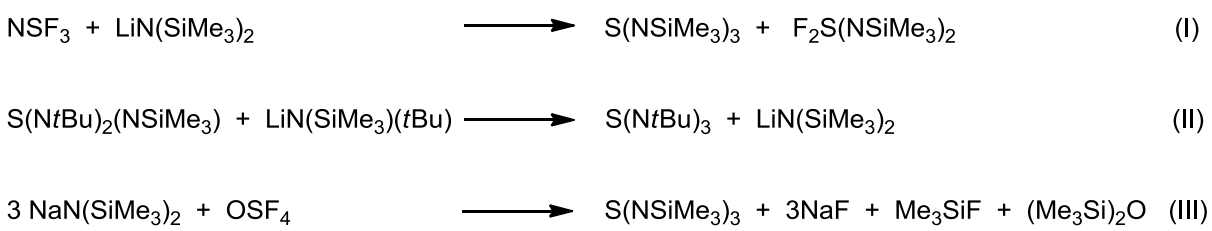

Scheme 1.2: Syntheses of sulfurtriimide.[28-30]

However, the yields of these reactions were very low because the substances are highly reactive. Thus, a new synthesis was developed realizing the oxidation of sulfur +IV to sulfur +VI of the iminosulfindiamide by bromine or iodine.[22, 31] The involvement of halides suggests a radical mechanism with the characterized dimeric product given by Scheme 1.3.

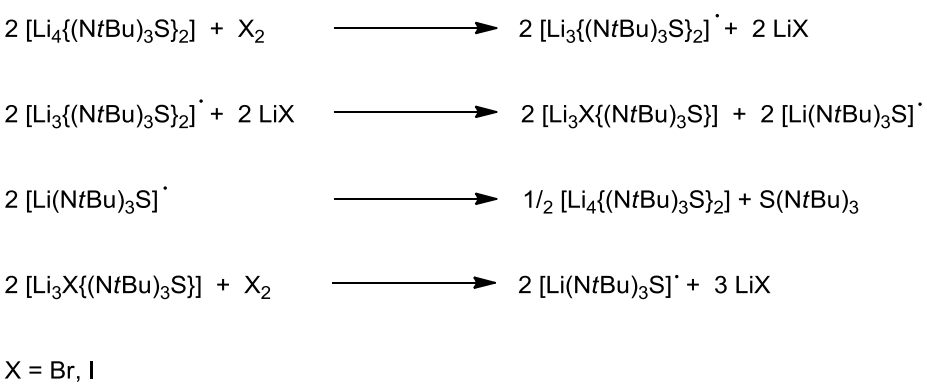

Scheme 1.3: Synthesis of sulfurtriimide.[22, 31]

The first sulfur atom with fourfold coordination and consequently the first known analog of the sulfate anion SO_4^{2-} was synthesized by *Appel* and *Ross* in 1968.[32] The *S,S*-dimethylsulfurdiimide reacted with potassium amide in liquid ammonia to give the tripotassium salt of sulfodiimine $[K_3(HN)_3SN \cdot NH_3]$ (Scheme 1.4).[32]

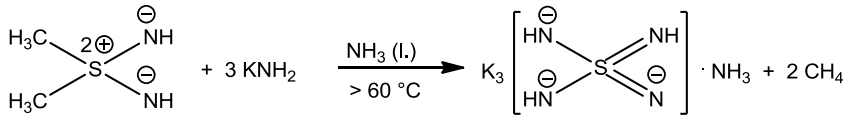

Scheme 1.4: Synthesis of $[K_3(HN)_4SN \cdot NH_3]$.[32]

In 1995 *Dehnicke et al.* published the synthesis of a compound featuring a tetrahedrally coordinated sulfur atom, $S(NPMe_3)_4^{2+}$, with two chloride atoms as counter ions.[33] In addition, a lithiated tetrakis(*tert*butyl)imidosulfate $[(thf)_4Li_2(NtBu)_4S]$ was reported in 1997 by *Stalke et al.* (Figure 1.2, top).[22] For this purpose, *n*BuLi and *t*BuNH$_2$ were used to form the lithiated compound LiNH*t*Bu. $[(thf)_4Li_2(NtBu)_4S]$ (**1**) could be obtained in the synthesis of this precursor and addition of sulfurtriimide. At this, each lithium atom is coordinated by two nitrogen atoms and two THF molecules.[22] This dianionic ligand is stable in THF, but oxidizes when exposed to air, which can be seen by color change from colorless to blue (Figure 1.2).

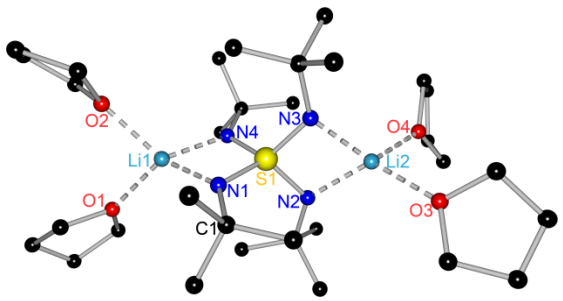

Figure 1.2: Crystal structures of $[(thf)_4Li_2(NtBu)_4S]$ (**1**).

One year later *Stalke et al.* presented the first transmetalation of $[(thf)_4Li_2(NtBu)_4S]$ by means of barium bis(bis(hexamethylsilyl)-amine).[21] The crystallized product $[(thf)_4Ba_2\{N(SiMe_3)_2\}_2\{NtBu)_4S\}]$ contains two barium atoms, which are coordinated by the sulfur-nitrogen ligand (Figure 1.3, left).

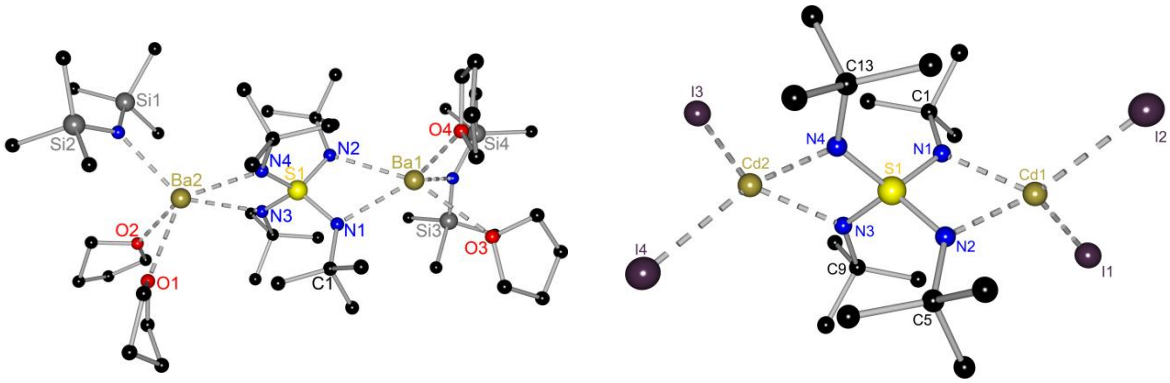

Figure 1.3: Crystal structures of $[(thf)_4Ba_2\{N(SiMe_3)_2\}_2\{NtBu)_4S\}]$ (left) and $[\{(thf)_4Li\}_2\{I_4Cd_2(NtBu)_4S\}]$ (right). $Li(thf)_4$ and hydrogen atoms are omitted for clarity.

Each barium atom is surrounded by one $N(SiMe_3)_2$ group and two THF molecules.[21] In a previous work,[34] another transmetalation product of $S(NtBu)_4^{2-}$ was synthesized. Remarkably, in the reaction of cadmium iodide and $[(thf)_4Li_2(NtBu)_4S]$ the unprecedented complex $[\{(thf)_4Li\}_2\{I_4Cd_2(NtBu)_4S\}]$ could be obtained (Figure 1.3, right). Interestingly, the anticipated salt elimination, which should be the driving force for the reaction did not occur. The cadmium cation is still coordinated by two iodide anions. Thus, the remaining lithium ions are solvated by four THF molecules.

Moreover, in my diploma thesis I could synthesis a new complex of the lithiated $S(NtBu)_4^{2-}$ ligand was synthesized, in which the lithium atom is coordinated by dioxane molecules instead of THF molecules (Scheme 1.5).

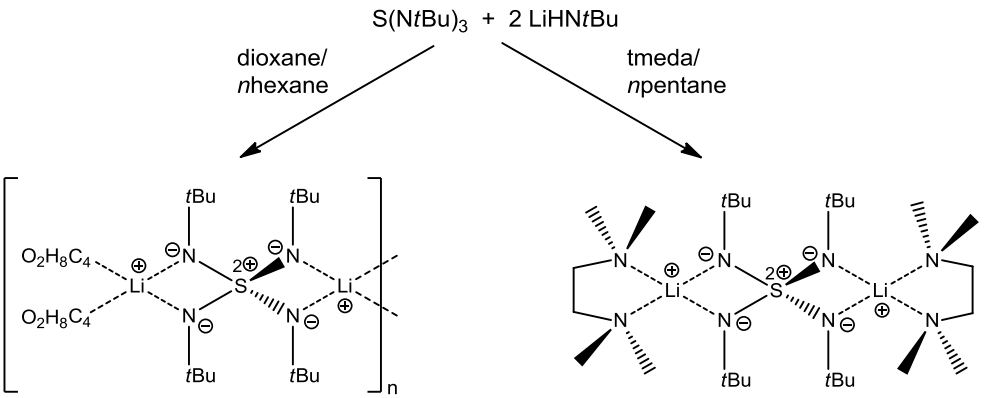

Scheme 1.5: Syntheses of $[(C_4H_8O_2)_2Li_2(NtBu)_4S]_n$[34] and $[(tmeda)_2Li_2(NtBu)_4S]$[35].

The synthesis of $[(C_4H_8O_2)_2Li_2(NtBu)_4S]_n$ could be achieved[34] and furthermore, *Carl et al.* could obtain the TMEDA coordinated monomeric compound $[(tmeda)_2Li_2(NtBu)_4S]$.[35] The donor bases were changed to give more stable species of the $S(NtBu)_4^{2-}$. The dioxane and TMEDA coordinated systems could be better for transmetalation reactions. The comparison of these both complexes with the $[(thf)_4Li_2(NtBu)_4S]$ could give more information which starting material would be the best for following reactions.

1.2. Transition and main group metal complexes of homoleptic polyimido anions ($E(NR)_4^{m-}$)

Due to the large variety of coordination modes for sulfate anions with metal atoms, polyimido compounds, $E(NR)_4^{m-}$ (E = transition or main group metal atom) are indicative of new diverse ligand systems for syntheses and hold interesting electronic and stereochemical properties (Figure 1.4).[36] By introducing organic aliphatic moieties at the chelating nitrogen atoms, the polyanion becomes more lipophilic, thus, the resulting complexes are often soluble even in non-polar hydrocarbons.

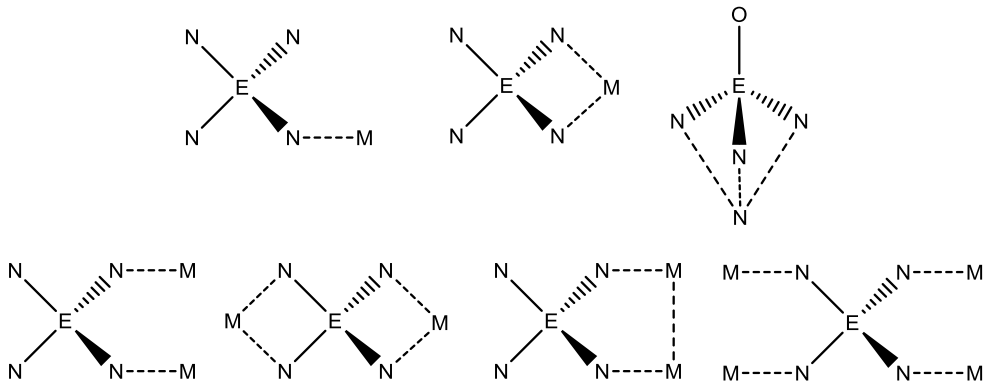

Figure 1.4: Coordination modes for metal ions with $E(NR)_4^{m-}$. R is omitted for clarity.

During the last 40 years many articles on transition metal and main group analogs of polyimido anions like $E(NR)_4^{m-}$ have been published. In 1989 the work groups around *Wilkinson* and *Hursthouse* reported on a homoleptic rhenium complex, [(tmeda)Li(N*t*Bu)$_4$Re] (**I**), synthesized *via* the [Re(NH*t*Bu)(N*t*Bu)$_3$] intermediate (Scheme 1.6).[37, 38] In the same year they published two further transition metal complexes of a polyimido ligand coordinated by two lithium atom [Li$_2$(N*t*Bu)$_4$M], (M = W (**II**), Mo (**III**)).[37, 39] Both complexes were synthesized *via* an intermediate [M(NH*t*Bu)$_2$(N*t*Bu)$_2$] (M = W, Mo), which reacts with methyllithium in diethyl ether.[37-39] One year later, the fourth complex of this type was published. The same work groups accomplished the synthesis of [Li$_2$(N*t*Bu)$_4$Cr] (**IV**) under the same conditions as for the tungsten- and molybdenum complexes.[40, 41] In addition, the osmium complex Os(N*t*Bu)$_4$ was obtained from OsO_4 and *t*BuNH(SiMe$_3$).[40] In the same year *Wilkinson et al.* and *Hursthouse et al.* presented the first transmetalation of the tungsten complex

with aluminum chloride to $W[(NtBu)_4(AlCl_2)_2]$ and with trimethyl aluminum to $[W(NtBu)_4(AlMe_2)_2]$.[42] Both compounds are sensitive towards water but thermally stable. In 1994 the same groups reported different polyimido manganese species $[Mn(NHtBu)(NtBu)_3]$ (**V**).[43] The lithium complex $[(dme)_2Li(NtBu)_4Mn]$ (**VI**) was obtained by using five equivalents of $Li(NHtBu)$ in DME.

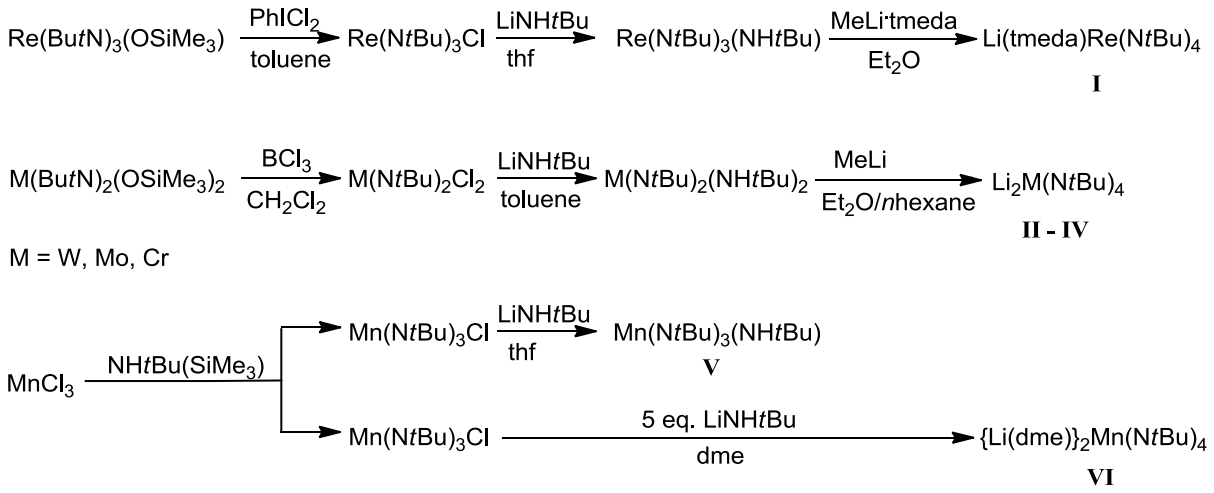

Scheme 1.6: Syntheses of $[(tmeda)Li(NtBu)_4Re]$[37, 38], $[(dme)_2Li(NtBu)_4Mn]$[43] and $[Li_2(NtBu)_4M]$[39-41].

Apart from polyimido anions ($E(NR)_4^{m-}$) which include transition metals main group metal coordination is also feasible. The group 16 sulfur-nitrogen homologes include selenium and tellurium. In 1977 *Shreeve et al.* synthesized the first selenium polyimido compound $[\{Me_2M(NR)_2\}_2Se]$ (**G**) with a fourfold coordination from $[Me_2M\{NLi(R)\}_2]$ (M = Si, Sn; R = $C(CF_3)_2Me$) and selenium tetrachloride (Figure 1.5).[44] This selenium(IV) compound could be obtained as low-melting stabile solid.[44] One year later *Roesky* and *Ambrosius* introduced a $Se(NR)_2(NR')_2$ complex (R = NMe; R' = $NC_6H_4CF_3$) (**H**), in which two nitrogen atoms coordinate a carbonyl group.[45] This complex was so unstable that it decomposed at 120°C towards red elementary selenium.[45] Several years later *Roesky et al.* obtained a $Te(NtBu)_4$ (**I**) species in the reaction of tellurium chloride with bis[*tert*butyl(lithio)amino]phenylboran.[46] Like **H** this tellurium(IV) compound decomposed at 195°C forming elementary tellurium.[46] Moreover, in 1995 *Chivers et al.* presented a $Te(NtBu)_4$ complex (**J**) with a coordinated $P(NtBu)Ph$ fragment.[47] In 2006 *Wrackmeyer et al.* reported a selenium compound in the oxidation state +IV with coordinated iron cyclopentadienyl (**K**).[48]

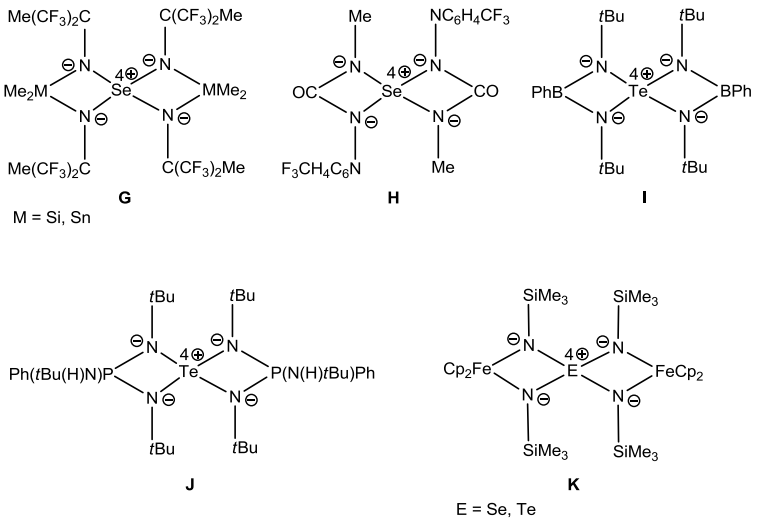

Figure 1.5: Published selenium- and tellurium polyimido compounds.[44-48]

The polyimido ($E(NR)_4^{m-}$) analogs of the third period contain silicon- and phosphorus ligands. *Russell et al.* presented the tetrakis(imido)phosphate anion (**L**) in 1997, which is isoelectronic to the phosphate anion PO_4^{3-} (Figure 1.6).[49] In the course of the reaction, P_2I_4 reacts first with 1-aminonaphtalene followed by lithiation with *n*BuLi to give [{(thf)$_4$Li}{(thf$_2$Li)$_2$(Nnaph)$_4$P}]. Like in the [(thf)$_4$Li$_2$(N*t*Bu)$_4$S] (**1**) species two lithium atoms are coordinated by two nitrogen atoms and two THF molecules. Also analogs to [{(thf)$_4$Li}$_2${I$_4$Cd$_2$(N*t*Bu)$_4$S}] a lithium atom is coordinated by four THF molecules forming an overall solvent separated ion pair.[49]

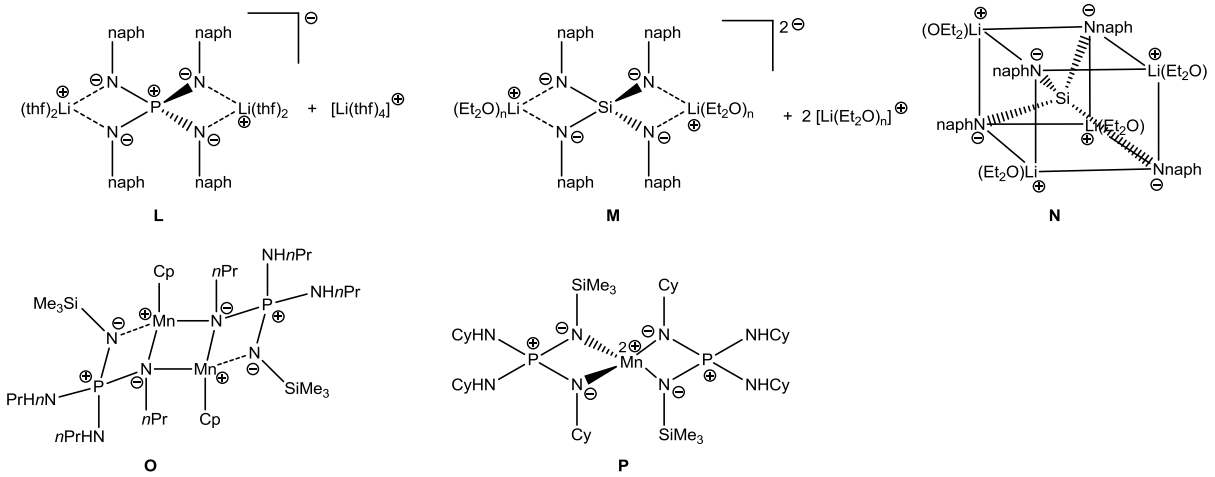

Figure 1.6: Published phosphorous- and silicon compounds.[49-51] **O** and **P** are possible but unproven structures.[51]

In 2000 *Chivers et al.* published the tetrakisimido tetraanions [{$(Et_2O)_nLi$}$_4${(Nnaph)$_4$Si}], which could be two possibly different species (**M**,**N**).[51] It could not be deduced which species was formed. **M** would be an analog to **1**, to [{Li(thf)$_4$}$_2${I_4Cd_2(N*t*Bu)$_4$S}], and the phosphor center compound **L**, while this is not the case for **N**. Furthermore, *Layfield et al.* synthesized manganese iminophosphate complexes in 2012 (**O**, **P**). In the first one, phosphorus atom is coordinated by four nitrogen atoms, two of which belong to a manganese cyclopentadienyl moiety (**O**) and in the second one phosphorus- and one manganese atom are coordinated by four nitrogen atoms (**P**). Both structures are possible but unproven (Figure 1.6).[50] The developments until 2001 in the chemistry of analogs of polyimido and imido/oxo anions of p- and d-block elements have been intensively reviewed by *Chivers et al*.[52]

1.3. $OS(NR)_3$ and $O_2S(NR)_2$ compounds

For this thesis, the topic of the oxo-sulfur imido compounds is of equally high importance. The decomposition of the lithiated tetrakis(*tert*butyl)imidosulfate (**1**) leads mostly to formation of the hydrolyzed products. This is why it is interesting to characterize and know the behavior of these compounds. The oxo species can be synthesized by oxidation of the sulfurtriimide.

In 1979 *Glemser et al.* published the compound $[OS(N\mathit{t}Bu)(NH\mathit{t}Bu)_2]$ (**R**), which contains an oxygen atom and three nitrogen atoms coordinated to the sulfur center.[53] Compound **R** is formed *via* the intermediate $O_2S(NH\mathit{t}Bu)_2$ (**Q**).[53] Furthermore, in 1991 *Okuma et al.* presented several complexes of $OS(NR)_3$, e. g. the positively charged 4,4'-sulfinyldimorpholine diethyl amine $[OS(C_4H_8NO)_2(NEt_2)]^+$ with BPh_4^- (**S**) as a counter ion.[54] Analogs with the ethyl moiety being replaced by other aliphatic groups have been synthesized as well.[54] The first metalated $OS(NR)_3$ complex was reported in 1998 by *Stalke et al*.[31] In the reaction of $[Li_2\{N\mathit{t}Bu)_3S\}_2]$ with iodine the trilithiated species $[(thf)_3Li_3(\mu_3I)\{(N\mathit{t}Bu)_3SO\}]$ (**T**) was obtained.[31] In 2001 we introduced a second lithiated $OS(NR)_3$ complex, $[OS(N\mathit{t}Bu)_3Li_2tmeda]_3$ (**U**), (Figure 1.7).[55]

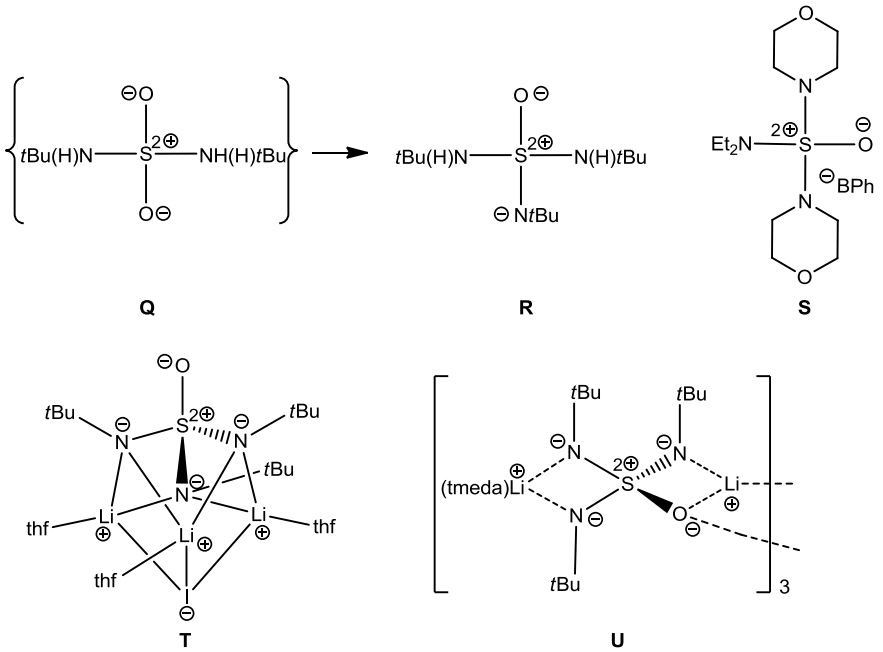

Figure 1.7: Examples for $OS(NR)_3$- and $O_2S(NR)_2$ compounds.[31, 53-55]

Stalke et al. designed a tentative mechanism for the oxidation of $[Li_4\{NtBu)_3S\}_2]$. Thereby, **T** could be obtained as the main product (Scheme 1.7).[31] In the first step the white compound turns blue as the radical species $[Li_3\{(NtBu)_3S^{IV}\}_2]^{\cdot}$ is synthesized, the existence of which has been proven by ESR spectroscopy. Applying heat, the intermediate $\{Li_2(NtBu)_3S^{IV}O\}$ was formed. After aqueous workup $O_2S(NtBu)_2$ was finally obtained.[31]

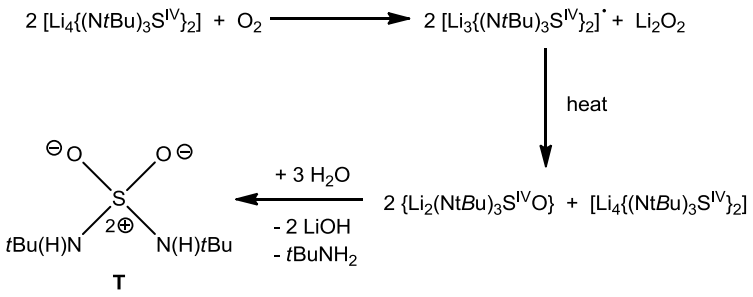

Scheme 1.7: Tentative mechanism for the oxidation of $[Li_4\{NtBu)_3S\}_2]$.[31]

In 2002 *Mews et al.* presented three crystal structures containing the the cationic $(Me_2N)_3SO^+$ species (Figure 1.8), the last publication on this topic.[56] In the reaction of $(Me_2N)_2S(O)F_2$ with fluorotrimethylsilane, the first complex $[(Me_2N)_3SO^+Me_3SiF_2^-]$ could be obtained, which reacted with MF_n (M = As, H, n = 5, 1) to yield $[(Me_2N)_3SO^+AsF_5^-]$ (**W**) and $[(Me_2N)_3SO^+HF^-]$ (**X**).[56]

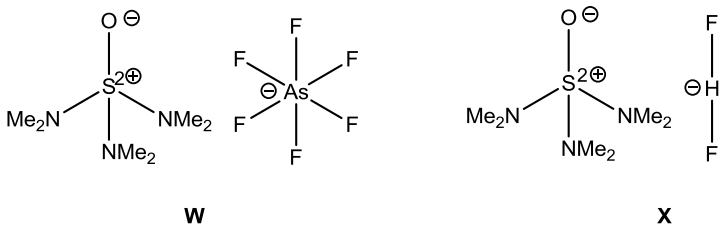

Figure 1.8: Examples of $(Me_2N)_3SO^+$ compounds.[56]

1.4. Sulfur-nitrogen and sulfur-oxygen bonding

In the mid-1980s, it was verified that *d*-orbitals do not participate in the sulfur-nitrogen and sulfur-oxygen bonding because of the large energy difference between the *p*- and *d*-orbitals of the sulfur atom.[57-60] MO-calculations of "hypervalent" molecules indicate that *d*-orbitals are necessary for the polarization functions and not for bonding.[61-63] *Cioslowski et al.* reported that the short bond consists of a highly polarized covalent and an ionic bond, whereby the octet rule is not violated for these compounds.[64, 65]

Stalke et al. published several experimental and theoretical charge density studies about sulfur nitrogen compounds.[66-69] For none of the investigated S–N bonds in methyl(diimido)sulfonic acid H(N*t*Bu)$_2$SMe (1.68 Å and 1.58 Å), methylene-bis(triimido)sulfonic acid H$_2$C{S(N*t*Bu)$_2$(NH*t*Bu)}$_2$ (1.52 Å to 1.65 Å), sulfurdiimide S(N*t*Bu)$_2$ (1.54 Å and 1.53 Å), and sulfurtriimide S(N*t*Bu)$_3$ (1.51 Å), a classical double bond formulation could be supported from charge density investigations.[69] These compounds were analyzed by high-resolution X-ray diffraction. Generally, the experimental and theoretical results of the geometry agree with the qualitative features of the spatial distribution of the Laplacian (shape of $\nabla^2\rho(r)$, number and position of nonbonding VSCCs (valence shell charge concentration)).[70] In each compound, the lone pairs of the nitrogen atom incline toward the electropositive sulfur atom as could be observed by VSCCs as critical points in the negative Laplacian.[70] *Chesnut* described this as lone-pair back-bonding of the *sp*^{3} hybridized SN$_x$ (Figure 1.9).[71]

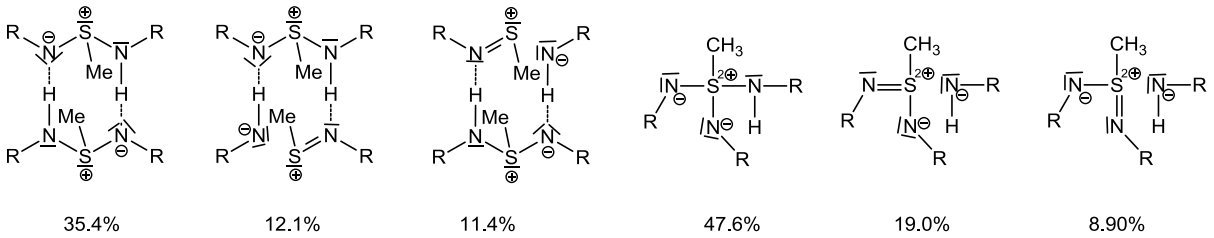

Figure 1.9: Results of NBO/NRT analysis of H(N*t*Bu)$_2$SMe and Me{S(N*t*Bu)$_2$(NH*t*Bu)}$_2$. For H(N*t*Bu)$_2$SMe 58.9 % and for Me{S(N*t*Bu)$_2$(NH*t*Bu)}$_2$ 75.5 % are covered by the distributed electronic structure. The weights are given below each resonance structure.[69]

Rundle described the "hypervalent" planar *sp*^{2} hybridized SN$_x$ and SO$_x$ molecules by the formation of an *m*-center-*n*-electron bond (Figure 1.10).[72] Due to this, S(N*t*Bu)$_2$ has a 3-

center-4-electron bond and S(N*t*Bu)$_3$ a 4-center-6-electron bond. In these compounds, the π-system is below and above the SN_x plane, which could be verified by NBO/NRT approaches (natural bonding orbital/natural resonance theory).[69, 73]

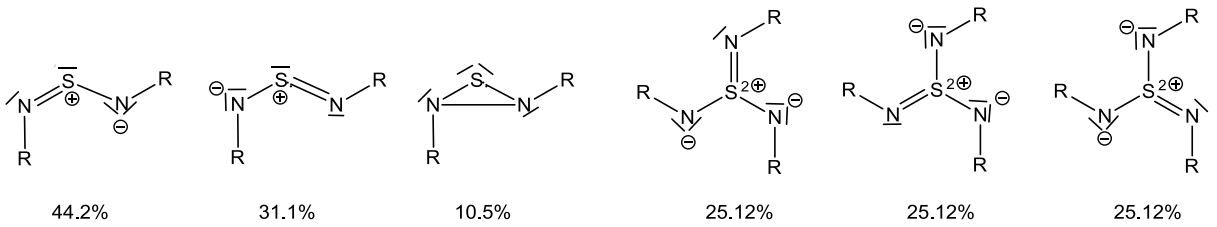

Figure 1.10: Results of NBO/NRT analysis of sulfurdiimide and sulfurtriimide. For S(N*t*Bu)$_2$ 85.8 % and for S(N*t*Bu)$_3$ 75.4 % are covered by the distributed electronic structure. The weights are given below each resonance structure.[69]

For the potassium sulfate, *Stalke, Gatti* and *Iversen* describe the S–O interaction as highly polarized, covalent bonds.[74] This could be characterized by multipole modeling of experimental synchrotron X-ray diffraction data and periodic DFT calculations.[74]

Summarizing, the S–O and the S–N bond can be described as a polarized bond (S^+–O^-, S^+–N^-).[69, 74] In H(N*t*Bu)$_2$SMe and H_2C{S(NtBu)$_2$(NH*t*Bu)}$_2$, the short S–N bonds include covalent as well as ionic contributions.[69] In S(N*t*Bu)$_2$ and S(N*t*Bu)$_3$, the covalent influence on the S–N bonds results in decreased charge at the nitrogen atoms.[69] Moreover, the ionic part is slightly raised in the short S–N bonds.[69] In K_2SO_4, the S–O bond is also highly polarized with a ionic part and cannot be described as a typical covalent bond only.[74] Finally, the valence expansion at the sulfur atom with more than eight electrons can be excluded to explain the bonding.

1.5. Di(*tert*butyl)seleniumdiimide

The higher homolog of the disubstituted sulfur atom in $S(NtBu)_2$ is the selenium atom in di(*tert*butyl)seleniumdiimide, $Se(NtBu)_2$. In 1976 *Sharpless et al.* described the importance of this selenium compound in the amination of olefins and acetylenes.[75] Ten years later *Herberhold et al.* published the synthesis of $Se(NtBu)_2$ and cycle selenium species.[76] In this, *tert*butylamine was added dropwise to a suspension of selenium tetrachloride and diethyl ether. The resulting salt, $tBuNH_3Cl$, was filtrated and the solvent was removed. Moreover, they reported that the product is dependent on the temperature. At room temperature $Se(NtBu)_2$ melts and after a few days they could obtained yellow crystals, which indicated formation of the five-member cycle $[Se_3(NtBu)_2]$. In ^1H NMR studies of $Se(NtBu)_2$ they found only one signal at rt and two signals at –30°C, which they attributed to the *Z*/*E*-isomers with the *syn, syn* and *anti, anti* isomers giving the same signal (Scheme 1.8).[76]

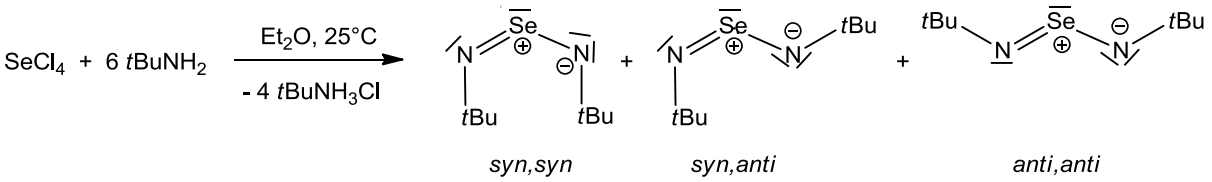

Scheme 1.8: Synthesis of di(*tert*butyl)seleniumdiimide.[76]

In 1993 the work groups of *Wrackmeyer* and *Herberhold* published studies of this di(*tert*butyl)seleniumdiimide and other selenium-nitrogen compounds. By means of ^{15}N and ^{77}Se NMR spectroscopy, they identified the type of heterocycle or Se–N product as well as their formation by signal shifting.[77] In 1996 a new method of an amination with a seleniumdiimide was reported by *Sharpless et al.* (Scheme 1.9).[78] This work combined with the results from *Sharpless et al.*[75] in 1976 shows the application of the selenium compounds in different redistribution reactions.

In 1998 and 2000 *Chivers et al.* reported about the relative stabilities of monomeric and dimeric structures.[79, 80] Employing DFT molecular orbital techniques for $E(NMe)_2$ (E = S, Se, Te) they found that the *syn, syn* conformation is more stable than the *anti, anti* conformation. The *syn, anti* conformation is nearly equal to the *syn, syn* conformation in electronic interaction but regarding steric aspects it is energetically between the *syn, syn*

and *anti, anti* conformation.[79] *Chivers et al.* determined these compounds by means of ^{77}Se NMR studies.[80] The ^{77}Se NMR studies concurred on the results of *Wrackmeyer* and *Herberhold*[77] and *Chivers et al.* enhanced the list of selenium-nitrogen cycles and their ^{77}Se NMR spectra.[80]

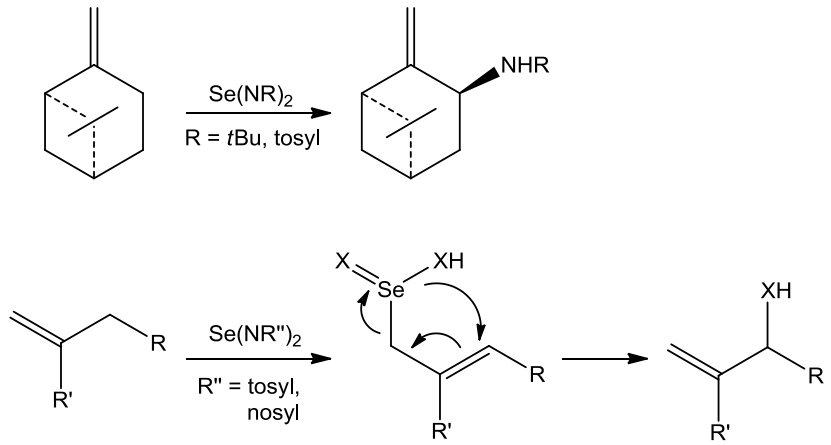

Scheme 1.9: Amination of β-pinene[75] and allylic amination by means of a seleniumdiimide[78].

Shortly afterwards, the same work group published a new seleniumdiimide, the $Se(NAd)_2$ and the dimeric hydrolyzed $[OSe(NtBu)]_2$ (Figure 1.11).[81] Furthermore, they determined the conformation and energetics of chalcogen diimides with different calculation programs drawing the conclusion that calculations cannot tell yet, whether dimerization is favored.[82]

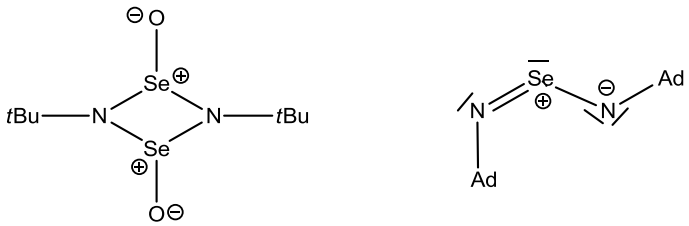

Figure 1.11: The dimeric hydrolyzed $[OSe(NtBu)]_2$ and $Se(NAd)_2$.[81]

2. Scope

This thesis is based on the work accomplished during my diploma thesis, in which the reproduction of the lithiated tetrakis(*tert*butyl)imidosulfate [(thf)$_4$Li$_2$(N*t*Bu)$_4$S] (**1**) was essential (Figure 2.1). Moreover, the first complex of this type with a coordinated transition metal, [{(thf)$_4$Li}$_2${I$_4$Cd$_2$(N*t*Bu)$_4$S}] could be synthesized and a second four coordinated starting material [(C$_4$H$_8$O$_2$)$_2$Li$_2$(N*t*Bu)$_4$S]$_n$ with a coordinated 1,4-dioxane was obtained.

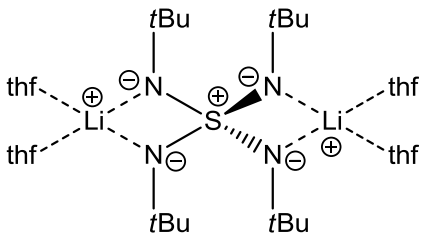

Figure 2.1: Lithiated starting material tetrakis(*tert*butyl)imidosulfate [(thf)$_4$Li$_2$(N*t*Bu)$_4$S] (**1**) for further transmetalation reactions.

Herein, the focus lays on the transmetalation of the lithiated tetrakis(*tert*butyl)-imidosulfate (**1**) to synthesize novel metal complexes of the S(N*t*Bu)$_4^{2-}$ ligand. Moreover, the behavior of the associated complexes in the solid state and their differences in bond lengths and angles should be investigated by single crystal X-ray diffraction experiments.

The first and main part describes the transmetalation of **1** by different synthetic approaches. The second part centers on the synthesis of [(thf)$_4$Li$_2$(N*t*Bu)$_4$S] (**1**) with the THF molecules being replaced by other solvent molecules, which is a more convenient to handle starting material. The third part is about the synthesis of novel S(NR)$_4^{2-}$ ligands to ease the transmetalation and the syntheses of heterobimetallic complexes. The last part focuses on the reproduction of di(*tert*butyl)seleniumdiimide and a potential synthesis of a higher homolog of the sulfur-nitrogen compounds and the potential metal complexes.

3. Results and discussion

Lithiated compounds can be transmetalated in different ways. The aim is to exchange the lithium atoms with a different metal atom and educe a new metal complex. In this work, two possibilities to synthesize metalated tetrakis(*tert*butyl)imidosulfate compounds are presented. On the one hand, there is the transmetalation of $[(thf)_4Li_2(NtBu)_4S]$ (**1**) and on the other hand, there is the option to implement the transmetalation into the reaction of the sulfurtriimide to $[(thf)_4Li_2(NtBu)_4S]$ (**1**). Scheme 3.1 shows the different possibilities. One option is the reaction of sulfurtriimide and a metal alkyl (yellow). Furthermore, there are the reactions of sulfurtriimide and metal hydrides (orange) or metal *tert*butanolates (red) (chapter 3.6). For the transmetalation reaction starting from the lithiated tetrakis(*tert*butyl)imidosulfate (**1**), there are two options with a metal acetylacetonate (pink/purple) (chapter 3.4 and 3.5). The complex with the coordinated metal bis(trimethylsilyl)amide can be synthesized in the reaction of a mixture of $M(N(SiMe_3)_n)$, *tert*butylammonium chloride and the $[(thf)_4Li_2(NtBu)_4S]$ (**1**) (turquoise)[21] (chapter 3.3) or in the reaction of metal chlorides and lithium bis(trimethylsilyl)amide (blue) (chapter 3.2). Also a transmetalation reaction can be induced by metal halides or coordinated metal halides. With the coordinated species, there are two possible products (green): The elimination of lithium halide to synthesize $[(R_2M)_2(NtBu)_4S]$ and the elimination of LiR to synthesize $[(X_2M)_2(NtBu)_4S]$ (chapter 3.1). This second product can be also obtained in the reaction of metal halides with $[(thf)_4Li_2(NtBu)_4S]$ (**1**) (brown) (chapter 3.1). By this reaction is it possible to separate the lithium halide by filtration and the metal atom is now coordinated by two THF molecules and the sulfur-nitrogen ligand (gray) (chapter 3.1).

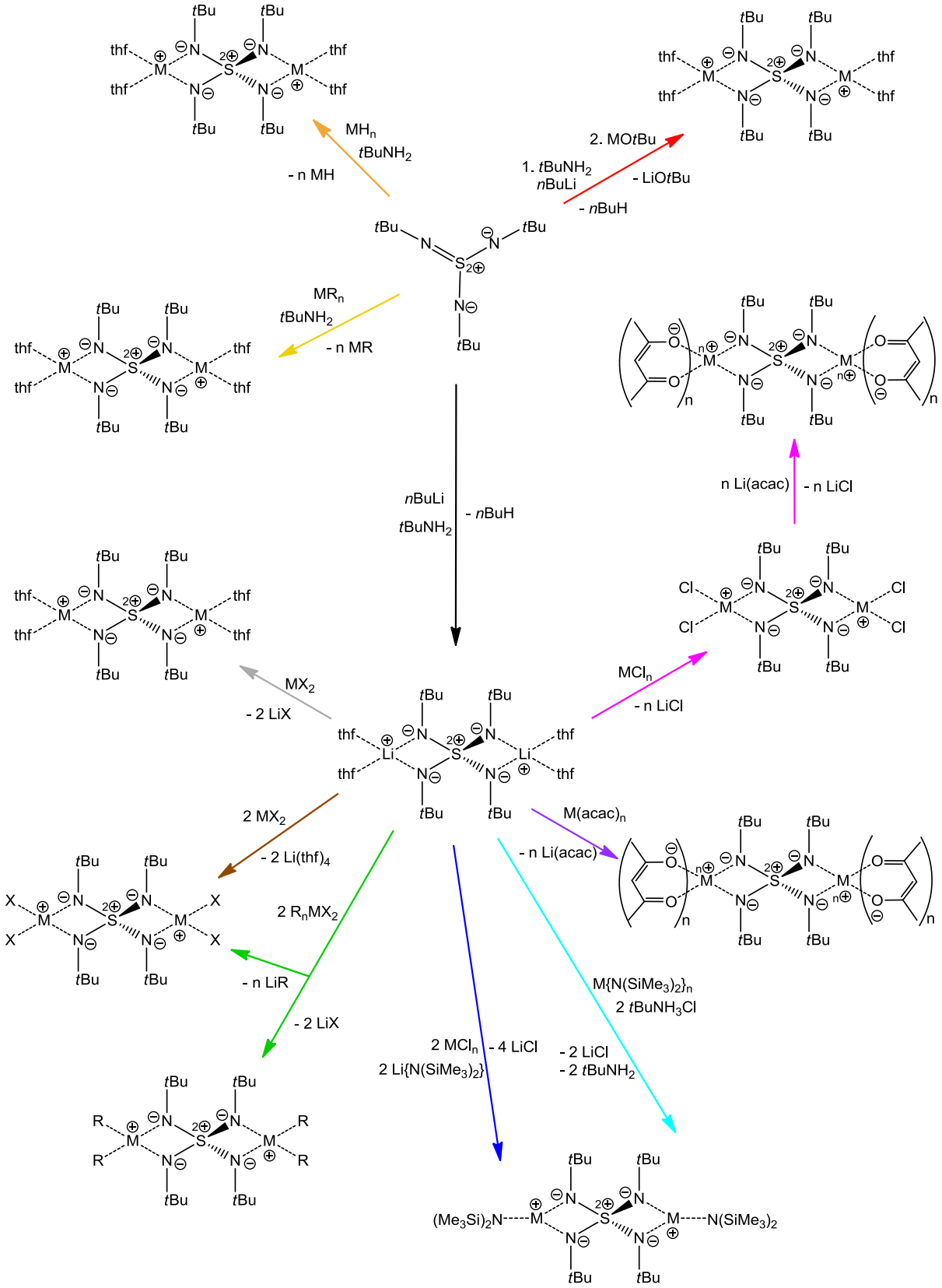

Scheme 3.1: Possible transmetalation reactions for novel metalated tetrakis(*tert*butyl)imidosulfate compounds.

3.1. Transmetalation reaction with metal halides

In the transmetalation of tetrakis(*tert*butyl)imidosulfate (**1**) by means of metal halides, driving force is to react $[M_2(NtBu)_4S]$ and the corresponding lithium halide. However, the transmetalation can also proceed without the salt elimination. This was confirmed by the results of my diploma thesis,[34] wherein the cadmium iodide complex $[\{(thf)_4Li\}_2\{I_4Cd_2(NtBu)_4S\}]$ was synthesized. Based on this work, different metal halides were tested for the transmetalation reaction. The metal halides had been stored in the glove box. It had been assumed that these metal halides were dry and usable for transmetalation reactions. The metal halide and $[(thf)_4Li_2(NtBu)_4S]$ (**1**) in a mixture of THF/toluene were stirred over two hours at 0°C and then two days at room temperature. After removing the solvent *in vacuo*, pentane was added and the reaction mixture was stirred for one hour. In the next step, the precipitated lithium halide was filtered off and the resulting solution was then stored at –24°C. Scheme 3.2 shows the expected reactions.

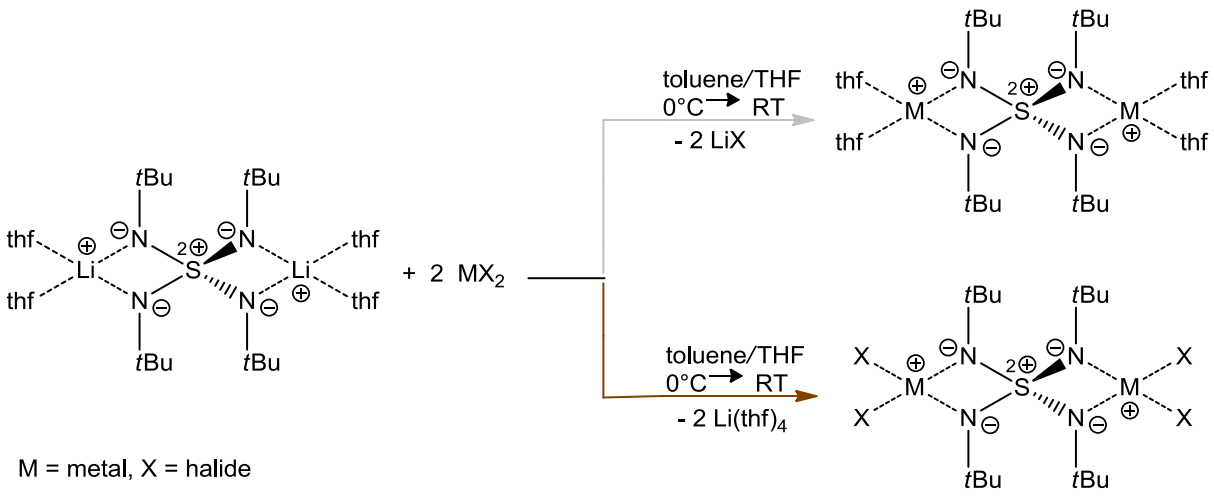

Scheme 3.2: Expected reactions of the transmetalation of **1** with metal halides.

In the reaction of aluminum-, gold-, and nickel chloride colorless crystals were obtained, which were analyzed by X-ray structure determination. All the crystals turned out to consist of lithium bromide coordinated by THF molecules. The bromide originates from a previous step, the formation of $S(NtBu)_3$ by oxidation. In the reaction of iron- and copper bromide, as well as copper-, iron-, ruthenium- and samarium chloride and iron

iodide an amorphous solid lithium halide could be filtered off. The desired product did not crystallize. The ^{1}H and ^{13}C NMR showed several signals, which could not be assigned. Table 3.1 shows the applied substances.

Table 3.1: Metal halides, which were used for the transmetalation reaction of $[(thf)_4Li_2(NtBu)_4S]$ (**1**).

metal halides	*solution color (toluene/THF)*	*solution color (pentane)*	*crystals*
$FeBr_2$	green-blue	brown	colorless $O_2S(NtBu)_2$
$CuBr_2$	blue	colorless	colorless $[(thf)_2LiBr]_2$
$ZnBr_2$		blue	
$MnBr_2$	blue	blue	colorless $[(thf)_2LiBr]_2$
$FeCl_2$	green		
$CuCl_2$	black		
$NiCl_2$	brown		colorless $[(thf)_2LiBr]_2$
$SmCl_2$	yellow		
$AlCl_3$	colorless		colorless $[(thf)_2LiBr]_2$
$AuCl_3$	colorless		colorless $[(thf)_2LiBr]_2$
$RuCl_3$	brown		
FeI_2	black		

The experimental proceedings were changed because the reaction product did not crystallize at 0°C, –24°C, –35°C and –78°C. Also the analytic control mostly gave too many signals for unambiguous assignment of signals of the desired compounds. Only the ^{1}H NMR spectrum of the reaction mixture with $CuBr_2$ showed a signal at 1.37 ppm for the *tert*butyl groups, which might be assigned to the desired product. Instead of toluene and THF, the reactions of iron-, copper-, zinc- and manganese bromide were carried out in pentane to realize the crystallization. Like before, only lithium bromide and the hydrolyzed product $O_2S(NtBu)_2$ could be obtained, which were analyzed by X-ray diffraction.

Summarizing, the reactions with metal halides as transmetalation reagents were not successful. Instead, coordinated metal halides may yield the desired products because these substances should be more stable and due to the coordination of ally-, alkyl- and other CH-groups the new transmetalation products might crystallize easier.

For the coordinated metal halides, R_nMX_2, there are two possible products. The elimination of lithium halide to synthesize $[(R_2M)_2(NtBu)_4S]$ and the elimination of LiR to synthesize $[(X_2M)_2(NtBu)_4S]$ are possible (Scheme 3.3).

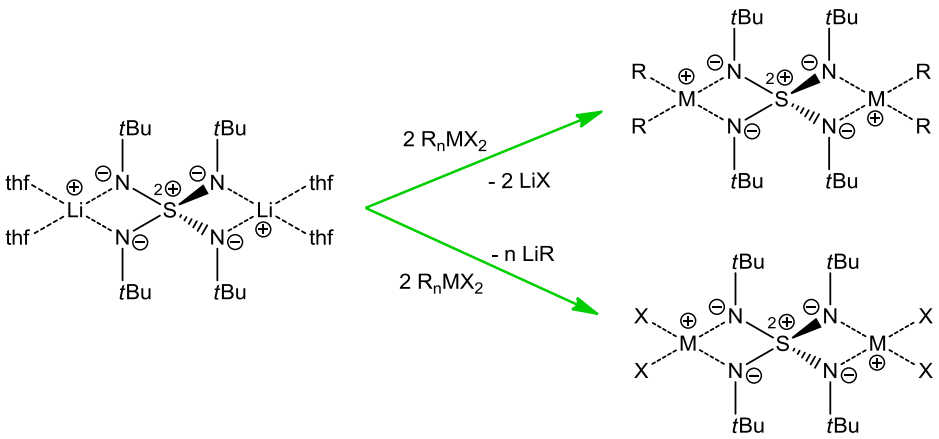

Scheme 3.3: Expected reactions of the transmetalation with coordinated metal halides.

The lithiated starting material is extremely water sensitive so that the utilized metal halides need to be dried again *in vacuo* applying heat before they can be used for the metalation of the sulfur-nitrogen ligand. In the reaction with coordinated metal halides, THF was added to a mixture of $[(thf)_4Li_2(NtBu)_4S]$ and followed by the metal halide at –30°C. After the filtration of lithium salt, pentane or toluene was added. After two weeks half of the solvent was removed *in vacuo*. It had been assumed that used metal halides and donor stabilized metals were dry and usable for transmetalation reactions. These metal halides and donor stabilized metals, their color in solution and whether crystals were obtained are summarized in Table 3.2.

In the reaction of the rhodium compound $(PPh_3)_3RhCl$ and $[(thf)_4Li_2(NtBu)_4S]$ crystals were obtained. Unfortunately, these crystals turned out to consist of hydrolyzed PPh_3-ligand and lithium cations form $Li(OPPh_3)_4$ species. The phosphane are inert against water but they react readily with oxygen to give the phasphanoxides. This lithium-phosphane compound could be formed because the triphenylphosphane might be better stabilizing the complex with the coordinated lithium atom than the sulfur-nitrogen ligand, $S(NtBu)_4^{2-}$. This compound is not completely characterized because the quality of the X-ray diffraction data was too poor for a detailed structure refinement. The synthesis of this $Li(OPPh_3)_4$ species was also not reproducible. The ^1H NMR spectrum of the

crystals dissolved in d_8-THF showed multiplets of the phenyl rings at 7.36 and 7.67 ppm. NMR studies of the reaction mixture were inconclusive. Also EI-MS and elemental analysis could not clarify which products had formed.

Table 3.2: Utilized coordinated metal halides and outcome of the reaction.

substance	*solution color*	*product*	*substance*	*solution color*	*product*
$TiCl_3 \cdot (thf)_3$	brown	powder	$FeI(C_3H_5)(CO)_3$	red	
$CrCl_3 \cdot (thf)_3$	brown		$NiBr(NO)(PPh_3)_2$	green	powder
$FeBr_2 \cdot thf$	black		$PPh_4VO(mnt)_2$	brown	powder
Ph_2SnCl_2	yellow	microcrystals	$Cl_2Cu(N(H)_2tBu)_2$	red	powder
Cp_2TiCl_2	brown	microcrystals	$[(p\text{-cymene})RuCl_2]_2$	green	powder
Cp_2ZrCl_2	yellow	$tBuNH_3Cl$	$(PPh_3)_3RhCl$	red	"$Li(OPPh_3)_4$"
$TiCl_3 \cdot AlCl_3$	brown		$[(\eta^3\text{-}C_3H_8)PdCl]_2$	green	
$TiCl_3(C_8H_7)$	red		$[(\eta^3\text{-}C_4H_7)PdCl]_2$	yellow	
FeTPP-Cl	brown		$[(\eta^3\text{-}1,3\text{-}Ph_2\text{-}C_3H_3)PdCl]_2$	yellow	powder
NHC-AgCl	blue		$[(\eta^3\text{-}1,1,3\text{-}Ph_3\text{-}C_3H_2)PdCl]_2$	orange	
$[Ni_2Cp_3]BF_4$	brown	powder	$[(\eta^3\text{-}1,3\text{-}C_6H_9)PdCl]_2$	brown	
$[Fe_2Cp_2]PF_6$	yellow	$FeCp_2$	$Fe(OAc)_2$	yellow	$tBuNH_3Cl$
$[Fe_2Cp_2]BF_4$	yellow	$FeCp_2$	$Pd(OAc)_2$	brown	powder
$(COD)PdCl_2$	brown	powder	$Cu(OAc)_2$	yellow	powder
K-Selectride™	yellow	microcrystals			

In the reaction of Ph_2SnCl_2, Cp_2TiCl_2, and K-Selectride™ some yellow and brown solids were obtained, the NMR analysis of which was inconclusive. The size of the crystals could not be increased by recrystallization from THF, toluene or pentane. The crystals from the reaction of $[Fe_2Cp_2]PF_6$ and $[Fe_2Cp_2]BF_4$ could be identified as $FeCp_2$. Most attempts did not yield crystals. Some reaction mixtures resulted in powder being formed, which was, however, not the desired product.

3.2. Metal chlorides and lithium bis(trimethylsilyl)-amide

An alternative route to achieve transmetalation is based on the reaction of a metal chloride and lithium bis(trimethylsilyl)amide. Probably, these substances react to the intermediate $ClM\{N(SiMe_3)_2\}$ by the elimination of lithium chloride, followed by a reaction with the starting ligand $[(thf)_4Li_2(NtBu)_4S]$ to the transmetalation product (Scheme 3.4).

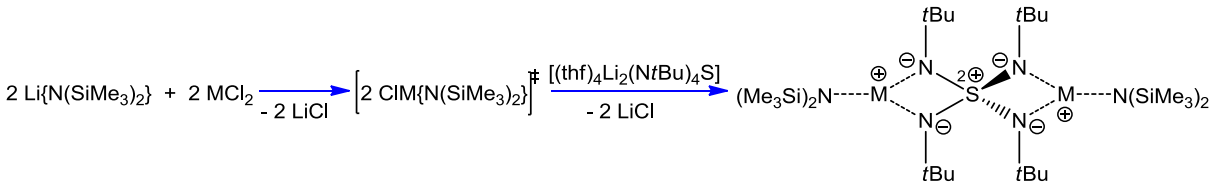

Scheme 3.4: Potential reaction of metal chlorides with $Li\{N(SiMe_3)_2\}$ and $[(thf)_4Li_2(NtBu)_4S]$.

In this reaction, there exist two possibilities for the removal of lithium chloride. Either lithium chloride was removed before or after addition of $[(thf)_4Li_2(NtBu)_4S]$. This was carried out with different metal chlorides.

The metal halides, which had been stored in the glove box, were assumed to be dry and usable for transmetalation reactions.

For this purpose, two equivalents of the metal chloride and two equivalents of the lithium bis(trimethylsilyl)amide were dissolved in toluene and stirred for four hours. One equivalent of $[(thf)_4Li_2(NtBu)_4S]$ was added to the reaction mixture and stirred over night. After the precipitated solid, which might be lithium chloride, was filtered off and half of the solvent was removed *in vacuo*. The resulting solution was stored at –24°C to obtain crystals.

In the reaction with aluminum- and cobalt chloride colorless crystals in a brown solution could be obtained, which were, however, not suitable for single crystal X-ray structure analysis. These crystals melted and changed their colors after a few seconds. While no stable crystals could be obtained during this work. Also the ^1H NMR spectrum shows signals, which are not usable to identify the solution mixture.

In the reaction of manganese-, magnesium- and nickel chloride, crystals of *t*BuNH$_3$Cl were obtained. A trace of the solvent *tert*butylamine, used in the syntheses of **1**, might be in the starting material. This *tert*butylamine may crystallize first as *t*BuNH$_3$Cl in the following reaction. NMR studies of the solutions only showed several peaks, which could not be assigned. In the reaction of copper chloride and palladium chloride with [(thf)$_4$Li$_2$(N*t*Bu)$_4$S] (**1**), Cl$_2$Pd(*t*BuNH$_2$)$_2$ and Cl$_2$Cu(*t*BuNH$_2$)$_2$ could be obtained, which had already been characterized earlier by *Boag et al.*[83] and *Chivers et al.*[84], respectively.

In these reactions of sulfur-nitrogen compounds, lithium bis(trimethylsilyl)amide and metal chlorides, different decomposition products could be obtained if water was unexpectedly present in the reaction mixture. Mostly *tert*butylammonium chloride or the hydrolyzed stabile product hexamethyldisiloxane was obtained. Additionally, O$_2$S(NH*t*Bu)$_2$[31, 53] could be formed if two oxygen atoms of water reacted with the sulfur compound and two equivalents of *t*BuNH$_3$Cl precipitated.

An interesting copper-nitrogen cycle was obtained in the reaction of copper(II)chloride, lithium bis(trimethylsilyl)amide and the lithiated starting material **1** (Scheme 3.5). Remarkably, the copper atoms in compound **2** were reduced to the oxidation state +I. With the exchange of the *tert*butylamine groups with oxygen atoms in the starting material, the stabile O$_2$S(NH*t*Bu)$_2$ was formed.

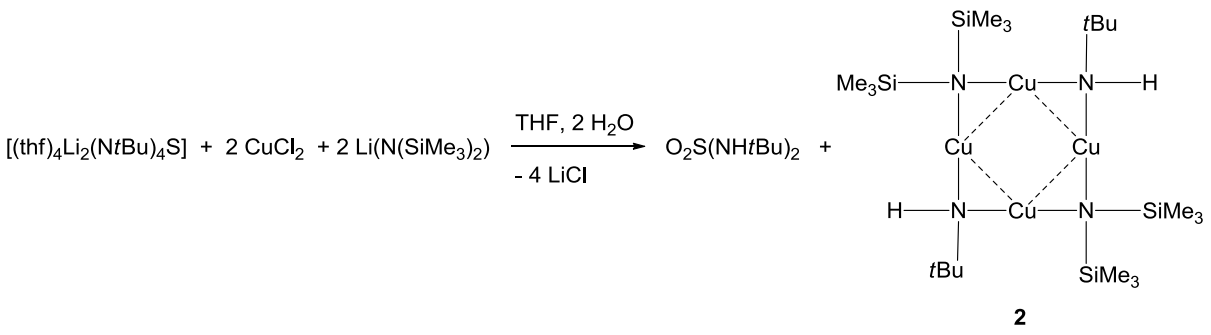

Scheme 3.5: Synthesis of the copper-nitrogen cycle [Cu(NH*t*Bu)Cu(N(SiMe$_3$)$_2$)]$_2$ (**2**).

Colorless crystals of [Cu(NH*t*Bu)Cu(N(SiMe$_3$)$_2$)]$_2$ (**2**) could be obtained after one week storage in THF at –24°C. This compound crystallizes in the monoclinic space group

$P2_1/n$ with half of the molecule in the asymmetric unit (Figure 3.1). The hydrogen atom H2 at the nitrogen atom N2 is found in the Fourier difference map and is refined freely.

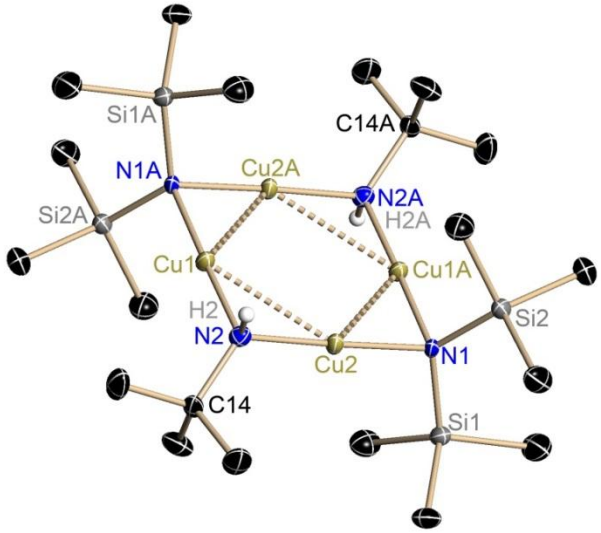

Figure 3.1: Crystal structure of **2**. Hydrogen atoms H2 was found in the Fourier difference map and refined freely. The other hydrogen atoms are omitted for clarity. Displacement ellipsoids are at 50 % probability.

Moreover, in the ^{1}H NMR spectrum, the hydrogen atom of the NH group gives a signal at 3.73 ppm. This proves the reaction pathway to the hydrolyzed $O_2S(NtBu)_2$ and compound **2** (Scheme 3.6). This type of copper-nitrogen cycle is literature known. In 1998 and 2000, *Dehnicke et al.*[85] and *Fenske et al.*[86] published similar cycles, in which a copper(I) atom is coordinated by nitrogen atoms, wherein one nitrogen atom is protonated (Figure 3.2).

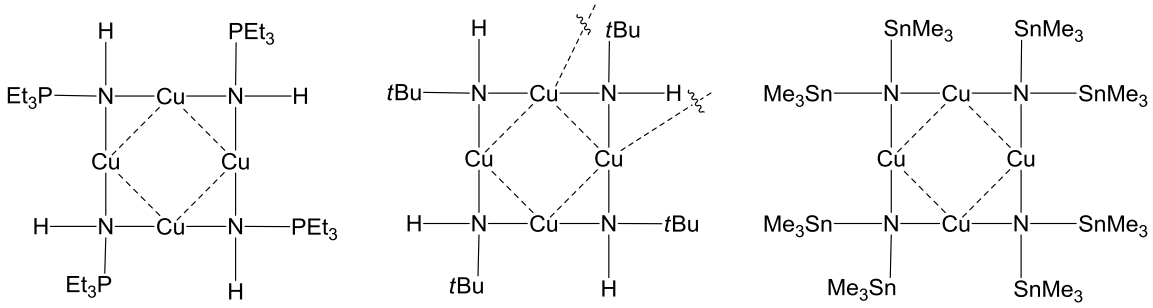

Figure 3.2: Published copper-nitrogen cycles of *Dehnicke et al.*[85] and *Fenske et al.*[86] Left: $[Cu(NHPEt_3)]_4$,[85], middle: the dimer $[Cu(NHtBu)]_8$,[86], right: $[Cu(N(SnMe_3)_2)]_4$.[86]

Compound **2** is nearly equal in bond lengths and angles to these published complexes. In **2**, the distances between the two copper cations are averagely 2.7040 Å and the Cu–N bond lengths are averagely 1.9073 Å (Table 3.3). The Cu–Cu–Cu and the Cu–N–Cu angles in these four compounds are nearly right angles, whereby the N–Cu–N angle becomes almost 180°.

Table 3.3: Selected, averaged bond lengths/*Å* and angles/° of **2**, $[Cu(NHPEt_3)]_4$,[85] $[Cu(NHtBu)]_8$,[86] $[Cu(N(SnMe_3)_2)]_4$.[86]

	3	$[Cu(NHPEt_3)]_4$	$[Cu(NHtBu)]_8$	$[Cu(N(SnMe_3)_2)]_4$
Cu–Cu	2.7040	2.6365	2.7305	2.7075
Cu–N	1.9073	1.9185	1.8795	1.8830
Cu–Cu–Cu	90.00		89.93	89.97
Cu–N–Cu	90.70	86.80	92.80	91.85
N–Cu–N	178.34	167.98	176.70	178.00

In this part, newly purchased metal chlorides and lithium bis(trimethylsilyl)amide were used for the transmetalation reaction. The same conditions as before were used for the respective synthesis. $[Cu\{(NtBu)_2(N(H)tBu)SO\}_2]$ (**2**) was obtained in the reaction of copper chloride with lithium bis(trimethylsilyl)amide and $[(thf)_4Li_2(NtBu)_4S]$ (Scheme 3.6).

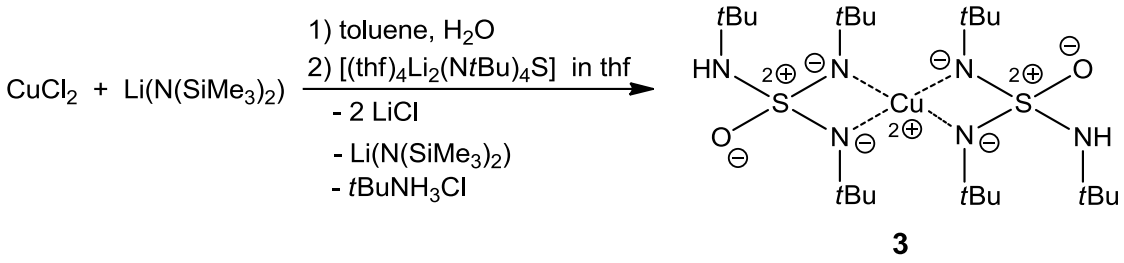

Scheme 3.6: Synthesis of $[Cu\{(NtBu)_2(N(H)tBu)SO\}_2]$ (**3**).

The difference to the synthesis of compound **2** was the copper chloride being newly purchased and toluene instead of THF being used in the first step of the reaction. In the course of the syntheses of **3** a *tert*butylammonium chloride splits off and a water molecule reacts with the starting material **1**. So, traces of water must have been present

either in the metal halides. To prove this, the reaction under identical conditions yet in the presence of a certain amount of water was repeated and the synthesis of **3** is reproducible in good yields (60 %) (Figure 3.3).

[Cu{(N*t*Bu)$_2$(N(H)*t*Bu)SO}$_2$] was formed colorless blocks from a THF/toluene solution at –24°C after one week. The crystals were suitable for single crystal X-ray diffraction analysis. The compound crystallizes in the triclinic space group $P\bar{1}$ with one molecule in the asymmetric unit.

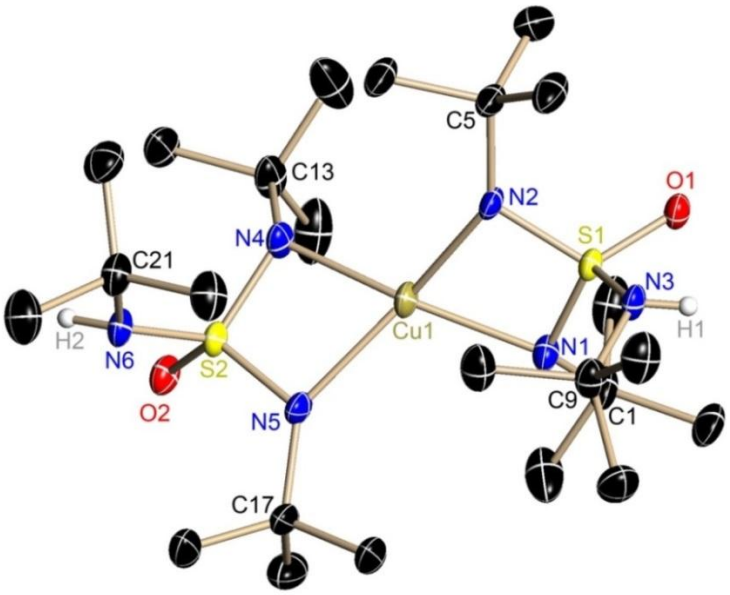

Figure 3.3: Crystal structure of [Cu{(N*t*Bu)$_2$(N(H)*t*Bu)SO}$_2$] (**3**). Hydrogen atoms H1 and H2 were found in the Fourier difference map and refined freely. The other hydrogen atoms are omitted for clarity. Displacement ellipsoids are at 50 % probability.

In this complex, the sulfur atom is almost tetrahedrally bonded by one oxygen atom and three *tert*butylimido groups, whereas one nitrogen atom is protonated and two nitrogen atoms coordinate a cooper cation. In total, the copper(II) atom is coordinated by four nitrogen atoms of two OS(N*t*Bu)$_2$(N(H)*t*Bu) species in a compressed tetrahedral fashion. This complex is in geometry nearly equal to the known compounds methylenebis(triimido)sulfonic acid H$_2$C{S(N*t*Bu)$_2$(NH*t*Bu)}$_2$.[55, 69] Both compounds have one protonated and two non-protonated *tert*butylimido groups. In **3**, an oxygen atom is present instead of the methylene group. The average S–N bond length of the coordinated nitrogen atoms in **3** is 1.575 Å (Table 3.4). This is slightly shorter than in the starting material (**1**) (1.601 Å)[22] and a little bit longer than in H$_2$C{S(N*t*Bu)$_2$(NH*t*Bu)}$_2$ (1.532 Å)[67, 69]. The longer S–N bond length in comparison to

$H_2C\{S(NtBu)_2(NHtBu)\}_2$ results of the coordination of the copper atom. The S–N bond length of the protonated nitrogen atoms is 1.633(2) Å, which is shorter than in $H_2C\{S(NtBu)_2(NHtBu)\}_2$ (1.6722 Å)[69].

Table 3.4: Selected bond lengths and angles of **3**.

bond lengths/Å		*angles/°*	
Cu1–N1	1.9936(19)	N1–Cu1–N2	72.20(8)
Cu1–N4	1.9945(19)	N4–Cu1–N5	72.19(8)
Cu1–N2	2.037(2)	N2–S1–N1	97.90(11)
Cu1–N5	2.039(2)	N2–S1–N3	110.75(11)
S1–N2	1.5647(19)	N1–S1–N3	113.28(11)
S1–N1	1.585(2)	O1–S1–N3	100.97(10)
S1–N3	1.632(2)	O1-S1–N2	117.27(11)
S2–N5	1.566(2)	O1–S1–N1	117.24(10)
S2–N4	1.585(2)	N5–S2–N4	97.90(11)
S2–N6	1.634(2)	N5–S2–N6	111.07(11)
S1–O1	1.4592(17)	N4–S2–N6	113.51(11)
S2–O2	1.4591(17)	O2–S2–N4	117.01(11)
		O2–S2–N5	117.13(11)
		O2–S2–N6	100.86(10)

The S–O bond length are also equal (1.4592(17) Å and 1.4592(17) Å) and are in the same range as the S–O bond length in sulfate K_2SO_4 (averagely 1.475 Å)[74]. The shortened sulfur nitrogen and sulfur oxygen bonds in **3** can be explained by the electron-density studies of *Stalke,*[66-69, 74] *Gatti*[74] and *Iversen*[74] *et al.* about the sulfur–nitrogen and sulfur–oxygen bonds (Chapter 1.4). It can be assume that the results are transferable to the S–O and S–N bonds in **3**. Similar to methyl(diimido)sulfonic acid $H(NtBu)_2SMe$ and methylenebis(triimido)sulfonic acid $H_2C\{S(NtBu)_2(NHtBu)\}_2$, they can be described as highly polarized single bonds with a mostly covalent character. The S–N and S–O bonds are being shorter than usual results from the ionic part. Although **3** contains a transition metal, the behavior of the backbone $S(NtBu)_4^{2-}$ is nearly constant in bond length and angles in comparison with the lithiated starting material **1**. This consistence of the backbone supports the assumption of polarized S–N and S–O distances.

The Cu–N bond lengths differ (2.038 Å for Cu1–N2/5 and 1.994 Å for Cu1–N1/4 on average) and are with an average length of 2.016(2) Å longer than the Li–N bond in the starting material (**1**). This difference in Cu–N bond lengths as well as the overall higher bond length results from the strife between the copper cation favoring a square planar geometry and the OS(N*t*Bu)$_2$(N(H)*t*Bu) ligands, the steric repulsion of which forces the geometry in the direction of tetrahedral.

The N–S–N angle, which encloses the metal atom, is 97.90(11)° and is larger than in the starting material (**1**) (94.70(1)°) because of the repulsion of the two sulfur-nitrogen species OS(N*t*Bu)$_2$(N(H*t*Bu). The N–M–N angle (average 72.20(8)°) is smaller than the starting material (**1**) because the copper atom is slightly smaller than the lithium atom. In addition, the two OS(N*t*Bu)$_2$(N(H)*t*Bu) species repel each other, which increases the Cu–N distance and therewith the average N–Cu–N angle becomes more acute.

Both N–S–N planes are twisted by an angle of 47.45° to create for more space for the bulky *tert*butylimido groups. The angle between the copper atom and the N–S–N plane is 178.93°, respectively, so that the coordination mode of these four atoms is nearly planar (Figure 3.4).

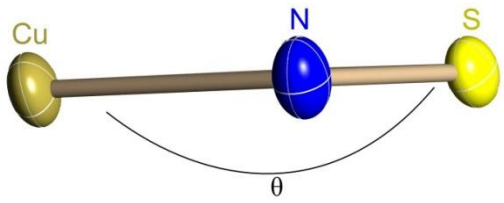

Figure 3.4: θ = 178.93°, angle between the N–S–N plane and the copper atom of **3**.

The hydrogen atoms of the imido group interact with the oxygen atom of the complex in the adjacent unit. For N–H···O, the H···O distance is 2.259 Å, which could be described as a strong donor-acceptor interaction.[87] Due to this coordination a chain of [Cu{(N*t*Bu)$_2$(N(H)*t*Bu)SO}$_2$] molecules is formed (Figure 3.5).

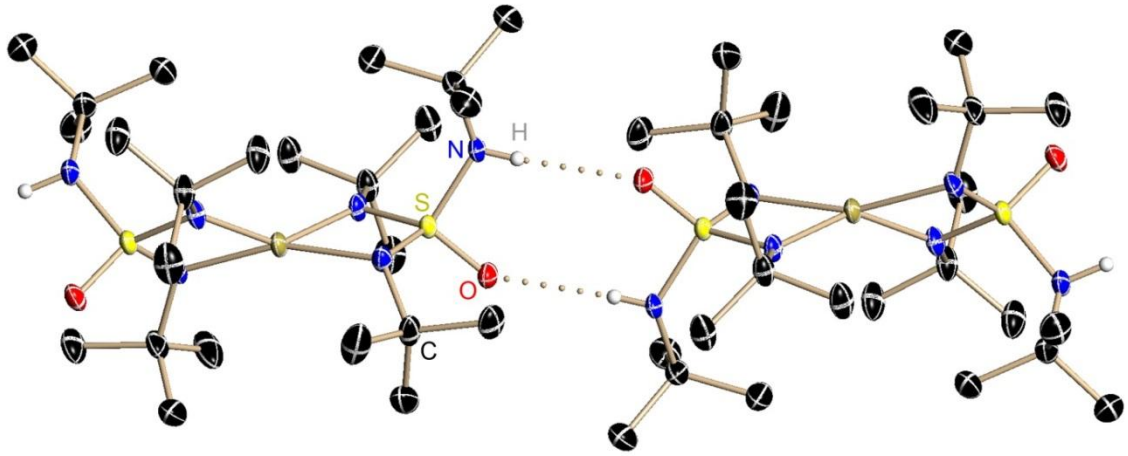

Figure 3.5: Packing plot of [Cu{(N*t*Bu)$_2$(N(H)*t*Bu)SO}$_2$] (**3**) with the interaction between the hydrogen atom of one molecule to the oxygen atom of the next molecule shown as dots. Hydrogen atoms H1 and H2 were found in the Fourier difference map and refined freely. The other hydrogen atoms are omitted for clarity. Displacement ellipsoids are at 50 % probability.

Compound **3** could be confirmed to exist even in solution by NMR spectroscopy experiments. Two signals are present in the ^{1}H NMR; one at 5.45 ppm the proton of the NH-group, which is not observed in the spectrum of the starting material (**1**), and the one at 1.29 ppm is due to protons of the methyl groups, which are shifted from the signal of the methyl groups of the starting material (**1**) (1.27 ppm).

In the reaction with zinc chloride, lithium bis(trimethylsilyl)amide and [(thf)$_4$Li$_2$(N*t*Bu)$_4$S] the hydrolyzed compound [Zn{(N*t*Bu)$_2$(N(H)*t*Bu)SO}$_2$] (**4**) was obtained (Scheme 3.7).

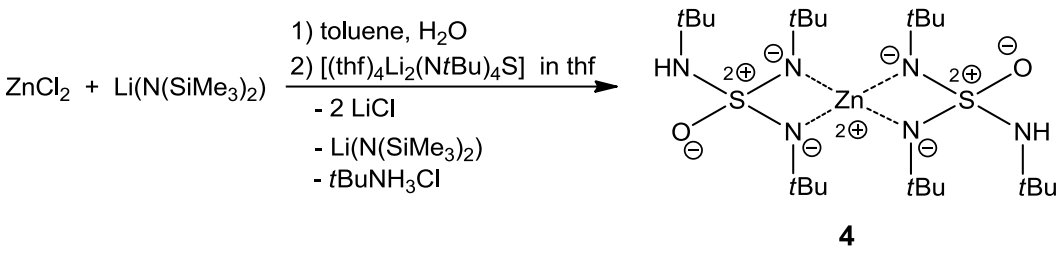

Scheme 3.7: Synthesis of [Zn{(N*t*Bu)$_2$(N(H)*t*Bu)SO}$_2$] (**4**).

[Zn{(N*t*Bu)$_2$(N(H)*t*Bu)SO}$_2$] (**4**) was obtained as colorless blocks from THF/toluene at –24°C after one week. The resulting crystals were suitable for X-ray experiments. The

compound crystallizes in the orthorhombic space group *Pccn* with a half of a molecule in the asymmetric unit (Figure 3.6).

The structural motive of compound **4** resembles that of [Cu{(N*t*Bu)$_2$(N(H)*t*Bu)SO}$_2$] (**3**). In **4**, the sulfur atom is also bonded to an oxygen atom and three *tert*butylimido groups. The two nitrogen atoms, which are not protonated, coordinate a zinc(II) atom. Similarly to the copper atom in **3**, the zinc cation in **4** is coordinated by four nitrogen atoms, whereas always two of them belong to a OS(N*t*Bu)$_2$(N(H)*t*Bu) species.

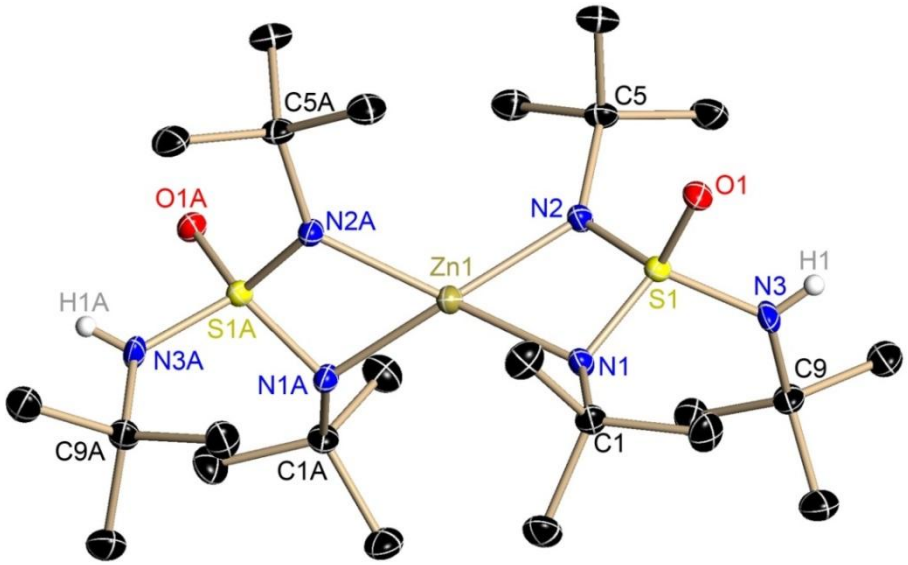

Figure 3.6: Crystal structure of [Zn{(N*t*Bu)$_2$(N(H)*t*Bu)SO}$_2$] (**4**). Hydrogen atoms H1 and H1A were found in the Fourier difference map and refined freely. The other hydrogen atoms are omitted for clarity. Displacement ellipsoids are at 50 % probability.

In **4**, the S–N bond lengths of the coordinated nitrogen atoms are 1.5741 Å on average. The electrostatic interaction shortens the bonds. The S1–N3 bond length (1.6240(2) Å) of the protonated nitrogen atoms is like the S–N bond length of **3**. Similar to compound **3**, it can be assumed that polarized S–N and S–O bonds are present. The average Zn–N bond lengths (2.0188 Å) and the average N–S–N angle (97.10°), which is orientated towards the zinc atom, are also similar in **3** (2.016 Å and 97.90 , respectively). The minimally longer Zn–N distance and the smaller N–S–N angle result from the slightly larger radius of the Zn^{2+} ion (0.74 Å)[88] compared to Cu^{2+} ion (0.71 Å)[88]. The N1–Zn1–

N2 angle (71.52(7)°) is smaller than the average N–Cu–N angle in **3** (72.20(8)°). The important bond lengths and angles are summarized in Table 3.5.

Table 3.5: Selected bond lengths and angles of **4**.

bond lengths/Å		*angles/°*	
Zn1–N1	2.0164(19)	N1–Zn1–N2	71.52(7)
Zn1–N2	2.0211(18)	N1–S1–N2	97.10(10)
S1– N1	1.5701(19)	N1–S1–N3	110.80(11)
S1–N2	1.5781(19)	N2–S1–N3	114.12(11)
S1–N3	1.6240(2)	O1–S1–N1	117.55(10)
O1–S1	1.4566(16)	O1–S1–N2	116.25(9)
		O1–S1–N3	101.65(10)

The two N–S–N planes are twisted by 75.43° to create more space for the bulky *tert*butylimido groups. The angle between the zinc atom and the N–S–N plane is 104.57°. Furthermore, the zinc atom is located out of the sulfur-nitrogen plane giving the zinc atom more space (Figure 3.7).

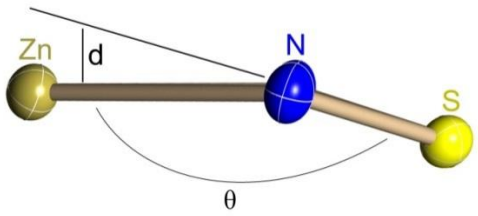

Figure 3.7: θ = 104.57°, angle between the N–S–N plane and the zinc atom and d = 0.4931(34) Å, distance between the zinc atom and the N–S–N plane in **4**.

NMR spectroscopic experiments confirm that compound **4** could be synthesized successfully in solution. The ^{1}H NMR spectrum shows a signal at 5.55 ppm, which originates from the proton of the NH group and one signal at 1.30 ppm, which belongs to the hydrogen atoms of the methyl groups. These signals are similar to the signals of compound **3**. The signal of the methyl groups are shifted in comparison with the starting material (**1**) (1.27 ppm).

Another resemblance of **3** and **4** is that the hydrogen atoms of the imido group interact with the oxygen atom of the complex in the adjacent unit. In **4**, the donor-acceptor interaction of the oxygen- and hydrogen atom amounts to 2.227 Å, which indicates a strong interaction.[87] Due to this coordination a chain of $[Zn\{(N\textit{t}Bu)_2(N(H)\textit{t}Bu)SO\}_2]$ molecules like in **4** is formed (Figure 3.7).

The superposition plot of compound **3** and **4** is shown in Figure 3.8, in order to illustrate the structural differences caused by the coordination of different metal atoms. The zinc atom is clearly outside of the sulfur-nitrogen plane whereas the copper atom is located in the plane formed by the sulfur- and nitrogen atoms.

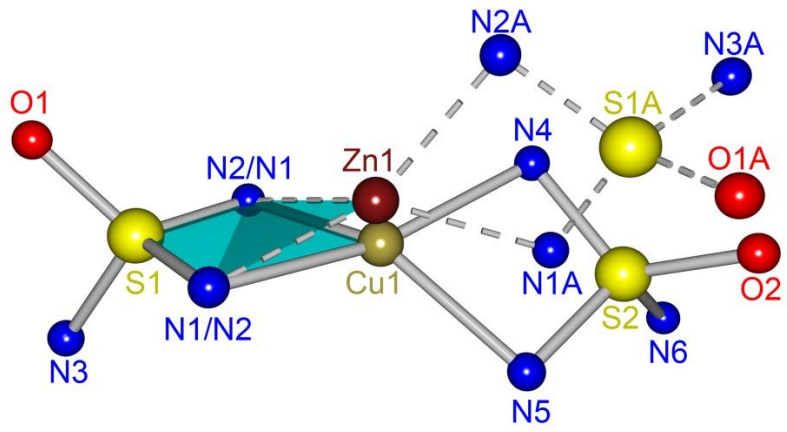

Figure 3.8: Superposition plot of **3** (Cu) and **4** (Zn). The atoms S1, N1 and N2 are projected onto each other with a deviation of 0.0081 Å.

Moreover, the Figure 3.8 visualizes the similar environment at the sulfur atom (S1) in both compounds. There are no significant differences in the O–S and S–N bond lengths and N–S–N and O–S–N angles. Possibly, the hydrogen atom at the nitrogen atom is removed and a second metal atom is coordinated by the deprotonated nitrogen atom to form a heterobimetallic compound.

The reactions described in the previous section were done with metal chlorides which were seemingly not dry enough leading to **3**, **4**, $OS(N\textit{t}Bu)_3$ or $O_2S(N\textit{t}Bu)_2$, or the side products or *tert*butylammonium chloride, being crystallized. In order to obtain the non-hydrolyzed products, all metal chlorides were dried again *in vacuo* ($5.0 \cdot 10^{-2}$ bar) applying heat (50°C or 200°C).

Magnesium chloride and palladium chloride were dried at $2.0 \cdot 10^{-6}$ bar and 200°C. An alternative approach was drying magnesium-, nickel- and aluminum chloride with thionyl chloride, $SOCl_2$. The metal chlorides were refluxed in $SOCl_2$, filtered off, washed with heptane and finally dried *in vacuo* at elevated temperature.[89-91]

By running the transmetalation of the lithiated compound $[(thf)_4Li_2(N\mathit{t}Bu)_4S]$ by means of $SOCl_2$ dried metal chlorides, the same reaction method as described in chapter 3.2. were applied (Scheme 3.8).[89-91]

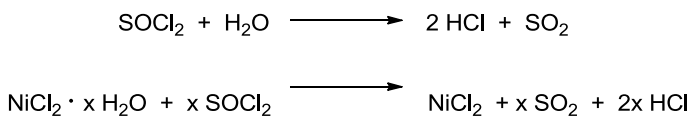

Scheme 3.8: Common reaction of thionyl chloride and water (top) and the drying of nickel chloride (bottom).[89-91]

In the synthesis with the dried aluminum chloride and the lithiated starting material very small crystals were obtained, which were not suitable for X-ray diffraction experiments. Another approach using magnesium chloride and $[(thf)_4Li_2(N\mathit{t}Bu)_4S]$ was executed. However, the colorless crystals from this reaction turned out to be *tert*butylammonium chloride. In the reaction with the dried nickel chloride, no crystals could be obtained. NMR experiments could not clarify which compounds were formed in solution.

In the synthesis of the transmetalation product with zinc chloride, colorless crystals were obtained after four days. Remarkably, the first heterobimetallic complex (**5**) of the tetrahedrally coordinated sulfur compound was synthesized (Scheme 3.9). Interestingly, only one $Zn(N(SiMe_3)_2)$ group is coordinated, while one lithium atom is still coordinated by the $S(N\mathit{t}Bu)_4^{2-}$ ligand. It might be assumed that the second exchange of the lithium cation with the zinc atom uses more equivalents of zinc chloride and lithium bis(trimethylsilyl)amide.

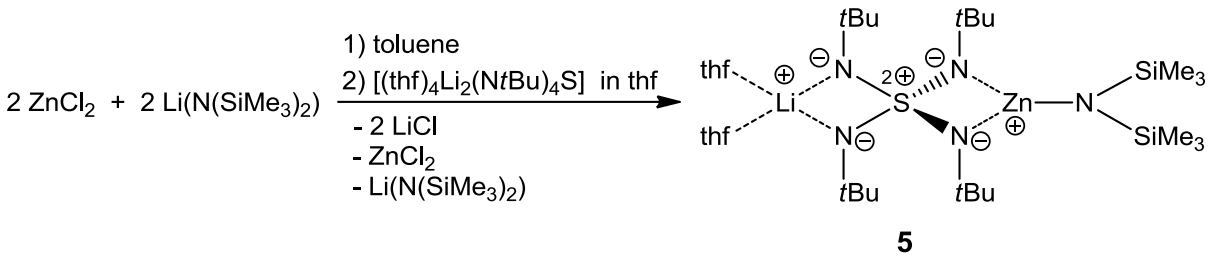

Scheme 3.9: Synthesis of $[(thf)_2Li(N(SiMe_3)_2)Zn(NtBu)_4S]$ (**5**).

The novel compound $[(thf)_2Li(N(SiMe_3)_2)Zn(NtBu)_4S]$ (**5**) crystallizes from THF/toluene at −24°C as colorless blocks, which were suitable for X-ray diffraction experiments. The compound crystallizes in the monoclinic space group $C2/c$ with half a molecule per asymmetric unit. At one side of the $S(NtBu)_4^{2-}$ ligand the zinc atom is coordinated, while the other side, the zinc atom is complexed in a trigonal planar fashion by the two nitrogen donor atoms of the ligand and an additional $N(SiMe_3)_2$ group. The tetrahedral coordination sphere around the lithium atom is formed by two THF donor molecules and the remaining two nitrogen atoms of the ligand, which is equal to the starting material with two equally coordinated lithium atoms (Figure 3.9).

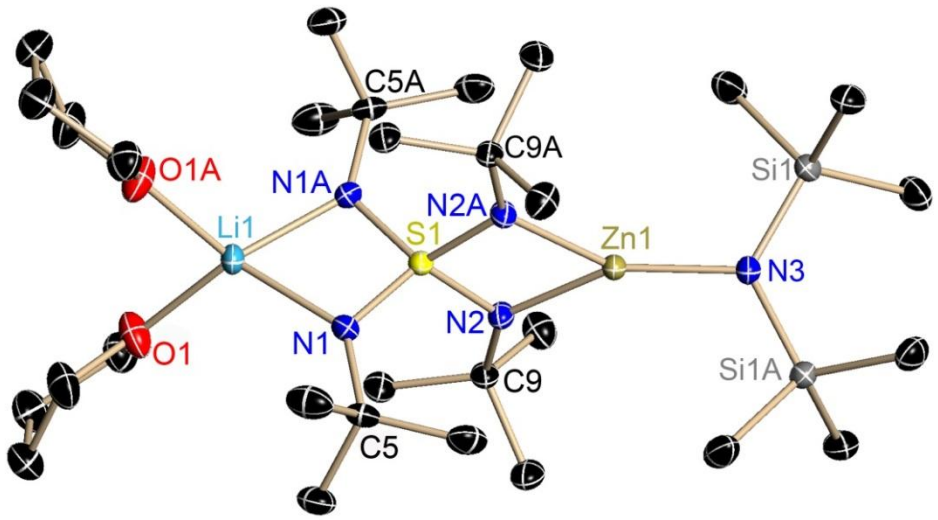

Figure 3.9: Crystal structure of $[(thf)_2Li(N(SiMe_3)_2)Zn(NtBu)_4S]$ (**5**). Hydrogen atoms are omitted for clarity. Thermal ellipsoids are at 50 % probability.

Complex **5** presents the second transition metal complex of the $S(NtBu)_4^{2-}$ ligand. Afore, only the cadmium compound[34] and main group metal complexes of this tetrahedral

sulfur-nitrogen ligand were known.[21, 22] Due to the presence of a transition metal, the bonding environment between the metal atom and the nitrogen atoms of the ligand slightly changes (Figure 3.10). While the lithium atom in the starting material **1** interacts with the sp^2-orbitals of the nitrogen atoms *via* its *s*-orbital, the zinc atom in complex **5** interacts *via* its *d*-orbital. Due to this, the bond length (S–N, M–N) and angles (N–S–N, N–M–N) may be different.

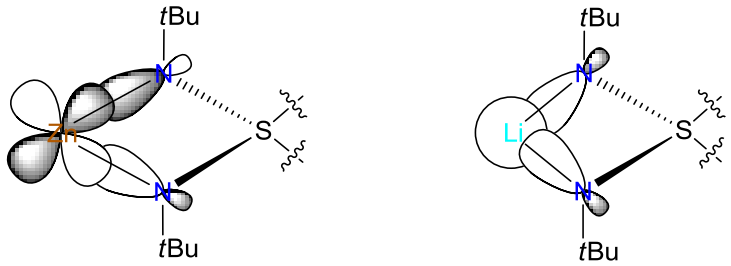

Figure 3.10: Assumed bonding situation in **5** of the zinc atom with the nitrogen atoms of the $S(NtBu)_4^{2-}$ ligand (left) and in **1** between the lithium atom and the nitrogen atoms of the $S(NtBu)_4^{2-}$ ligand (right). The non-bonding *p*-orbitals of the zinc- and nitrogen atoms are omitted for clarity.

The S1–N1 bond in **5** is 1.5668(15) Å and the S1–N2 bond is 1.6315(15) Å (Table 3.6). The four S–N bond distances sum up to 6.40 Å, which is similar to the S–N bond distances of the known compound $[\{(thf)_4Li\}_2\{I_4Cd_2(NtBu)_4S\}]$ (6.36 Å) and the starting material (**1**) (6.40 Å). Hence, the electropositive sulfur responds to the metal-polarized negative charge at the outside of the $[S(NR)_4]^{2-}$ tetrahedron. The assumption about the bonding environment *Stalke,*[66-69, 74] *Gatti*[74] and *Iversen*[74] *et al.* could be adopted to the complexes including a tetrahedrally coordinated $S(NtBu)_4^{2-}$. From constancy of the backbone $S(NtBu)_4^{2-}$ it may be concluded that the polarized S–N bonds are still present even though the change from main group metals to transition metals was carried out. In **5**, the S1–N1 bond (1.5668(15) Å) is a bit shorter than the S–N bond (1.601 Å) of the starting material (**1**).

The N2A–S1–N2 angle (91.31(11)°) is smaller than the N1A–S1–N1 angle (96.74(11)°) because the tetrahedral coordination sphere of the lithium atom widens the N1A–S1–N1 angle compared to the trigonal planar coordination sphere of the zinc atom. Furthermore, the bis(trimethylsilyl)imido group requires more space than the THF molecules leading to an increasing of the N2–Zn1 distance and a more acute N–S–N

angle. As expected, the angle N2A–Zn1–N2 (73.21(9)°) is a bit larger than N1A–Li1–N1 (72.26(16)°) as a result of the slightly larger ionic radius of Zn^{2+} (0.74 Å, Li^{+}: 0.73 Å)[88].

The Li–N distance is 1.986(4) Å which is typical for Li–N bonds. Published distances between a lithium ion, which is coordinated by two THF molecules and two nitrogen atoms, are on average 2.066 Å in the Cambridge Crystallographic Data Center (CCDC). The Zn–N(amide) distance is 1.880(2) Å which is only marginally shorter than the mean average of Zn–N(amide) bonds in the CCDC.

Table 3.6: Selected bond lengths and angles of **5**.

bond lengths/Å		*angles/°*	
Li1–N1	1.986(4)	N1–Li1–N1A	72.26(16)
N2–Zn1	1.9568(15)	N3–Zn1–N2	143.40(4)
N3–Zn1	1.880(2)	N2–Zn1–N2A	73.21(9)
N1–S1	1.5668(15)	N2A–S1–N2	91.31(11)
N2–S1	1.6315(15)	N1A–S1–N1	96.74(11)
N3–Si1	1.7126(11)	Si1–N3–Zn1	118.11(6)
Li1–O1	1.978(3)	O1–Li1–O1A	94.48(19)
		O1–Li1–N1	117.73(7)

Interestingly, both N–S–N planes are twisted in an angle of 89.8°, which is close to the ideal 90° for tetrahedral environment of the sulfur atom. The zinc atom as well as the lithium atom lay exactly in the N–S–N plane, by which a square planar coordination mode is formed. This results in a 180° angle between the cation and the N–S–N plane (Figure 3.11).

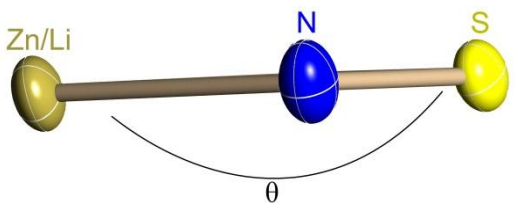

Figure 3.11: θ = 180°, angle between the N–S–N plane and the zinc/lithium atom in **5**.

NMR experiments in THF verify the presence of compound **5** in solution. A singlet at 1.30 ppm for the *tert*butyl- and trimethylsilyl groups and signals at 3.59–3.57 and 1.74–1.71 ppm for the THF molecules can be observed in the ^{1}H NMR spectrum. Whereas, the signal of the hydrogen atoms of the *tert*butyl groups in the starting material (**1**) is at 1.27 ppm. The ^{13}C NMR spectrum shows signals at 30.4 ppm for the carbon atoms of the methyl groups and at 57.6 ppm for the tertiary carbon of the *tert*butyl groups. The signals at 67.5 and 26.3 ppm belong to the THF molecules. Furthermore, the ^{15}N HMBC spectrum shows two signals at –355.7 ppm for the nitrogen atom of the (trimethylsilyl)amides and at –218.8 ppm for the nitrogen atoms of the *tert*butylimides.

In the reaction of iron chloride and the lithiated tetrakis(*tert*butyl)imidosulfate pale crystals were obtained, which could be characterized as the new, unprecedented transmetalation product [{(thf)$_3$Li}$_2$(FeCl)$_2$(N*t*Bu)$_4$S] (**6**) (Scheme 3.10). [{(thf)$_3$Li}$_2$-(FeCl)$_2$(N*t*Bu)$_4$S] (**6**) could be obtained as colorless crystals after one week at –24°C. The crystals are of monoclinic symmetry and crystallize in the space group $C2/c$ (Figure 3.12).

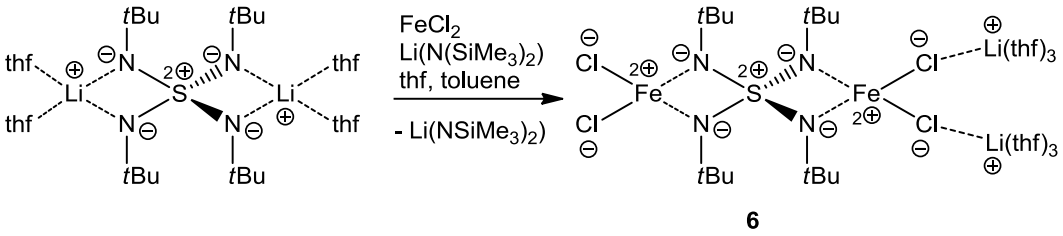

Scheme 3.10: Synthesis of [{(thf)$_3$Li}$_2$(FeCl)$_2$(N*t*Bu)$_4$S] (**6**).

It is remarkable that the expected reaction of $FeCl_2$ and Li-HMDS (HMDS = bis(trimethylsilyl)amine) did not occur. The Li-HMDS might not be take part in the reaction. The expected pre-coordination to the possible intermediate Cl-Fe-HMDS did not occur, which may be explained by the prospective instability of this intermediate. The coordination of $FeCl_2$ with the $S(NR)_4^{2-}$ ligand could be observed. Each iron atom is tetrahedrally coordinated by two nitrogen atoms of the sulfur-nitrogen ligand and by two chloride atoms. On one side of the ligand the chloride ions coordinate

and additional, a lithium atom, which is also in a distorted tetrahedral environment, consisted by three THF molecules.

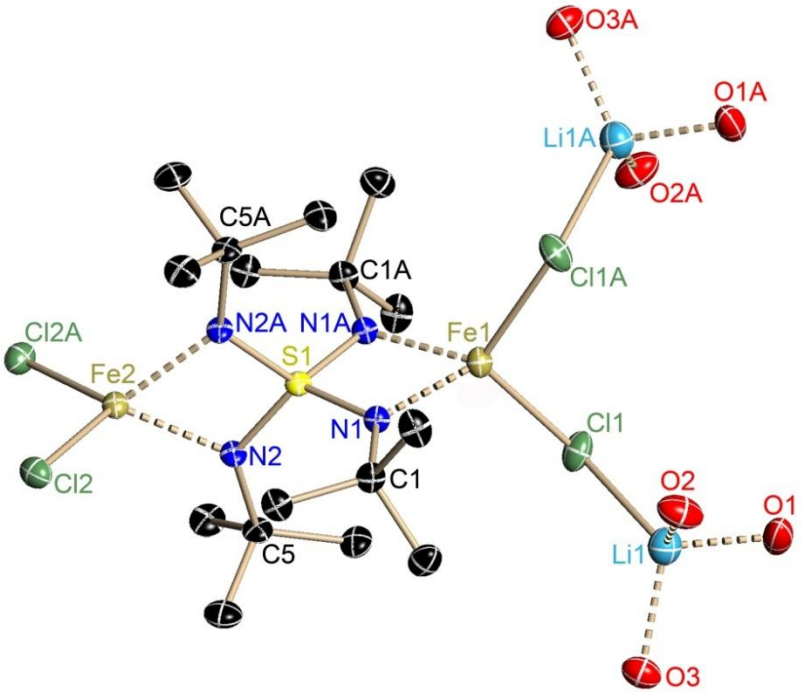

Figure 3.12: Crystal structure of [{(thf)$_3$Li}$_2$(FeCl)$_2$(N*t*Bu)$_4$S] (**6**). Hydrogen atoms and the carbon atoms of the THF molecules are omitted for clarity. Displacement ellipsoids are at 50 % probability.

This FeCl(Li(thf)$_3$) moiety is known but infrequent. The work group of *Siemeling*[92] reported the [(Me$_3$Si)$_2$N]$_2$Fe(μ-Cl)Li(thf)$_3$][92] and *Kays*[93] the [1,8-C$_{10}$H$_6$(NSi*i*Pr$_3$)$_2$Fe(μ-Cl)Li(thf)$_3$][93] compound, which show a similar coordination motive of this FeCl(Li(thf)$_3$) moiety. An iron atom is coordinated by a ligand and is bonded to a chloride. The lithium atom is coordinated tetrahedrally by this chloride and three THF molecules.

Selected bond lengths and angles of compound **6** are given in Table 3.7. The S–N-bond length of [{(thf)$_3$Li}$_2$(FeCl)$_2$(N*t*Bu)$_4$S] (**6**) amounts to averagely 1.595Å and the S–N bond lengths of the lithiated starting material (**1**), the [(thf)$_4$Ba$_2$\{N(SiMe$_3$)$_2$\}$_2$\{N*t*Bu)$_4$S\}], the [{(thf)$_4$Li}$_2$\{I$_4$Cd$_2$(N*t*Bu)$_4$S\}] as well as the heterobimetallic compound **5** amount between 1.587 Å and 1.593 Å. The S–N bond lengths vary only marginally between the different metal atoms (sum up to 6.38–6.40 Å). This indicates that the S(N*t*Bu)$_4^{2-}$ unit is similar in all complexes and does not dependent on the coordinated metal atom and

their oxidation state. As for the above described complexes, highly polarized S–N bonds are present.

Table 3.7: Selected bond lengths and angles of **6**.

bond lengths/Å		*angles/°*	
Fe1–N1	2.012(10)	N1A–Fe1–N1	70.1(5)
Fe2–N2	2.048(10)	N2–Fe2–N2A	68.8(5)
N1–S1	1.599(8)	N2–S1–N1	118.2(4)
N2–S1	1.590(7)	N1A–S1–N1	92.5(6)
Fe1–Cl1	2.305(10)	N2–S1–N2A	93.4(5)
Fe2–Cl2	2.285(13)	Cl1A–Fe1–Cl1	109.9(5)
Li1–Cl1	2.340(10)	Cl2A–Fe2–Cl2	108.9(6)
O1–Li1	1.907(12)	Fe1–Cl1–Li1	116.6(6)
O2–Li1	1.93(2)	O1–Li1–O2	107.5(5)
O3–Li1	1.931(10)	O1–Li1–O3	101.5(3)
		O2–Li1–O3	112.8(2)

In contrast to the Li–N bond length (1.95 Å)[21] of the starting material, the Cd–N bond length (2.22 Å)[34] of the cadmium iodide coordinated ligand and the Ba–N bond length (2.67 Å)[21] of $[(thf)_4Ba_2\{N(SiMe_3)_2\}_2\{N\textit{t}Bu)_4S\}]$, the Fe–N distance (2.03 Å) of compound **6** is shorter than the Ba–N and Cd–N distances and longer than the Li–N bond length. This corresponds to the ionic radii of the lithium-, iron-, cadmium- and barium cations (Li^+: 0.73 Å, Fe^{2+}: 0.77 Å, Cd^{2+}: 0.92 Å, Ba^{2+}: 1.35 Å)[88]. The tendency shows that the metal-nitrogen bond length is shorter for smaller metal atoms than for bigger metal atoms.

The Fe1–Cl1 distance (2.31 Å) is a little longer than the Fe2–Cl2 distance (2.29 Å). This is explicable by the coordination of the Cl1 atom to the Li1 atom, whereby the iron-chloride bond is weakened. In contrast to the Fe–Cl bond length in iron(II) chloride (2.22 Å)[94] the Fe–Cl bond length (2.30 Å) in **6** is 0.08 Å longer, which might be due to the π-donor interaction of the nitrogen atom which bonds to the iron atom.

Generally, a tendency of the bond lengths and angles can be observed. If the metal atom is bigger, the metal-nitrogen bond length is longer than in complexes with smaller metal

atoms. The N–S–N angle with a bigger η^2-bridged metal atom is wider and the N–M–N angle is smaller than in smaller metal atom coordinated compounds (Figure 3.13).

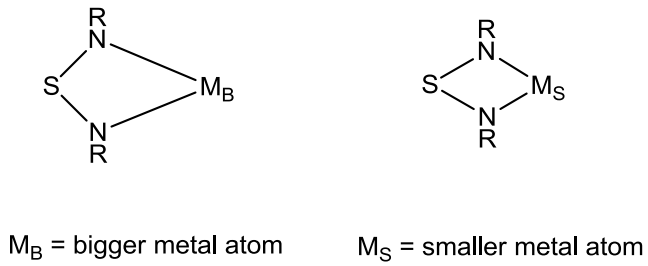

Figure 3.13: General tendency of the bond length and angles in metalated sulfur-nitrogen compounds.

The tendency of the angle between the N–S–N plane in $[(thf)_4Ba_2\{N(SiMe_3)_2\}_2\{N\textit{t}Bu)_4S\}]$ (96.26°), $[\{(thf)_4Li\}_2\{I_4Cd_2(N\textit{t}Bu)_4S\}]$ (95.40°), **6** (92.95°) and **1** (94.70°), which coordinate a metal atom, follows the same tendency as the S–N distance. This means, that the complexes with a smaller metal atom have a smaller N–S–N angle. However, the N–S–N angle of **6** is smaller than the angle in compound **1**, even though the ionic radius of the lithium atom is smaller than the ionic radius of the iron atom. This deviation from the normal tendency might originate from the geometrical difference of the *s*-, *p*- and *d*-orbitals. In **1**, only the *s*-orbitals of the lithium atom take part in the lithium-nitrogen bond, while in **6** the *p*- and *d*-orbitals of the iron atom could be involved additively. Furthermore, the charge of the atoms influences the angle; while the lithium atom is only in the oxidation state +I, the iron atom is +II, which may be why the N–S–N angle is bigger in **1** than in **6**.

The angle between the iron atoms and the N–S–N plane is exactly 180° so that the iron atom is located directly in this plane and hence, a planar coordination mode is formed. (Figure 3.14).

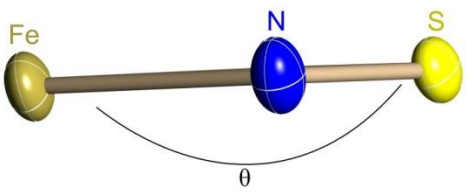

Figure 3.14: θ = 180°, angle between the N–S–N plane and the iron atom in **6**.

As can be decided from the crystal structure, both iron atoms in compound **6** are present in the oxidation state +II, which could be proven by Mößbauer experiments. The Mößbauer spectrum of **6** is shown in Figure 3.15.

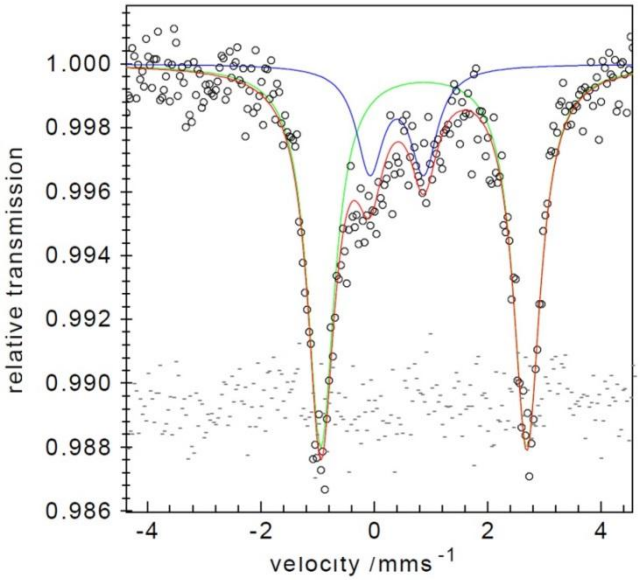

Figure 3.15: Mößbauer spectrum of [{(thf)$_3$Li}$_2$(FeCl)$_2$(N*t*Bu)$_4$S] (**6**). Green: Fe(II) high spin; Blue: Fe(III) high spin; Red: Fe(II) and Fe(III) high spin.

In the sample, the iron(II) high spin (green) is present in 78.47 % and the iron(III) high spin (blue) in 21.53 %. This implies that some iron(III) chloride is in the sample but the main species is the iron(II) in the complex. The middle, $\delta_{exp}/(mm/s)$, the quadrupole splitting, $|\Delta E_a|/(mm/s)$ and the full width at half maximum, $\Gamma_{FWHM}/(mm/s)$ are given in Table 3.8. An shift at 0.88 mm/s is consistent with high spin iron(II) and at 0.40 mm/s with high spin iron(III). Both values are in the same range as observed compounds with high spin iron(II/III).[95-104] The quadrupole splitting of 3.63 mm/s and 0.95 mm/s is also in the observed range of high spin iron(II) and the high spin iron(III) complexes.[95-104]

Table 3.8: Values of the magnetic measurement; c = correlated.

	Fe(II)	*Fe(III)*
$\delta_{exp}/(mm/s)$	0.88	0.40
$\|\Delta E_a\|/(mm/s)$	3.63	0.95
$\Gamma_{FWHM}/(mm/s)$	0.58	0.58 c

The iron(II) high spin species is congruent with the crystal structure. Both iron cations are presente in the oxidation state +II. The iron(III) high spin could not be in this complex because no iron cation with the oxidation state +I was found in the Mößbauer spectrum. If one iron(III) atom is presented, the second iron atom must be +I to counterpoise the negative charge of the sulfur-nitrogen ligand and the chloride ions. Maybe, a part of the sample had decomposed prior to the Mößbauer experiment to iron(III) chloride, which may be explained the presence of the iron(III) high spin.

Furthermore, ^{1}H, ^{13}C and ^{7}Li NMR experiments could confirm that compound **6** was formed in solution. In the ^{1}H NMR spectrum, a signal at 1.31 ppm shows the methyl groups, which are shifted from the starting material signal at 1.27 ppm. The signals of the protons of the THF molecules are at 3.42–3.68 ppm and 1.64–1.83 ppm. In the ^{7}Li NMR spectrum, a signal at 3.5 ppm shows both lithium ions. In the ^{13}C NMR spectrum, signals can be found of the THF molecules at 67.4 ppm and at 25.3 ppm and of the *tert*butyl groups at 29.8 ppm.

Compound **6** closely resembles the known complex $[\{(thf)_4Li\}_2\{I_4Cd_2(NtBu)_4S\}]$ (Figure 3.16). In both reactions a salt elimination did not occur, which indicates, that the syntheses of the other possible product was not achieved. It is well known that $Fe\{N(SiMe_3)_2\}_2$, which was used to form complex **6**, is very unstable. The formed complex stabilizes the iron(II) chloride by coordination of the $S(NtBu)_4^{2-}$ unit.

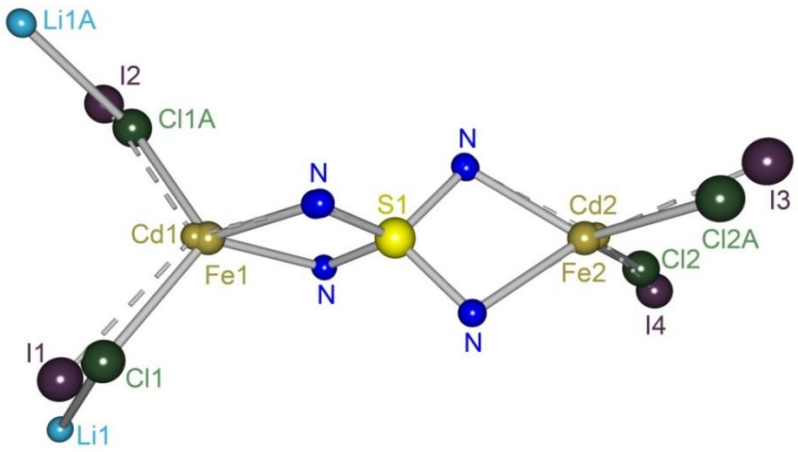

Figure 3.16: Overlay plot of **6** and $[\{(thf)_4Li\}_2\{I_4Cd_2(NtBu)_4S\}]$. The atoms S1, N1 and N2 are projected onto each other with a deviation of 0.0117 Å.

The important difference between these compounds is that in **6** the co-coordinated cation species is directly bonded to the chloride atom and in the cadmium compound the lithium atom is not bonded to the ligand but coordinated by four THF molecules. In both compounds the lithium atoms are tetrahedrally coordinated. In Figure 3.16 it is shown that the two complexes are very similar in their coordination motive. As expected, the M–X bond length (M = metal atom, X = halide) of **6** is a little bit shorter than in the cadmium compound, due to the smaller size of the halide. In contrast to the iron atom, the cadmium atom is not exactly in the N–S–N plane. The angle between this plane and the cadmium atom amounts to 178.73° and the distance between the plane and the cation amounts to 0.042 Å. This small deviation may be caused by the bigger cation radius of the cadmium atom.

Literature known compounds[105, 106] with a coordinated iron atom in a similar coordination sphere are utilized for N_2 and O_2 activation, this might also be possible for complex **6**, which resembles the catalytically most promising Fe(II)–Cl···alkali metal bridge for these activations (Figure 3.17).

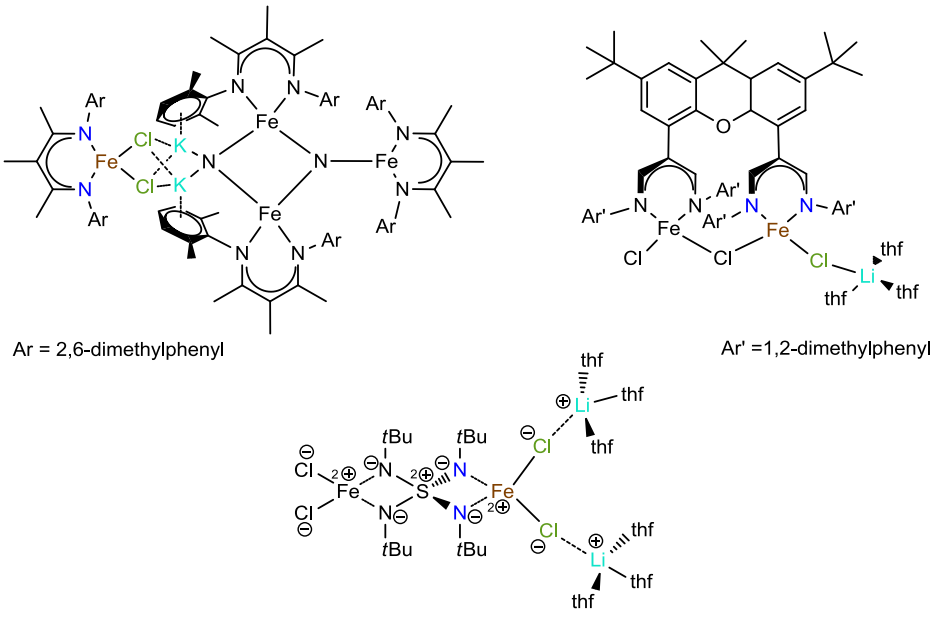

Figure 3.17: Top: Known Fe(II)–Cl···alkali metal complexes, reported by *Holland et al.*[105] (left) and by *Limberg et al.*[106] (right). Bottom: Complex **6**.

Holland et al. published the iron chloride complex $[MeC[C(Me)N(2,6\text{-}Me_2C_6H_3)]_2Fe(\mu\text{–}Cl)]_2$, which was induced with potassium and nitrogen to obtain the catalytically active complex.[105] With an excess of H_2 the protonated iron complex and ammonia could be synthesized.[105] *Limberg et al.* synthesized an iron metalated complex $[(Me_2C_6H_3)Fe_2Cl_3(Li(thf)_3)]$, which reacted with half an equivalent of O_2 to the Fe(III)···O···Fe(III) containing compound.[106] Based on the resemblances in the coordination sphere of the iron atom similar reactivity might be observed for **6**.

3.3. Metal bis(trimethylsilyl)amide

Stalke et. al. succeeded in synthesizing the first transmetalation product of the lithiated tetrakis(*tert*butyl)imidosulfate (**1**).[21] Barium bis{bis(trimethylsilyl)amide} and *tert*butylammonium chloride were reacted to $[(thf)_4Ba_2\{N(SiMe_3)_2\}_2\{(N\mathit{t}Bu)_4S\}]$. The same conditions as described by *Stalke et al.* were utilized for the following syntheses (Scheme 3.11).[21]

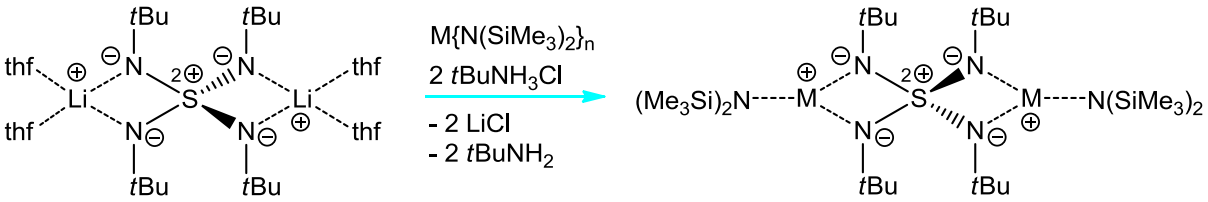

Scheme 3.11: Potential reaction pathway of metal chlorides with $M\{N(SiMe_3)_2\}_n$, $\mathit{t}BuNH_3Cl$ and $[(thf)_4Li_2(N\mathit{t}Bu)_4S]$.

To a mixture of $[(thf)_4Li_2(N\mathit{t}Bu)_4S]$ and $\mathit{t}BuNH_3Cl$ THF was added. After the solvent was removed *in vacuo*, the solid was resolved in pentane and lithium chloride was filtrated off. Afterwards, metal bis(trimethylsilyl)amide in THF was added. After the resulting solid was removed by filtration and the solvent *in vacuo*, heptane was added.

In the reactions with M-HMDS (M = Rb (I), Sn (II), Cu(II), Fe(II), Co (II)) microcrystals were obtained, which were not suitable for X-ray structure analysis. Recrystallization did not yield a better result. NMR experiments show several signals, which could not be identified. The metal bis(trimethylsilyl)amides were dried before syntheses but the desired products could not be synthesized by this approach.

3.4. Metal acetylacetonates

Another method to synthesize transmetalation products is the utilization of metal acetylacetonates ($M(acac)_n$). These ligands can be integrated into the N–S–N sphere to stabilize the $S(NtBu)_4^{2-}$ anion. Thereby, to the mixture of $[(thf)_4Li_2(NtBu)_4S]$ and metal acetylacetonate THF was added at rt. After stirring over night, the resulting lithium chloride was filtrated and the solution was layered with pentane (Scheme 3.12). Before the reaction the metal acetylacetonates were dried *in vacuo* and additional heat.

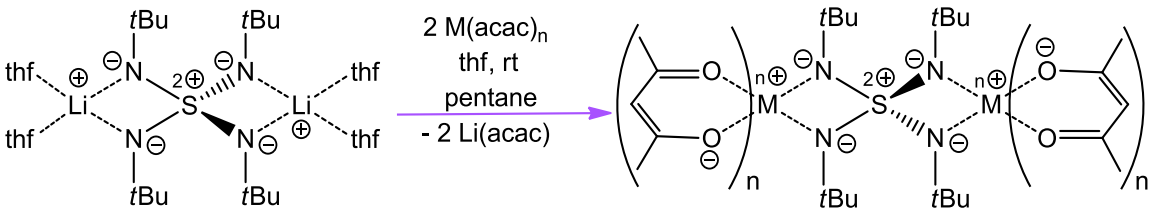

Scheme 3.12: Reaction of $[(thf)_4Li_2(NtBu)_4S]$ with $M(acac)_n$.

From the thus obtained reaction mixture of lithiated S–N ligand and manganese(II) acetylacetonate lithium bromide with coordinated THF molecules could be extracted and characterized by X-ray analysis (Table 3.9). After filtration and removing half of the solvent, NMR experiments show many signals, which could not be assigned to the desired product.

Table 3.9: Applied metal acetylacetonates and their results.

metal halides	*solution color*	*results*
$Ni(acac)_2$	violet	$Li_4(acac)_4(thf)$
$Cu(acac)_2$	green	$[(acac)_2Cu_2(NtBu)_4S]$
$VO(acac)_2$	brown	powder
$Mn(acac)_2$	yellow	LiBr·thf
$Pd(acac)_2$	yellow	$[(acac)Pd(NtBu)_2$ $(N(H)tBu)SO]$
$Fe(acac)_3$	brown	powder
$Mn(acac)_3$	brown	powder
$Co(acac)_3$	green	$Co(acac)_3$
$TiO(acac)_4$	orange	powder

From the reaction of $Co(acac)_3$ and $[(thf)_4Li_2(NtBu)_4S]$ only the starting material cobalt acetylacetonate was crystallized. While colorless crystals were formed in the reaction with $VO(acac)_2$. These crystals were not suitable for X-ray analysis. NMR experiments could not clarify which compounds were formed. In the reaction with manganese(III)-, iron(III)- and titanium(IV) acetylacetonates, powder could be obtained, which was not suitable for X-ray analysis. NMR experiments were inconclusive.

In the reaction of nickel acetylacetonate and $[(thf)_4Li_2(NtBu)_4S]$ (**1**), an unexpected product was obtained. Interestingly, after crystallization the coordination of the nickel atom and the sulfur-nitrogen ligand was not observed by X-ray analysis. Instead an unknown product **7** was found, which features three differently coordinated lithium environments (Figure 3.18).

$Li_4(acac)_4(thf)$ (**7**) crystallizes in the monoclinic space group $P2_1/n$ with one molecule in the asymmetric unit. One lithium atom (Li1) is nearly square planarly coordinated by two acetylacetonate groups (O1, O2, O3, O4), another lithium atom (Li2) by four oxygen atoms of different acetylacetonate groups (O2, O4, O5, O7) and the third lithium atom (Li3) has a fivefold coordination by two acetylacetonate groups (O5, O6, O7, O8, O9) and a THF molecule. The fourth lithium atom (Li4) is coordinated by two acetylacetonates of one asymmetric unit (O6, O8) and by two other acetylacetonates of the next unit. A lithium atom, which is coordinated by five atoms, is literature known.

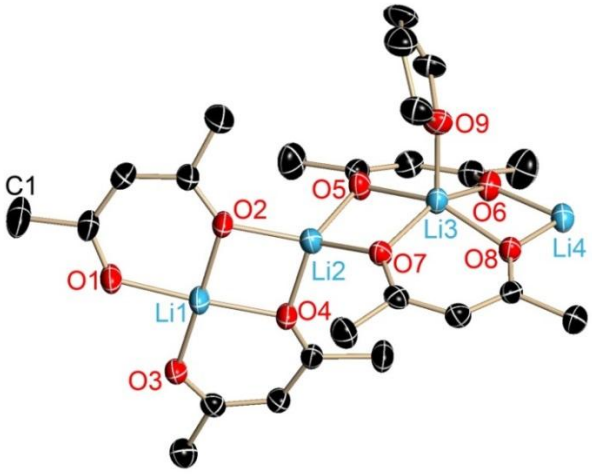

Figure 3.18: Crystal structure of $Li_4(acac)_4(thf)$ (**7**). Hydrogen atoms are omitted for clarity. Displacement ellipsoids are at 50 % probability.

A few complexes are similarly coordinated by five oxygen atoms, in which the Li–O bond length is around 2.000 Å.[107-113] In **7** the Li–O bond length is 2.000 Å on average for lithium atom (Li3), which concurs with the published length. In the packing model, this $Li_4(acac)_4(thf)$ fragment forms a coordination polymer chain of continually repeated fragments (Figure 3.19).

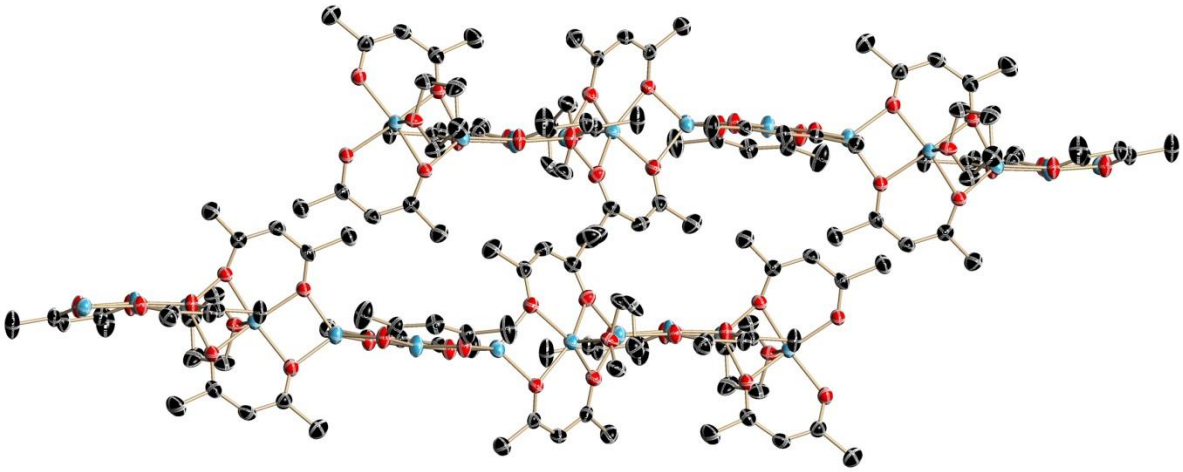

Figure 3.19: Packing model of $Li_4(acac)_4(thf)$ (**7**). Hydrogen atoms are omitted for clarity. Displacement ellipsoids are at 50 % probability.

With the confirmation that the lithium acetylacetonate was formed, the assumption can be made that the synthesis of $Ni(acac)_2$ and **1** resulted in the formation of a sulfur-nitrogen complex with a coordinated nickel atom, $[(thf)_4Ni_2(N\textit{t}Bu)_4S]$. Alas, ^{1}H, ^{13}C and ^{15}N NMR experiments could not clarify this suggestion. The ^{1}H NMR shows a signal at 1.30 ppm, which could be the shifted protons of the *tert*butyl groups. A signal at 5.03 ppm indicates that the CH-group of the acetylacetonate was in the sample, but neither the other signals nor the integrals fit the expected spectrum of the desired product (Figure 3.20). In the ^{15}N NMR spectrum only one signal at –135.4 ppm is present confirming only one type of nitrogen atoms being in the compound. However, it does not prove that the desired product was synthesized.

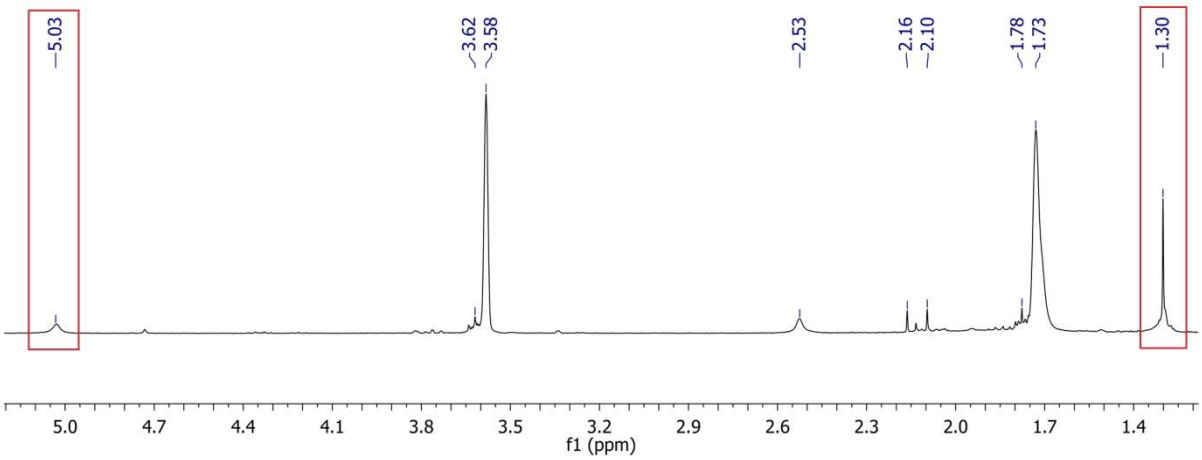

Figure 3.20: ^{1}H NMR spectrum (measured in d_8-THF) of the reaction mixture of Ni(acac)$_2$ and [(thf)$_4$Ni$_2$(N*t*Bu)$_4$S] (**1**).

However, the addition of the lithiated S–N ligand (**1**) to copper(II) acetylacetonate led to formation of a new stable metalated compound of the S(N*t*Bu)$_4^{2-}$ ligand (Scheme 3.13). The resulting complex [(acac)$_2$Cu$_2$(N*t*Bu)$_4$S] (**8**) was obtained after one week in THF, without layered pentane, at –24°C as colorless blocks suitable for X-ray structure determination.

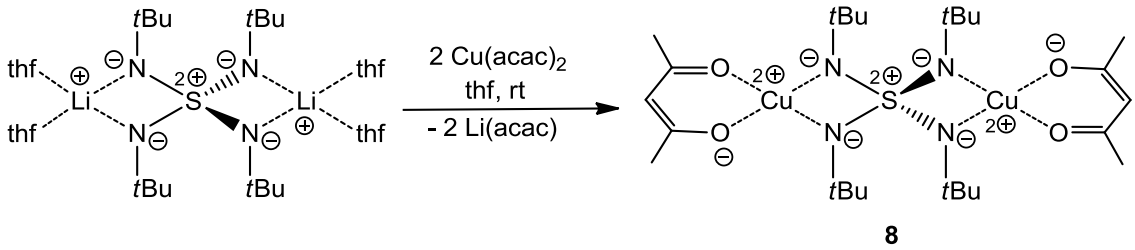

8

Scheme 3.13: Synthesis of [(acac)$_2$Cu$_2$(N*t*Bu)$_4$S] (**8**).

8 crystallizes in the monoclinic space group *P*2/*n* with one molecule in the asymmetric unit (Figure 3.21). Each copper(II) atom is nearly square planarly coordinated by the two oxygen atoms of the planar chelating acetylacetonate anion and by two nitrogen atoms at opposite sides of the [S(N*t*Bu)$_4$]$^{2-}$ tetrahedron (O1–Cu1–N1: 169.80°, O2–Cu1–N2: 169.33°).

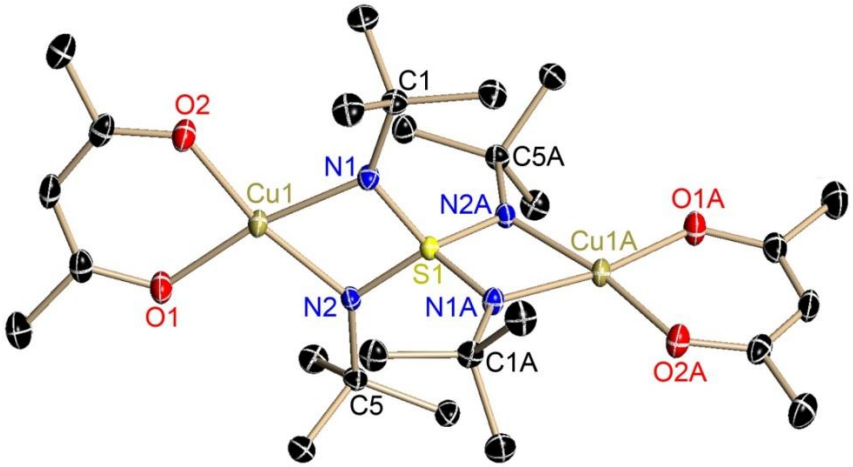

Figure 3.21: Crystal structure of $[(acac)_2Cu_2(NtBu)_4S]$ (**8**). The hydrogen atoms are omitted for clarity. Displacement ellipsoids are at 50 % probability.

The copper(II) cation is a d^9 metal with one single occupied *d* orbital. Complexes with copper(II) atoms have octahedral or tetrahedral geometries and are well known to be *Jahn-Teller* active.[114] The *Jahn-Teller* splitting in the tetrahedral coordination of the t_2 orbitals is reflected in the bond length and angles of the complexes.[115-117] The *d*-orbitals are shifted from the energy level of the tetrahedral ligand field, T_d, to the compressed tetrahedrally ligand field, D_{2d}.[117] Thereby, the d_{z^2}, d_{xz} and d_{yz} orbitals are stabilized and the $d_{y^2\text{-}z^2}$ and d_{xy} orbitals of the metal atom are destabilized (Figure 3.22).[117] Due to the steric and electronic repulsion of the metal atom and the ligand, the square planar geometry, D_{4h}, could not be finally formed.[116, 117]

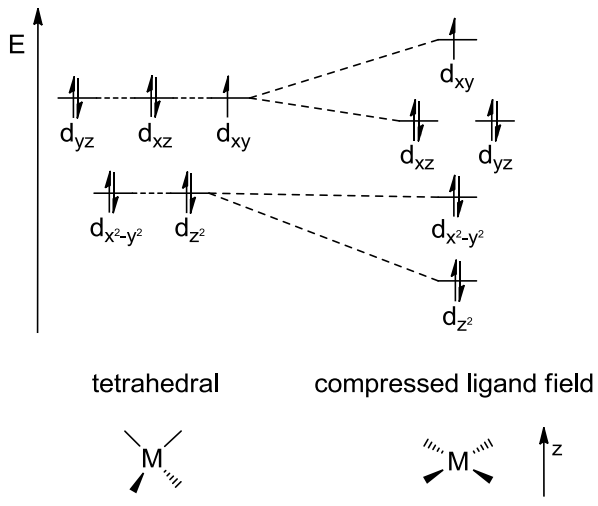

Figure 3.22: Splitting of the *d* energy levels in the tetrahedrally compressed ligand field. The energy level splitting is not true to scale.

This square planar environment of the copper atom differs considerably from the nearly tetrahedral N_2O_2-coordination of the lithiated starting material (**1**) (Figure 3.23). The two crystallographically independent S–N bond lengths in **8** (1.59 Å averagely and sum up to 6.34 Å) do not differ significantly from the S–N bond lengths in **1** (1.60 Å). Due to the similar bond lengths in **1** and **8** a distribution of the negative charges over the four nitrogen atoms of the $S(NR)_4^{2-}$ ligand can be assumed. The S–N bonds can also be described as polarized bonds with a mostly covalent and an ionic part, whereof the shorter bond results.

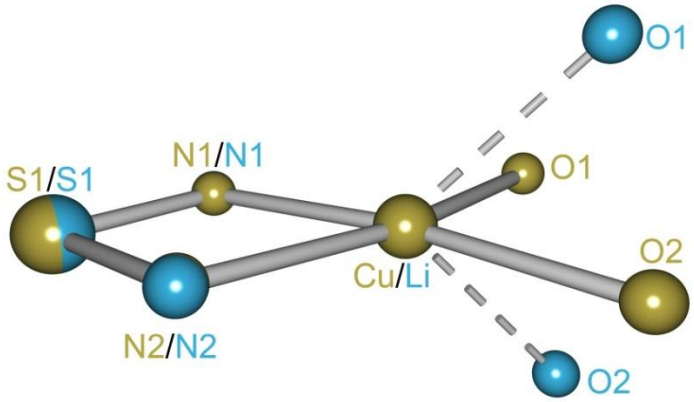

Figure 3.23: Superposition plot of **1** (Li) and **8** (Cu). The atoms S1, N1 and N2 are projected onto each other with a deviation of 0.0161 Å.

Furthermore, the average N–M distances (**8**: 1.958 Å, **1**: 1.957(6) Å) and the angles of N–M–N (**8**: 72.30(6)°, **1**: 73.95°) and N2–S1–N1 (**8**: 93.47(7)°, **1**: 94.70(1)°), which enclose the metal cation, are comparable (Table 3.13). This can be explained by the similar cationic radii of Cu(II) and Li(I) (Cu^{2+}: 0.71 Å, Li^{+}: 0.73 Å).[88] In published complexes with coordinated metal acetylacetonate at the nitrogen atom the N–M distances are 2.17 Å on average but the $Cu(acac)^{+}$ cation in a fourfold coordination sphere adopts N–M distances of 1.96 Å,[118] which is in excellent agreement with the corresponding bonds in **8** (Table 3.10).

Table 3.10: Selected bond lengths and angles of **8**.

bond lengths/Å		*angles/°*	
N1–Cu1	1.9599(14)	N2–Cu1 –N1	72.30(6)
N2–Cu1	1.9556(14)	N2A–S1–N2	117.72(11)
N1–S1	1.5868(14)	N2A–S1–N1	118.14(7)
N2–S1	1.5850(14)	N2–S1–N1	93.47(7)
O1–Cu1	1.9251(12)	N1–S1–N1A	118.06(11)
O2–Cu1	1.9207(13)	O2–Cu1–O1	92.56(5)

The angle between the copper atoms and the N–S–N plane is nearly 180° and the distance from the copper atom to the corresponding plane amounts to 0.0066 Å so that the copper atom is directly in this plane and hence, a planar coordination mode is formed (Figure 3.19). The N–S–N planes are twisted by 89.8° to give the maximum possible space between the *tert*butylimido groups.

The ^{1}H NMR experiment proves that compound **8** could be successfully synthesized. A signal at 3.88 ppm was identified as belonging to the methyl groups of the acetylacetonate, the signal at –16.74 ppm presents the CH group of the acac-unit and the singlet at 5.72 ppm the methyl groups of the *tert*butylimides. Also the EI-MS experiment confirms displaying a signal at 640 m/z the presence of this novel copper complex [(acac)$_2$Cu$_2$(N*t*Bu)$_4$S] as well.

Furthermore, the reaction of palladium acetylacetonate with [(thf)$_4$Li$_2$(N*t*Bu)$_4$S] was realized. Thereby, the hydrolyzed product [(acac)Pd(N*t*Bu)$_2$(N(H)*t*Bu)SO] (**9**) was synthesized. Possibly, the palladium acetylacetonate was not dried enough, so that impurities of water could react with the substances in the synthesis. In a following reaction with dried palladium acetylacetonate but addition of water, the same product could be obtained (Scheme 3.14). After Pd(acac)$_2$ was dried again, no crystals could be obtained in the reaction of palladium acetylacetonate and the lithiated starting material (**1**). NMR experiments of the solution could not confirm formation of the desired product [(acac)$_2$Pd$_2$(N*t*Bu)$_4$S].

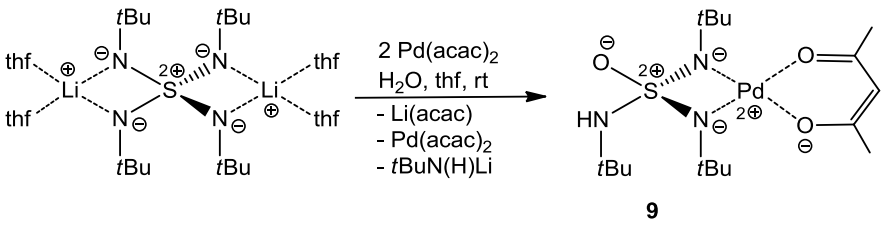

Scheme 3.14: Synthesis of [(acac)Pd(N*t*Bu)$_2$(N(H)*t*Bu)SO] (**9**) in the presence of water.

Crystals of [(acac)Pd(N*t*Bu)$_2$(N(H)*t*Bu)SO] were obtained as yellow-orange blocks after storing a THF/water suspension of **9** at –24°C for four weeks. The crystals were suitable for X-ray structure analysis. The compound crystallizes in the monoclinic space group $P2_1/c$ with one molecule in the asymmetric unit (Figure 3.24).

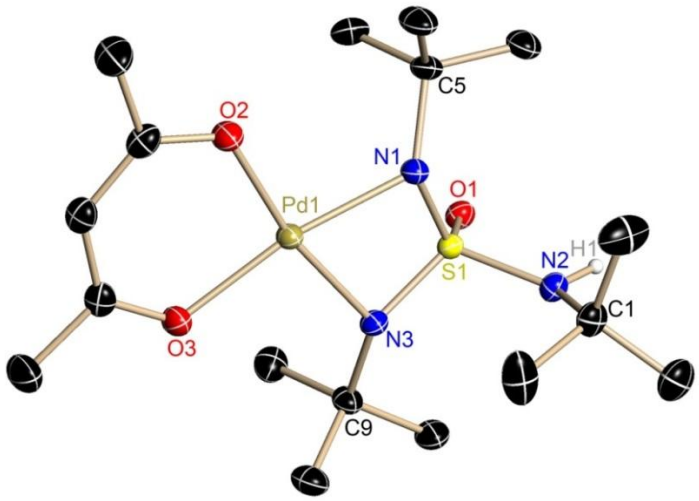

Figure 3.24: Crystal structure of [(acac)Pd(N*t*Bu)$_2$(N(H)*t*Bu)SO] (**9**). Hydrogen atoms H1 was found in the Fourier difference map. The other hydrogen atoms are omitted for clarity. Displacement ellipsoids are at 50 % probability.

In this complex the sulfur atom is nearly in a tetrahedral environment formed by one oxygen atom and three *tert*butylimido groups, which one protonated nitrogen atom and the two nitrogen atoms of the S(N*t*Bu)$_4^{2-}$ ligand coordinating a palladium atom, which is coordinated square planarly by two nitrogen atoms and two oxygen atoms of an acetylacetonate. As expected, the S–N bonds of **9** are 1.5842 Å on average and compared to all other sulfur-nitrogen complexes (Table 3.11). The three S–N and the S–O bond distances sum up to 6.24 Å, which is in the same range as **3** (6.24 Å) and **4** (6.23 Å). In

contrast, the metal-nitrogen bond in **9** is 2.0275 Å on average, which is longer than the M–N bonds in compound [Cu{(N*t*Bu)$_2$(N(H)*t*Bu)SO}$_2$] (**3**) (2.0160 Å) and [Zn{(N*t*Bu)$_2$-(N(H)*t*Bu)SO}$_2$] (**4**) (2.01875 Å). Complex **9** encourages the assumption made in chapter 3.2. (Page 42, Figure 3.13) that larger metal atoms form longer M–N bonds than smaller metal atoms.

Table 3.11: Selected bond lengths and angles of **9**.

bond lengths/Å		*angles/°*	
Pd1–N1	2.0316(19)	N3–Pd1–N1	70.82(7)
Pd1–N3	2.0233(18)	N3–S1–N1	95.72(9)
S1–N1	1.5951(19)	N3–S1–N2	109.57(11)
S1–N2	1.6165(19)	O1–S1–N1	117.72(10)
S1–N3	1.5733(19)	O1–S1–N2	102.73(10)
S1–O1	1.4535(16)	O1–S1–N3	118.51(10)
Pd1–O3	2.0155(16)	O3–Pd1–O2	91.55(6)
Pd1–O2	2.0174(16)		

Moreover, the N–Pd–N angle (70.82(7)°) is smaller than the N–M–N in **3** and **4** (M: Cu = 72.20° on average, Zn = 71.52(7)°) angle confirming the thesis that larger metal atoms form more acute N–M–N angles. Only the N–S–N angles in compounds **3**, **4** and **9** contradict the thesis described in Figure 3.13. In **9**, the N3–S1–N1 angle which encloses the metal atom is 95.72(9)°and hence, the smallest angle in compared to **4** (97.10(10)°) and **3** (97.90(11)°).

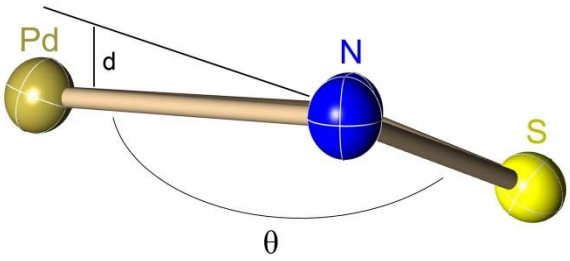

Figure 3.25: θ = 162.61°, angle between the N–S–N plane and the palladium atom and d = 0.4938(33) Å, distance between the palladium atom and the N–S–N plane.

In contrast to **3** and **4** the distance between the palladium atom and the N–S–N plane is 0.4938 Å. This is in the same range as **4** so that the assumption is given that bigger metal atoms move out of the plane because of their size. The angle between the N–S–N square and the palladium cation amounts to 162.61° (Figure 3.25).

Similar to compounds **3** and **4**, in [(acac)Pd(N*t*Bu)$_2$(N(H)*t*Bu)SO] an interaction between the hydrogen atom of the amino group and the oxygen atom of the next adjacent unit is observed. The distance between these atoms (O···H) amounts to 2.133 Å, which could be described as a strong donor-acceptor interaction.[87] By this interaction, one [(acac)Pd(N*t*Bu)$_2$(N(H)*t*Bu)SO] coordinates to a second complex of the next asymmetric unit.

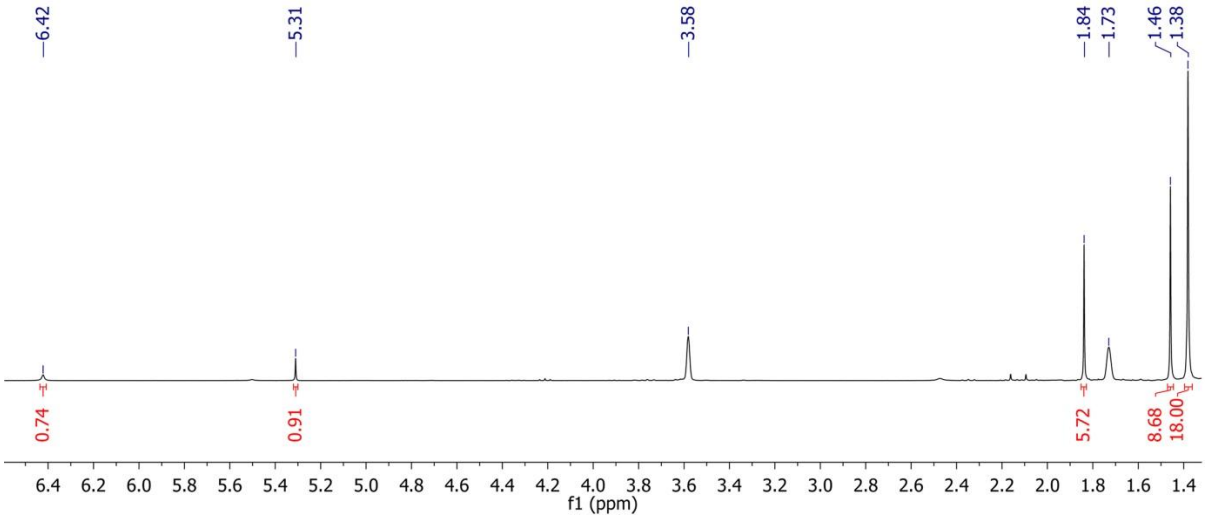

Figure 3.26: ^{1}H NMR spectrum (measured in d_8-THF) of [(acac)Pd(N*t*Bu)$_2$(N(H)*t*Bu)SO] (**9**).

In the ^{1}H, ^{13}C and ^{15}N NMR experiments it could be verified that complex **9** could be obtained in solution (Figure 3.26). A singlet at 6.42 ppm in the ^{1}H NMR spectrum coupling to a signal at –246.4 ppm in the ^{15}N HMBC spectrum was identified as the hydrogen atom of the protonated amino group. The *tert*butyl group forms a singlet at 1.46 ppm in the ^{1}H NMR spectrum which corresponds to the signal at 30.7 ppm in the ^{13}C NMR spectrum. The signals at 1.38 ppm in the ^{1}H NMR, at 31.3 ppm in the ^{13}C NMR and at –312.5 ppm in the ^{15}N HMBC spectrum were identified to belong to the other *tert*buylimido groups. The remaining signals were shown the acetylacetonate moiety.

3.5. Metal chlorides and Lithium acetylacetonate

This part is about the fact that metal chlorides should react with $[(thf)_4Li_2(NtBu)_4S]$ to give transmetalation product, in which metal atom is coordinated by metal chlorides. Addition of lithium acetylacetonate was added to the so-obtained complex resulting in the probably more stable product, which coordinated the metal acetylacetonate (Scheme 3.15).

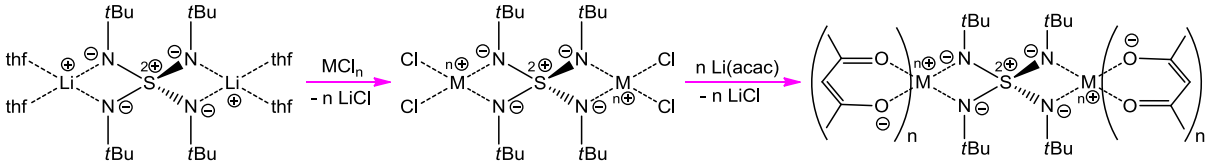

Scheme 3.15: Reaction path of $[(thf)_4Li_2(NtBu)_4S]$ with metal chloride and subsequent addition of lithium acetylacetonate.

A mixture of $[(thf)_4Li_2(NtBu)_4S]$ and dried metal chlorides was dissolved in THF and stirred over night at rt. After removal of the resulting solid by filtration, the reaction mixture was added to lithium acetylacetonate and stirred a few hours. Again, the solid was filtrated, half of the solvent was removed *in vacuo* and the resulting solution stored at –24°C. The applied metal chlorides and their results are summarized in Table 3.12.

Table 3.12: Used metal chlorides and their reaction products.

metal halides	*solution color*	*results*
$ZnCl_2$	yellow	powder
$CuCl_2$	green	powder
$FeCl_2$	brown	$tBuNH_3Cl$
$MnCl_2$	brown	powder
$NiCl_2$	yellow	powder
$CoCl_2$	brown	$tBuNH_3Cl$
$InCl_3$	yellow	$tBuNH_3Cl$
$CrCl_3$	green	$tBuNH_3Cl$
$GaCl_4$	brown	$tBuNH_3Cl$

Either *tert*butylammonium chloride or powder, which was not suitable for single crystal X-ray structure analysis, was obtained.

A possible explanation might be that the first step of this reaction did not work because ^{1}H, ^{13}C and ^{15}N NMR experiments were performed in order to trap the intermediate but gave only the signal of the *tert*butyl groups, which is no significantly shifted from the starting material.

3.6. Metal hydride and metal alkyls

In my diploma thesis,[34] several experiments with metal hydrides and S(N*t*Bu)$_3$ were carried out. These syntheses base on the work of *Stalke et al.*,[3] in which the metal hydride and the starting material were refluxed few hours. The metalated product should be obtained after filtration and crystallization from hexane. The reaction of S(N*t*Bu)$_3$ and MH$_n$ did not result in the desired product. Crystals could not be obtained; also NMR experiments could not clarify which compounds were formed. Therefore, the reaction conditions were changed. To the cooled (0°C) solution of a metal hydride and THF, *tert*butylamine was added and slowly warmed up to room temperature. After the solution was stirred over night, S(N*t*Bu)$_3$ dissolved in THF was added. On the next day, the resulting solid was removed by filtration and the filtrate was layered with pentane (Scheme 3.16). This experiment was realized with potassium-, calcium- and strontium hydride, but unfortunately no crystals were obtained. The NMR experiments show a lot of signals, which could not be assigned to one compound.

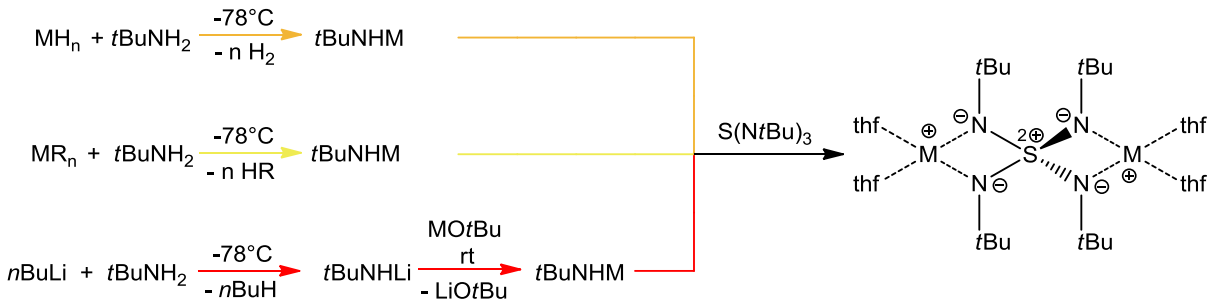

Scheme 3.16: Possible reaction pathways of metal hydrides or alkyls with S(N*t*Bu)$_3$ and *t*BuNH$_2$.

The reaction of metal alkyls, S(N*t*Bu)$_3$ and *t*BuNH$_2$ is based on the same idea as described above. This experiment was carried out with the following substances, dimethyl-, diethyl- and dimesityl zinc, dibutyl magnesium, trimethyl aluminum, and methyl potassium. The corresponding results are shown in Table 3.13.

Table 3.13: Used metal alkyls, –hydrides, -*tert*butanolate and their reaction products

metal alkyls	*solution color*	*results*
$ZnMe_2$	brown	$MeZn(NHtBu)_3Br \cdot thf$
$ZnEt_2$	yellow	powder
$ZnMes_2$	orange	colorless crystals
$MgBu_2$	brown	
$AlMe_3$	orange	powder
KMe	colorless	powder
KH	red	
CaH_2	orange	
SrH_2	orange	
CuO*t*Bu	orange	$(LiCl \cdot thf)_2$

Remarkable, in the reaction of dimethyl zinc, $S(NtBu)_3$ and $tBuNH_2$ colorless crystals were obtained, which consist of the $MeZn(NH_2tBu)_3^+$ cation with bromide counter ion (**10**) (Figure 3.27). The desired reaction pathway to *t*BuNHZn and methane could not be realized. Instead, a complex of the methyl zinc and the *tert*butylamine crystallized.

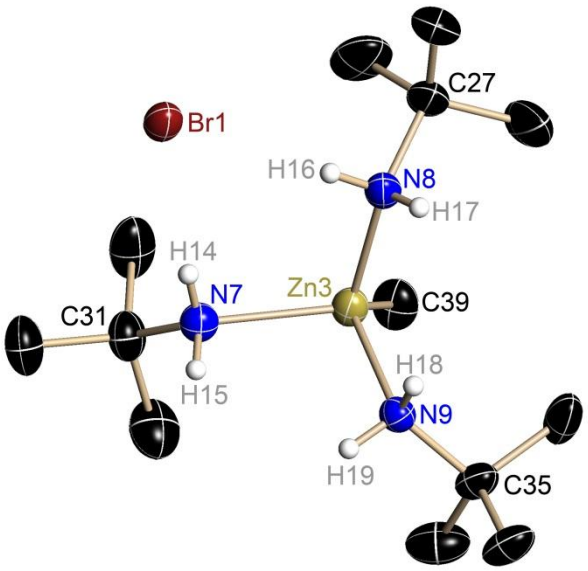

Figure 3.27: Part of the crystal structure of $[MeZn(NH_2tBu)_3Br]$ (**10**). Hydrogen atoms H14 – H19 were found in the Fourier difference map. The other hydrogen atoms are omitted for clarity. Displacement ellipsoids are at 50 % probability.

Compound **10** crystallized in the monoclinic space group $P2_1/c$ after two days storage at –24°C in a mixture of toluene and THF. Three molecules of $MeZn(NH_2tBu)_3Br$ are in one asymmetric unit. All hydrogen atoms attached to the nitrogen atoms are found in the Fourier difference map and refined using distance restrains.

In the syntheses with dimesityle zinc, $S(NtBu)_3$ and $tBuNH_2$ an exceptional complex was crystallized. The X-ray diffraction experiments did not result in a completely structure because the data set was incomplete. A detailed structure refinement could not be made because a lot of atoms were disordered and the quality of the X-ray diffraction data was too poor.

In my diploma thesis,[34] the reaction with potassium- and sodium *tert*butanolate were described, which are based on the work of *Izod et al.*[119] In the reaction with copper *tert*butanolate, $tBuNH_2$ was added dropwise to the cooled solution of *n*BuLi in *n*hexane (–78°C). After CuO*t*Bu was dissolved in toluene, the reaction mixture was added and stirred over night at rt. *t*BuNHCu was filtered off and dried *in vacuo.* The orange powder (*t*BuNHCu) and $S(NtBu)_3$ were dissolved in toluene and stirred over night at rt. The resulting solid was removed by filtration and after two weeks of storage at –24°C colorless crystals were obtained, which were identified by X-ray analysis as lithium chloride with one THF molecule being coordinated. After the lithium chloride was filtered off, no crystals were formed. ^{1}H, ^{13}C and ^{15}N NMR experiments were inconclusive.

3.7. Variation of the solvent

Another research project within this thesis was to vary the coordinating solvent molecules. In previous works,[34, 35] two compounds could be obtained, in which the THF molecules were exchanged by TMEDA, $[(tmeda)_2Li_2(NtBu)_4S]$, and by 1,4-dioxane, $[(C_4H_8O_2)_2Li_2(NtBu)_4S]_n$. Their effect on the structure geometry should be analyzed. Moreover, it should be investigated if the solvent exchange increases the stability of the complex and therewith, a reduced sensitivity towards oxygen and water. This is important for the consecutive reaction to the transmetalation product because hydrolyzed starting material caused obstacles.

The syntheses of novel Lewis bases coordinated starting materials is based on the syntheses of the lithiated tetrakis(*tert*butyl)imidosulfate.[22] $S(NtBu)_3$ dissolved in the respective solvent was added to the suspension of *n*BuLi and *tert*butylamine. After removing half of the solvent *in vacuo*, the solution was stored at –24°C (Scheme 3.17).

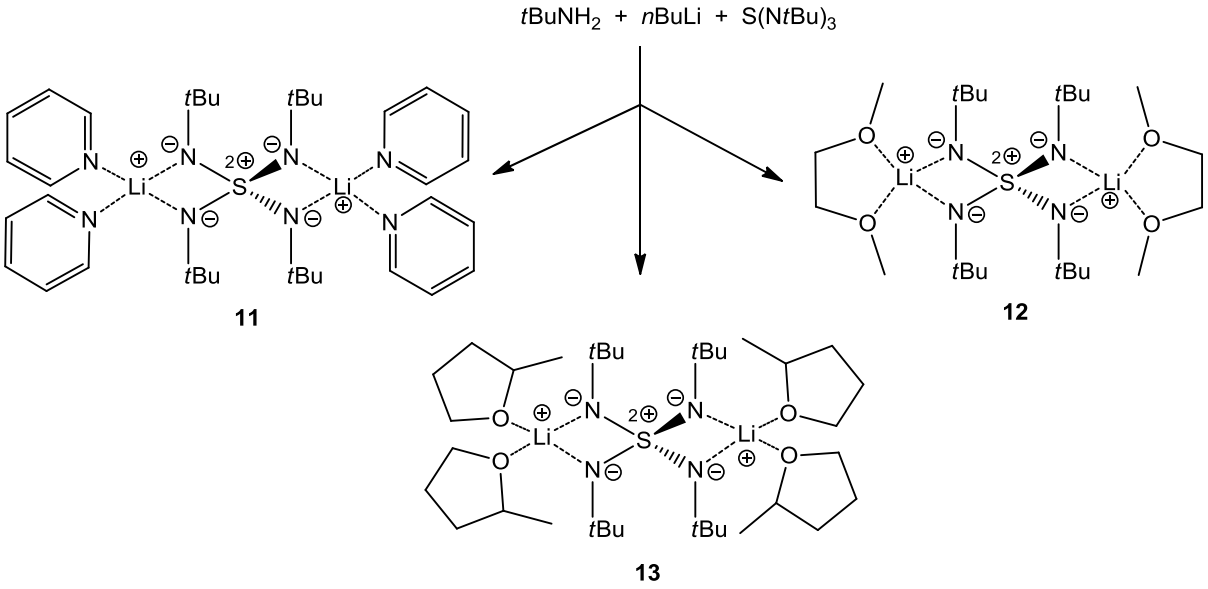

Scheme 3.17: Possible products of the reaction of *tert*butyl amine, *n*BuLi and $S(NtBu)_3$ in the presence of different Lewis bases.

The addition of 1,2-dimethoxyethane (DME), pyridine and 2-methyl-THF resulted each in a brown solution with colorless crystals, which turned blue in contact with air. This color change is an indication that the species containing the fourfold coordination of the

sulfur atom could be synthesized because the product is expected to be oxygen sensitive. Known complexes turn blue upon oxidation.[22]

Unexpectedly, these crystals are difficult to measure by X-ray diffraction experiments because the reflections in the diffraction pattern are not well separated. Only ring shaped reflections of powder and peaks indicative for a twin were found. The recrystallization of these compounds yielded crystals of the same quality.

The ^{1}H, ^{13}C and ^{15}N NMR spectrums of the DME- and pyridine compounds confirm the assumption that the desired products could be obtained in solution. Signals at 8.54–8.52, 7.68–7.62 and 7.27–7.22 ppm in the ^{1}H NMR spectrum (Figure 3.28) of compound **11** coupling to the signals at 150.6, 136.1 and 124.2 ppm in the ^{13}C NMR spectrum (Figure 3.29) identified the pyridine molecules. In the ^{15}N HMBC spectrum, a signal at –358.7 ppm corresponds to the nitrogen atoms of the Lewis bases. The *tert*butylimido groups form a singlet at 1.38 ppm in the ^{1}H NMR spectrum, at 51.4 and 34.2 ppm in the ^{13}C NMR spectrum and at –263.8 ppm a signal in the ^{15}N HMBC spectrum.

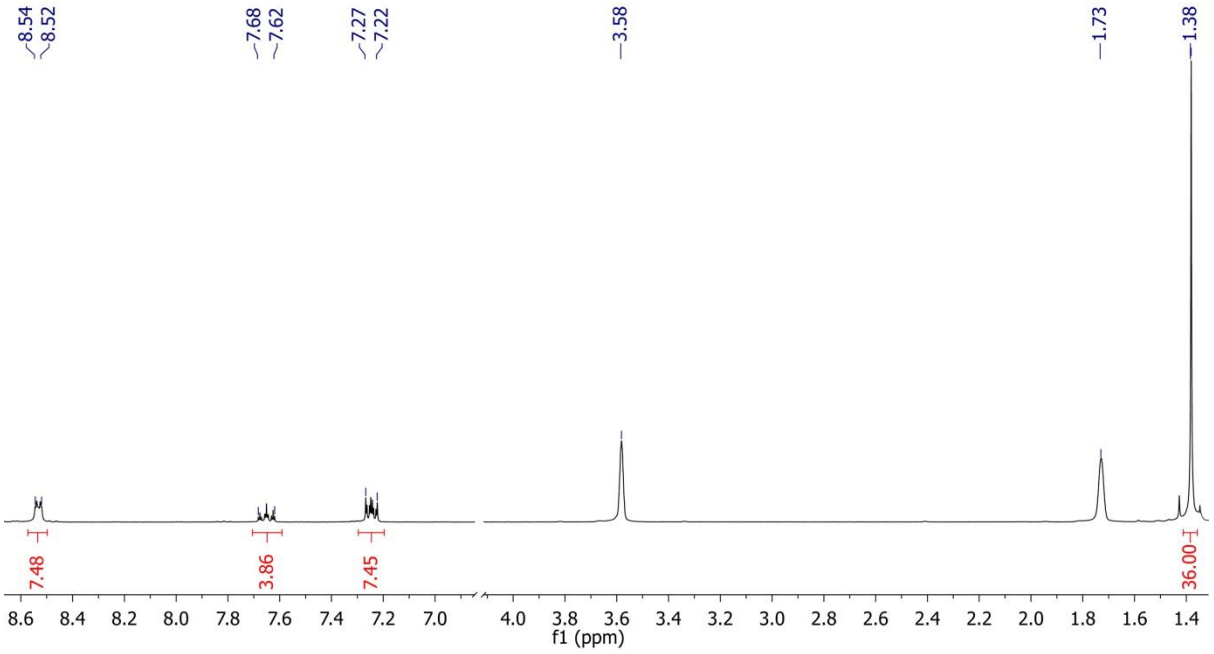

Figure 3.28: ^{1}H NMR spectrum (measured in d_8-THF) of $[(py)_4Li_2(NtBu)_4S]$ (**11**).

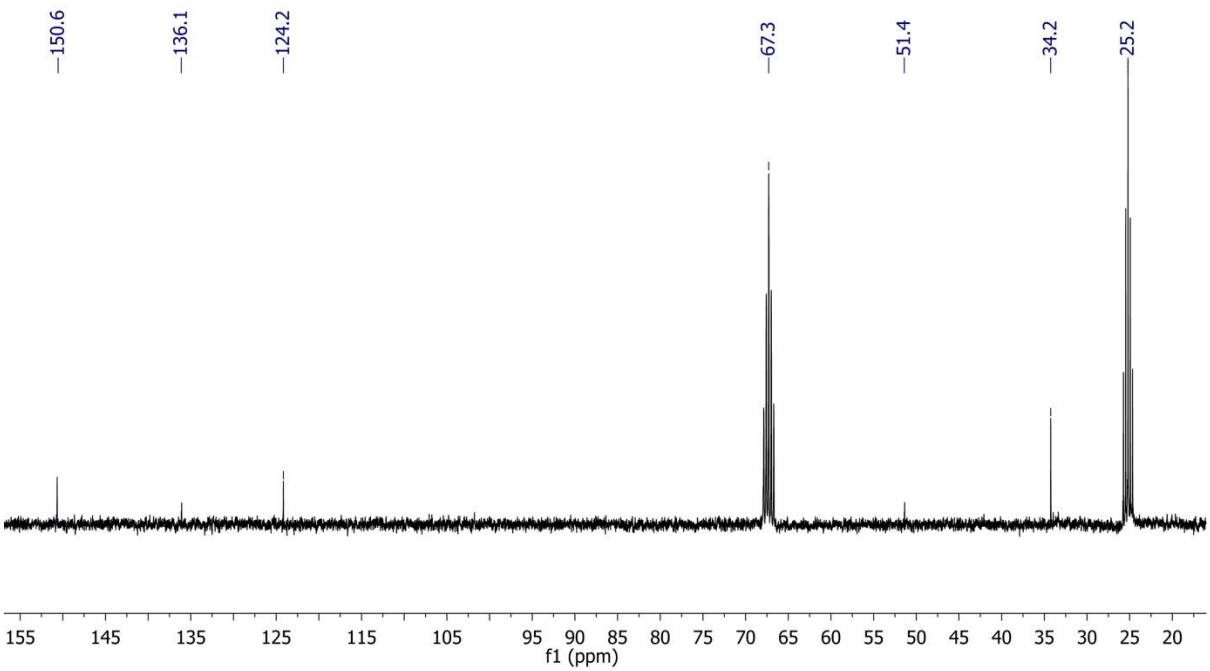

Figure 3.29: ^{13}C NMR spectrum (measured in d_8-THF) of [(py)$_4$Li$_2$(N*t*Bu)$_4$S] (**11**).

For compound **12**, a singlet at 1.38 ppm in the ^{1}H NMR spectrum (Figure 3.30) coupling to the signals at 51.4 and 34.3 ppm in the ^{13}C NMR spectrum (Figure 3.31) and a signal at –260.8 ppm in the ^{15}N HMBC spectrum was identified as the *tert*butylimido groups. In the ^{1}H NMR spectrum, a singlet at 3.43 ppm coupling to a signal at 72.7 ppm in the ^{13}C NMR spectrum could be identified as the CH_2 groups and a singlet at 3.27 ppm coupling with a signal at 58.8 ppm as the CH_3 groups of the DME.

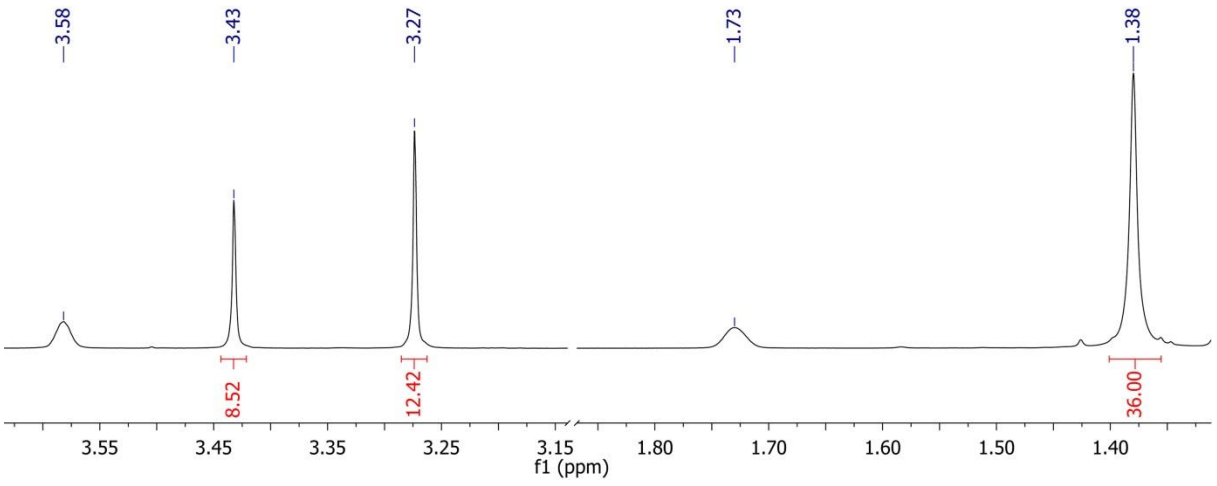

Figure 3.30: ^{1}H NMR spectrum (measured in d_8-THF) of [(dme)$_2$Li$_2$(N*t*Bu)$_4$S] (**12**).

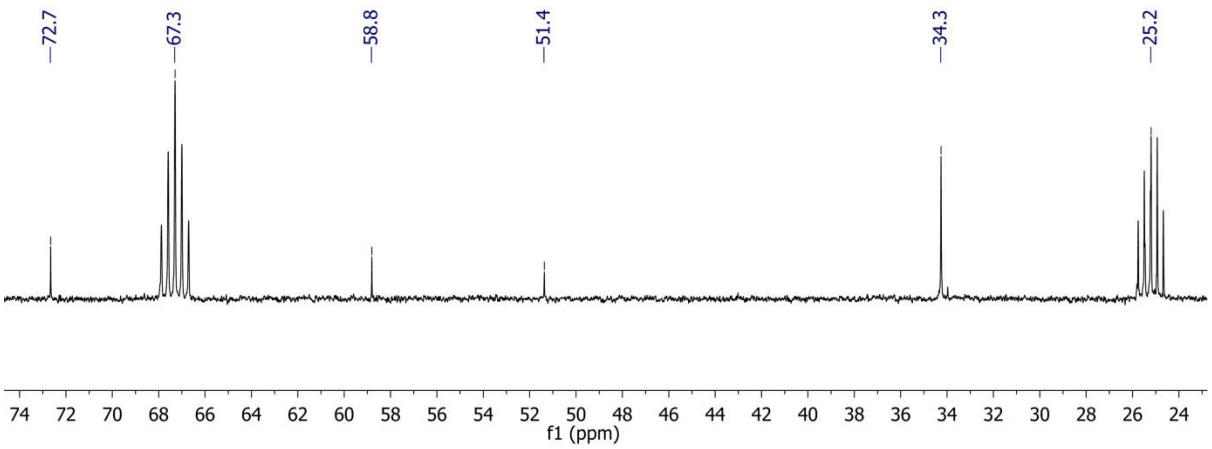

Figure 3.31: ^{13}C NMR spectrum (measured in d_8-THF) of $[(dme)_2Li_2(NtBu)_4S]$ (**12**)

The 2-Me-THF compound turned blue very rapidly, which makes the analytics of non-hydrolyzed products very difficult.

Summarizing, a different observations seem to prove that the desired products $[(py)_4Li_2(NtBu)_4S]$ (**11**) and $[(dme)_2Li_2(NtBu)_4S]$ (**12**) could be synthesized.

Further research should be directed at recrystallizing these compounds to get crystals of higher quality suitable for single crystal X-ray structure analysis to investigate the influence of the solvent on the structure in a more detailed way. Moreover, the transmetalation of these compounds should be carried out to compare them with the TMEDA and THF coordinated starting materials regarding the molecule stability.

3.8. Variation of the imido group

In this section novel sulfur-nitrogen ligands, $S(NR)_n(NR')_m$, for transmetalation reactions are presented. The known lithiated tetrakis(*tert*butyl)imidosulfate (**1**) includes bulky *tert*butyl groups, which seem to be important for the stability of the complex. Different moieties bonding to the nitrogen atoms would yield new sulfur-nitrogen ligands. In the past, a few phosphorous[120-123]- and silicon[124] centered compounds were published which included a center atom with two or three identical imides and one nitrogen atom, which is protonated or bonding to a different moiety. Two of these imido groups coordinate a lithium atom while the other does not coordinate. All of these complexes exist as dimers or in higher aggregates.

For the sulfur centered compounds, a range of different imido moieties was used as fourth imido group. Therefore, the reactions are based on the three known synthetic pathways to $S(NtBu)_2$[16] (A), $S(NtBu)_3$[31] (B) and $[(thf)_4Li_2(NtBu)_4S]$[22] (C) (Scheme 3.18). Instead of *tert*butylamine other amines which are listed in Table 3.17 were used. To a solution containing SCl_2 and diethylether the amine dissolved in diethylether was added at 0°C. After stirring over night at rt, the resulting solid was removed by filtration (A).

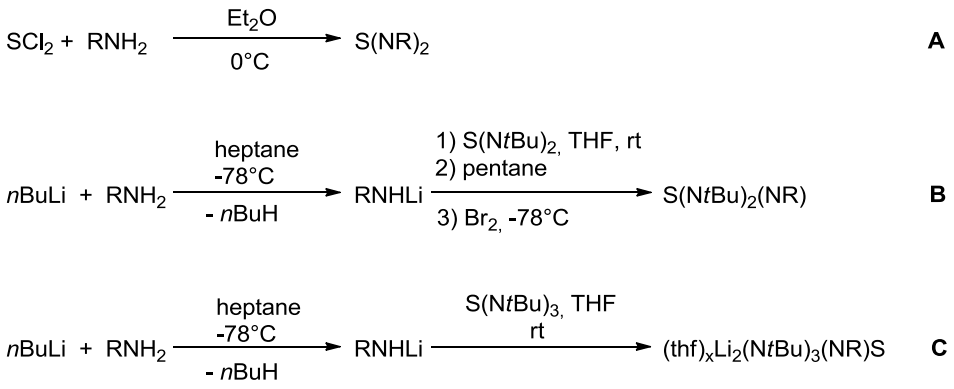

Scheme 3.18: General reactions A[16], B[31] and C[22] for the syntheses of novel sulfur-nitrogen compounds $S(NR)_n(NR')_m$.

For pathway B, *n*BuLi was cooled to –78°C before the amine dissolved in heptane was added dropwise. The solution was stirred for 1.5 h, followed by addition of $S(NtBu)_2$ and THF was added. The solvent was removed *in vacuo,* the resulting solid was dissolved in pentane, and bromine was added to the cooled solution for oxidation. In C, $S(NtBu)_3$

dissolved in THF was added to a solution of *n*BuLi and the respective amine. Two variants of procedure A were carried out for ethane-1,2-diamine. The first one is the reaction of 1.5 eq of the amine and 1.0 eq of the sulfur dichloride to get the single amination on one site of the sulfur (a). The second is the reaction of 3.0 eq of the amine and 1.0 eq of the SCl_2 to synthesize the possible amination with both nitrogen atoms (b).

Table 3.14: Used amines applied to the reaction pathways A, B, and C, and the corresponding reaction products.

amine	*A*	*B*	*C*
*n*butylamine	orange powder		brown powder
ethane-1,2-diamine	*a*) orange powder *b)* yellow powder	red, crystals: LiBr + ethane-1,2-diamine	red powder
N,N'-dimethylethane-1,2-diamine	yellow solution	yellow powder	yellow solution
2,6-diisopropylaniline	orange powder	red powder	brown crystals: $[(thf)_2Li(NtBu)_2(NHtBu)S(Ndipp)]$
2,6-dimethylaniline	red powder	yellow powder	brown crystals: $[(thf)_2Li(NtBu)_2(NHtBu)S(Ndmp)]$

Remarkably, addition of 2,6-diisopropylaniline (dipp) to tBuNH$_2$, nBuLi and S(NtBu)$_3$ led to formation of a new lithiated tetrahedrally coordinated sulfur ligand $[(thf)_2Li(NtBu)_2(NHtBu)S(Ndipp)]$ (**14**). Especially the coordination of three *tert*butylimido groups and one diisopropylaniline group give access to an unprecedented sulfur-nitrogen ligand species (Scheme 3.19).

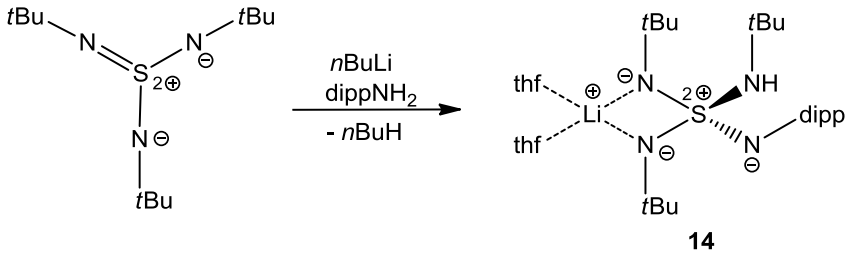

Scheme 3.19: Synthesis of $[(thf)_2Li(NtBu)_2(NHtBu)S(Ndipp)]$ (**14**).

Crystallization of [(thf)$_2$Li(N*t*Bu)$_2$(NH*t*Bu)S(Ndipp)] (**14**) at –24°C from a brown solution was successful and the crystals were suitable for single crystal X-ray diffraction experiments. **14** crystallizes in the monoclinic space group $P2_1/c$ with two molecules in the asymmetric unit. Figure 3.32 shows the crystal structure of [(thf)$_2$Li(N*t*Bu)$_2$-(NH*t*Bu)S(Ndipp)] (**14**).

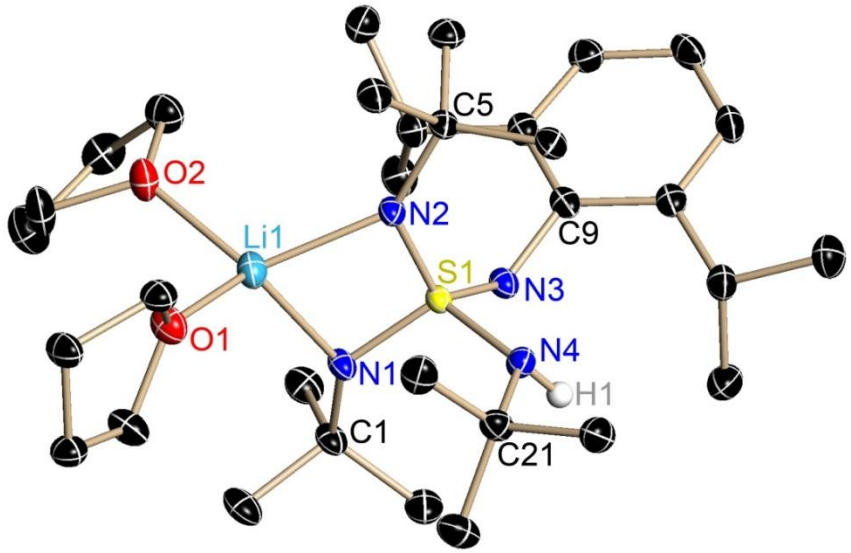

Figure 3.32: Crystal structure of [(thf)$_2$Li(N*t*Bu)$_2$(NH*t*Bu)S(Ndipp)] (**14**). Hydrogen atom H1 was found in the Fourier difference map. The other hydrogen atoms are omitted for clarity. Displacement ellipsoids are at 50 % probability.

In contrast to the known compounds with a phosphorous- or silicon atom this sulfur centered complex **14** exists as a monomer, which has not been reported before. This monomer results from the coordination of the lithium atom by two THF molecules instead of the coordination to a second ligand.

In **14**, two of the three *tert*butylimido groups coordinate the lithium atom. The third *tert*butylimido group is protonated and hence, the nitrogen atom forms a polarized single bond with the sulfur atom, which is confirmed by a longer S–N bond (1.7029 Å) (Table 3.15). The diisopropylaniline group is not protonated because the nitrogen atom of this group and the sulfur atom form a formal double bond, which is proven by a shorter S–N bond (1.5440 Å). In consideration of the results of *Stalke et al.*,[66-69, 74] the S1–N1, S1–N2 and S1–N3 bond lengths, which are 1.5526 Å on average and sum up to

6.3606 Å, can be described as polarized S–N distances. The non-protonated S–N bond lengths as well as the protonated S–N bond lengths in **14** are in the same range of methylene-bis(triimido)sulfonic acid $H_2C\{S(N\mathit{t}Bu)_2(NH\mathit{t}Bu)\}_2$. Slight differences in distances result of the variable oxidation state of the sulfur atom and the coordination of the lithium atom in **14**.

The average S–N bond length (S1–N1/2/3) in **14** is shorter than the corresponding bond length in compound **1**. This could be due to the different fourth imido moiety and the resulting monolithiation. The N–S–N angle is 100.29° on average, which encloses the metal atom, is larger in **14** than in **1**. Also the Li–N distance in this complex **14** is longer than in the dilithiated compound, which again results from the exchange of the imido moiety. A stronger THF coordination and a weaker coordination of the ligand to the lithium atom result in a shorter sulfur-nitrogen bond and a longer lithium-nitrogen bond.

Table 3.15: Selected average bond lengths and average angles of both fragments in the asymmetric unit of **14**.

bond lengths/Å		*angles/°*	
S1–N3	1.5440	N3–S1–N2	123.66
S1–N2	1.5531	N3–S1–N1	112.76
S1–N1	1.5606	N2–S1–N1	100.29
S1–N4	1.7029	N3–S1–N4	102.32
N1–Li1	2.001	N2–S1–N4	107.19
N2–Li1	2.007	N1–S1–N4	110.44
Li1–O2	1.947	N2–Li1–N1	73.23
Li1–O1	1.981		

In different NMR experiments (^1H, ^7Li, ^{13}C, ^{15}N) signals from compound **14** could be observed in solution. In the ^1H NMR spectrum, a signal at 7.25 ppm represents the proton of the NH group, signals at 6.85–6.83 and 6.53–6.51 ppm are identified as belonging to the CH groups at the aniline moiety, the signals at 2.96–2.93 ppm and 1.16 ppm represent the isopropyl groups and the singlets at 1.31 and 1.22 ppm the *tert*butyl groups. The signals of the THF molecules could be identified at 3.59–3.57 and 1.74–1.71 ppm.

Also a signal at 539.4 m/z in the EI-MS endorses that [(thf)$_2$Li(N*t*Bu)$_2$(NH*t*Bu)S(Ndipp)] could be synthesized and is considerably stable. Elemental analysis suggests that **14** is presented in a pure crystal (found (calc.)/ %): C 65.33 (67.09), H 9.45 (10.73), N 8.64 (9.78), S 5.13 (5.60)).

Comparing **14** to the phosphorous and silicon centered compounds, which were published in 2004 by *Chivers*[121] and in 1993 by *Hoffman*[124], respectively, it is apparent that these two compounds could be characterized as dimers, whereas this new lithiated complex **14** forms a monomer (Figure 3.33).

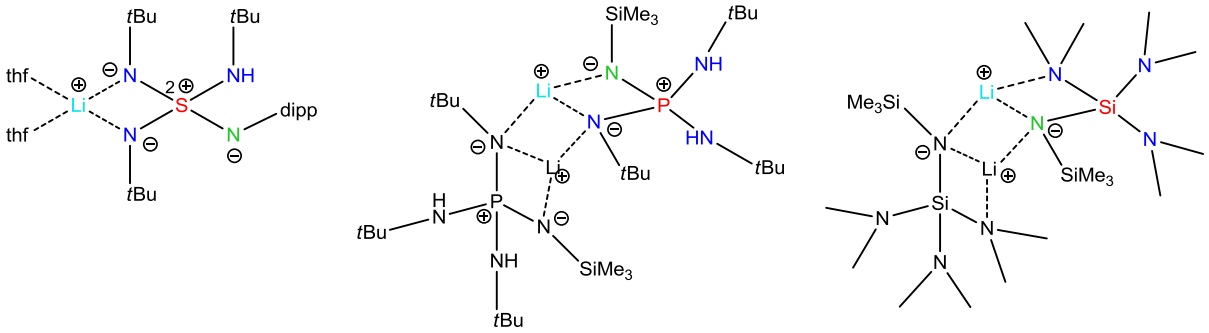

Figure 3.33: The sulfur centered complex **14**, phosphorous[121, 123]- and silicon[124] centered compounds.

Concerning bond lengths and angles no clear tendency can be observed. This may be explained by the different coordination sphere even though all compounds coordinate a lithium atom and contain three equivalent imido groups and one varying imido group. In [Li{P(N*t*Bu)(NH*t*Bu)$_2$(NSiMe$_3$)}] and [Li{Si(NMe$_2$)$_3$}(NSiMe$_3$)]$_2$, the lithium atom is coordinated by two different imido groups, whereas two identical imido groups coordinate the lithium atom in **14**. Due to this and the observation of **14** being a monomer, the typically tetrahedral coordination of the lithium atom could be formed with two additional THF molecules. A possible transmetalation of this sulfur centered complex could be easier due to the coordination of the lithium atom.

In the reaction of S(N*t*Bu)$_3$, *n*BuLi, and dmpNH$_2$ (dmp = dimethylphenyl) a second new lithiated, sulfur centered complex could be obtained (Scheme 3.20). This compound, [(thf)$_2$Li(N*t*Bu)$_2$(NH*t*Bu)S(Ndmp)] (**15**), differs from complex **14** containing a dmp group instead of the dipp group.

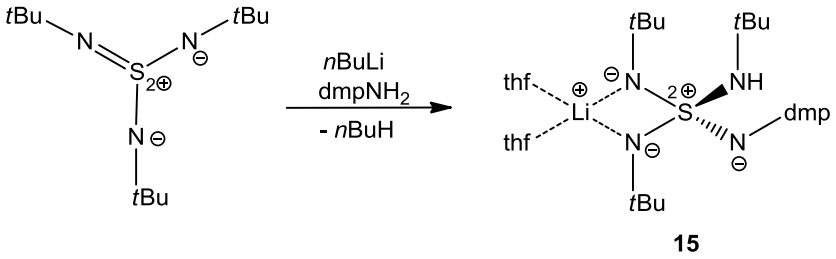

Scheme 3.20: Synthesis of $[(thf)_2Li(NtBu)_2(NHtBu)S(Ndmp)]$ (**15**).

15 could be obtained after storage in THF for five weeks at –24°C as brown crystals, which grow in the monoclinic space group $P2_1/c$ with one molecule in the asymmetric unit. The sulfur atom is coordinated tetrahedrally by four imido groups, of which three groups are *tert*butylimide and the fourth is a dimethylaniline. Two of the *tert*butylimido groups (N4–C17, N2–C9) coordinate the lithium atom, which is also coordinated by two THF molecules giving an overall fourfold coordination. The third *tert*butylamino group (N3) is protonated by H1 (Figure 3.34).

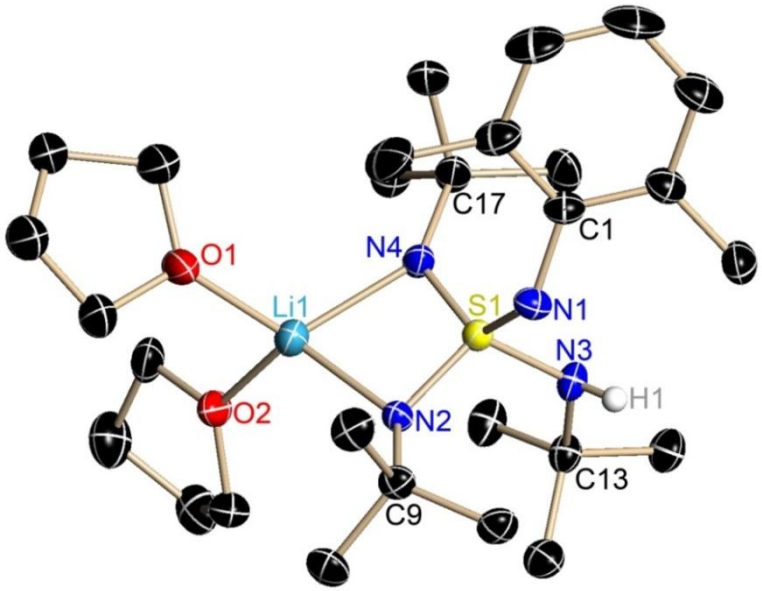

Figure 3.34: Crystal structure of $[(thf)_2Li(NtBu)_2(NHtBu)S(Ndmp)]$ (**15**). Hydrogen atom H1 was found in the Fourier difference map and refined freely. The other hydrogen atoms are omitted for clarity. Displacement ellipsoids are at 50 % probability.

Selected bond lengths and angles of **15** are given in Table 3.16. The average S–N bond length (S1–N2/3/4) is 1.5529 Å and sum up to 6.3585 Å, and hence, in the same range as in compound **14**. The distance between the nitrogen atoms and the lithium atom is

2.005 Å on average, as well as the bond between the oxygen- and lithium atom with a length of 1.974 Å on average are almost equivalent to **14**. The average angle between N–S–N is 101.03° and the N–Li–N angle amounts 73.61(15)°. These angles are nearly equivalent to the angles in complex **14**.

Table 3.16: Selected bond lengths and angles of **15**.

bond lengths/Å		*angles/°*	
S1–N1	1.5460(2)	N1–S1–N3	101.00(10)
S1–N4	1.5493(18)	N4–S1–N2	101.03(10)
S1–N2	1.5635(18)	N1–S1–N4	122.46(11)
S1–N3	1.6997(19)	N2–S1–N3	110.93(10)
Li1–O2	1.960(2)	N1–S1–N2	112.46(11)
Li1–O1	1.988(7)	N4–S1–N3	108.73(10)
Li1–N4	2.018(4)	N2–Li1–N4	73.61(15)
Li1–N2	1.992(4)		

The NMR experiments (^{1}H, ^{7}Li, ^{13}C, ^{15}N) confirm that compound **15** was formed in solution. In the ^{1}H NMR spectrum, a signal at 7.19 ppm represents the proton of the NH group, signals at 6.69–6.67 and 6.10–6.07 ppm were identified as belonging to the CH groups at the aniline moiety, the signal at 1.31 ppm represents the methyl group of the aniline and the singlets at 1.36 and 1.18 ppm the *tert*butyl groups. The signals at 3.60–3.56 and 1.75–1.72 ppm could be identified as protons of the THF molecules. These signals concur with the signals of **14**. Elemental analysis suggests that **15** is presented in a pure crystal.

Like complex **14**, complex **15** can also be compared with the compounds $[(thf)_4Li_2(N\mathit{t}Bu)_4S]$ (**1**), $[Li\{P(N\mathit{t}Bu)(NH\mathit{t}Bu)_2(NSiMe_3)\}]$[121, 123], $[Li\{Si(NMe_2)_3\}(NSiMe_3)]_2$[124] and $H_2C\{S(N\mathit{t}Bu)_2(NH\mathit{t}Bu)\}_2$[69] and the same assumptions and conclusion may be drawn. With these novel monolithiated, tetrahedrally coordinated starting materials a broad field of syntheses of new heterobimetallic compounds may result. As a starting procedure, the protonated nitrogen atom could be straight forwardly deprotonated and further metalated to obtain the heterobimetallic species. In a subsequent step, synthesis of these monomers may allow an easier transmetalation than the so far known complexes.

3.9. Di(*tert*butyl)seleniumdiimide

Due to the high potential of the di(*tert*butyl)seleniumdiimide in amination chemistry (Section 1.4),[75, 76, 78] this compound should be synthesized in order to explore new reaction pathways. Thereby, comparison with the analog sulfurdiimide would also be possible. For this, the reaction of selenium tetrachloride and *tert*butylamine in Et_2O was performed.[76] In the publication of *Herberhold et al.*[76] *tert*butylamine was added dropwise to a suspension of $SeCl_4$ and Et_2O. The tBuNH$_3$Cl was separated by filtration and the residue was washed with diethylether. After removing the solvent *in vacuo*, yellow crystals were obtained at –24°C, which turned into an orange oil at rt.[76] However, after single X-ray structure determination, these turned out to consist of the hydrolyzed product di(*tert*butyl)seleninyldiimide, OSe(NHtBu)$_2$ (**16**) (Scheme 3.21).

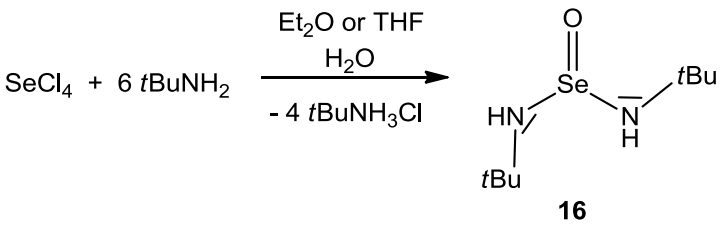

Scheme 3.21: Synthesis of di(*tert*butyl)seleninyldiimide (**16**).

From this the conclusion could be drawn that the selenium tetrachloride was dry enough. The selenium tetrachloride had been stored in the glove box. It had been assumed that this was dry and usable for reactions. The other starting materials, tBuNH$_2$ and Et_2O were dried and distilled before synthesis. Interestingly, in the ^{1}H and ^{13}C NMR spectra signals of three species were observed.

In the ^{1}H NMR spectrum, the three signals appear at 1.74, 1.24 and 1.18 ppm (Figure 3.35). One signal at 1.24 ppm has a three times higher integral than the other two signals. In the ^{13}C NMR spectrum there are also two signals (53.4 and 31.6 ppm), displaying the same integral (Figure 3.36). The signal at 5.17 ppm in the ^{1}H NMR spectrum presents the NH groups. *Herberhold et al.*[77] described the ^{13}C NMR spectrum (measured in $CDCl_3$) as exhibiting signals at 65.8 and 31.6 ppm indicating the Se(NtBu)$_2$ at 20°C and signals at 66.2, 65.6, 32.7 and 28.0 ppm of the *Z*- and *E*-isomers of Se(NtBu)$_2$ at –80°C.[76]

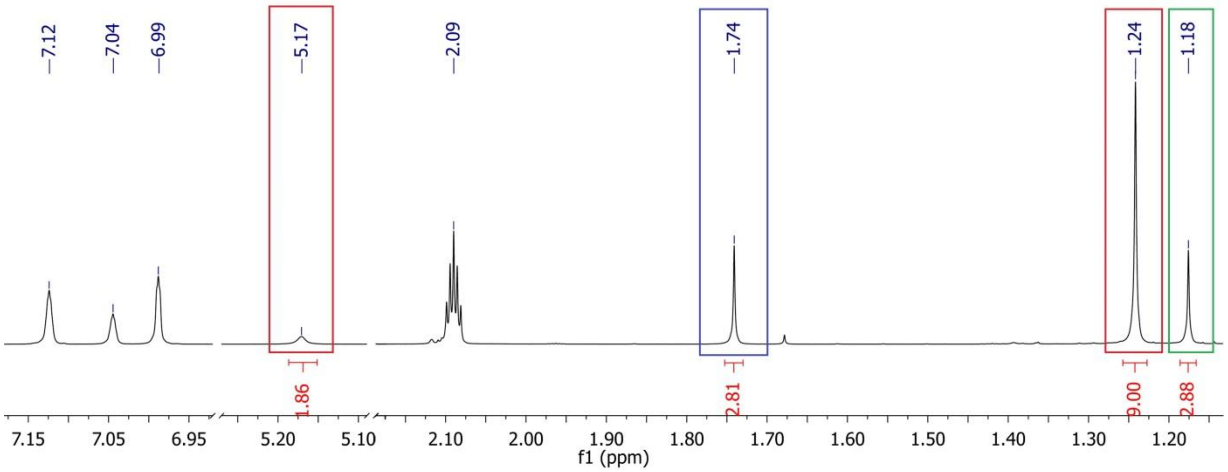

Figure 3.35: Section of the ^{1}H NMR spectrum (500.13 MHz, toluene–d_8) of **16** at –40°C. Blue: *E*-Se(N*t*Bu)$_2$, red: OSe(NH*t*Bu)$_2$ and green: *Z*-Se(NtBu)$_2$.

Compared it to the carbon spectrum of **16** the same six signals can be found, even though this spectrum was measured at –40°C. The assumption could be made that at –40°C one part of Se(N*t*Bu)$_2$ is present in the *Z*/*E*-isomers and another additional compound is formed, which is at the same shift as the converting species. However, the signals in the ^{1}H NMR spectrum of **16** do not correspond to the published signals of Se(N*t*Bu)$_2$, which are at 1.48 and 1.32 ppm at –30°C and were converged at 5°C (measured in $CDCl_3$).[76] In another publication of *Herberhold et al.* the signals of the *Z*/*E*-isomers in the ^{1}H NMR spectrum were reported to be at 1.56 and 1.13 ppm (measured in tolouene-d_8),[77] which are more similar to the observed signals of **14** but still different.

The similarities in the ^{13}C NMR spectrum and the differences in the ^{1}H NMR spectrum between the published data and **16** can be explained by formation of the hydrolyzed product OSe(NH*t*Bu)$_2$ giving the same signals in the ^{13}C NMR spectrum at –40°C as the converged signals of Se(N*t*Bu)$_2$ at 20°C. In the suspension of compound **16**, the hydrolyzed selenium compound was the main product and the *Z*/*E*-isomers of the non-hydrolyzed compound are the by-product, which did not crystallize.

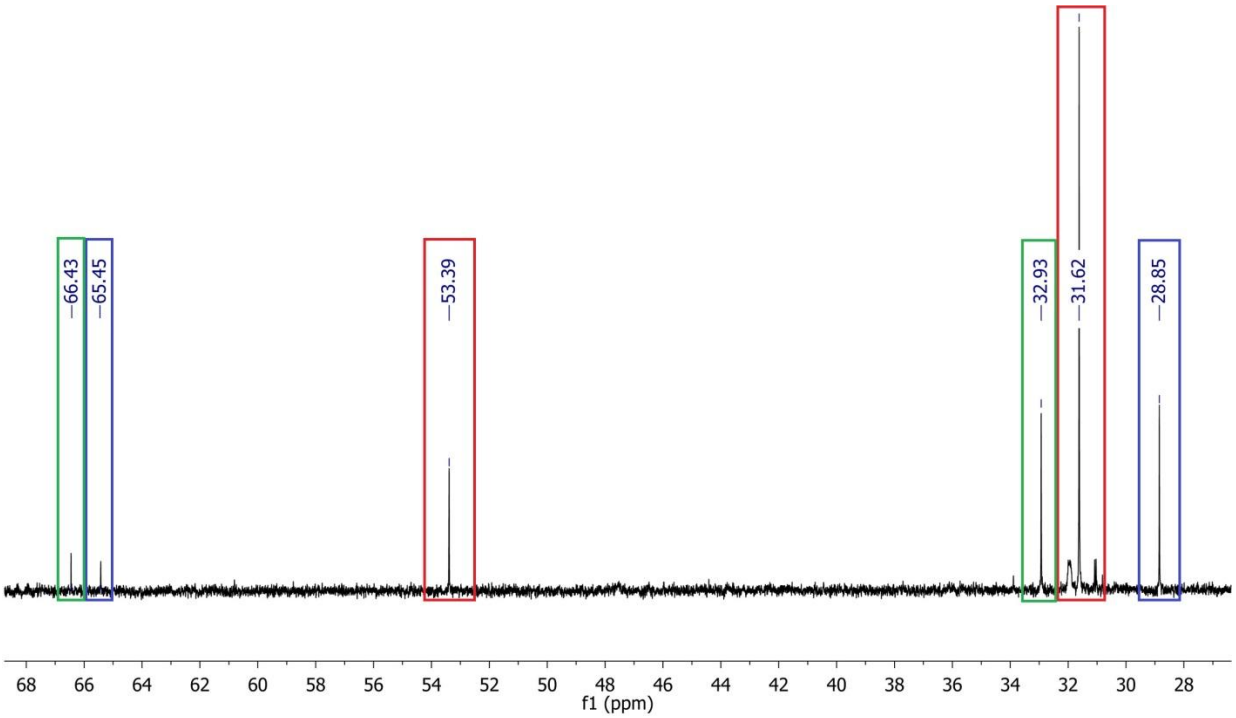

Figure 3.36: Extract of the ^{13}C NMR spectrum (125.758 MHz, toluene–d_8) of **16** at –40°C. Blue: *E*-Se(N*t*Bu)$_2$, red: OSe(NH*t*Bu)$_2$ and green: *Z*-Se(NtBu)$_2$.

In a next attempt to obtain Se(N*t*Bu)$_2$, first, selenium tetrachloride was dried. Still, only the hydrolyzed product was obtained. Due to this and the predication that the synthesis of di(*tert*butyl)selendiimide is temperature dependent, the reaction was rerun at 0°C and also at –78°C to impede the formation of heterocycles of selenium- and nitrogen atoms described by *Herberhold et al.*[76], *Wrackmeyer et al.*[77] and *Chivers et al.*[80] Although the filtrate was cooled (–24°C) after addition of *tert*butylamine, all different attempts led to the hydrolyzed product OSe(NH*t*Bu)$_2$. Changing the solvent from diethylether to THF yielded the same result. Hence, this reaction is so sensitive to oxygen and water, that it is hardly possible to synthesize the desired product. As the synthesis of Se(N*t*Bu)$_2$ was not successful, the starting material was changed. Instead of using selenium tetrachloride, selenium dichloride was tested because the sulfur centered analog S(N*t*Bu)$_2$ was obtained in the reaction of sulfur dichloride with *t*BuNH$_2$ (Scheme 3.22).[16, 80, 125]

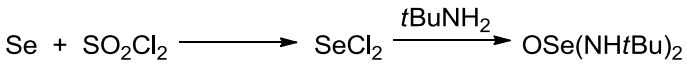

Scheme 3.22: Reaction of selenium, SO_2Cl_2 and *tert*butylamine.[80, 125]

Therefore, freshly distilled SO_2Cl_2 was added to a suspension of dried selenium powder and THF and after 30 min *t*BuNH$_2$ was added. After two days yellow crystals of OSe(NH*t*Bu)$_2$ were obtained.

Summarizing, different synthetic routes lead to the hydrolyzed product OSe(NH*t*Bu)$_2$ with quite a high yield especially considering that the selenium amides are very sensitive and difficult to handle. Only the dimeric OSe(μ-N*t*Bu)$_2$SeO[81], the hydrolyzed compound *t*BuNSe(μ-N*t*Bu)$_2$SO$_2$[80] and *t*BuNSe(μ-N*t*Bu)$_2$SeO$_2$[80] were known before.

The solid state structure of OSe(NH*t*Bu)$_2$ confirms that monomeric structures of a selenium-nitrogen compound are possible to synthesize. Figure 3.37 shows the crystal structure of **16**. It crystallizes in the triclinic space group $P\bar{1}$ with one molecule in the asymmetric unit. The selenium atom is tricoordinated by two nitrogen atoms with a *tert*butyl group and by one oxygen atom.

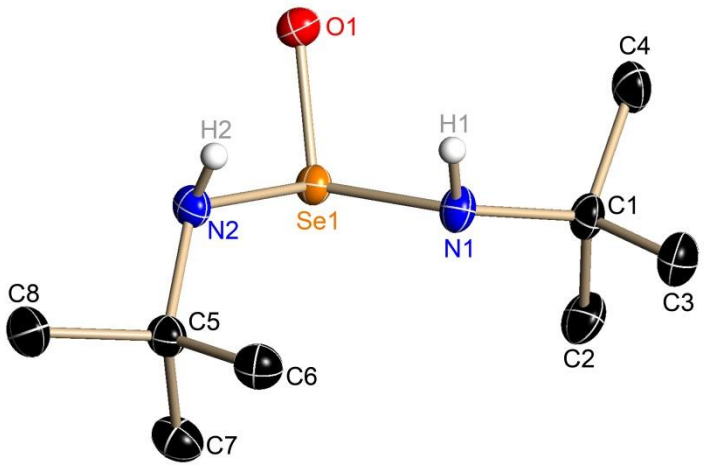

Figure 3.37: Crystal structure of OSe(NH*t*Bu)$_2$ (**16**). Hydrogen atoms H1 and H2 were found in the Fourier difference map. The other hydrogen atoms are omitted for clarity. Displacement ellipsoids are at 50 % probability.

The Se1–N1 bond length is 1.8377(15) Å and the Se1–N2 bond length is 1.8246(15) Å, which is in the same range of the Se–N bond lengths in the published hydrolyzed compounds.[77] The Se–O bond length of 1.6563(12) Å is similar to published hydrolyzed selenium compounds (Table 3.17). The angles are differing from the literature known compounds. The N–Se–N angle is wider than in the dimeric OSe(μ-N*t*Bu)$_2$SeO,[81] *t*BuNSe(μ-N*t*Bu)$_2$SO$_2$,[80] and *t*BuNSe(μ-N*t*Bu)$_2$SeO$_2$.[80] This could be explained by the

steric differences. In the dimeric complexes the nitrogen atoms are bonded to two selenium atoms which make the movement of the imido groups more restricted than in the monomer resulting in the wider angle in **16**. Consequently, the N–Se–O angle shows different values to the known compounds.

Table 3.17: Selected bond lengths and angles of **16**.

bond lengths/Å		*angles/°*	
Se1–N1	1.8377(15)	N1–Se1–N2	98.42(7)
Se1–N2	1.8246(15)	N1–Se1–O1	106.92(7)
Se1–O1	1.6563(12)	N2–Se1–O1	98.78(7)

In the following, $OSe(NH\textit{t}Bu)_2$ should be metalated. The electron pairs on the nitrogen atoms offer a good coordination site for metal cations. THF was added to solution containing the starting material **16**, the pre-coordinated and Cp_2TiCl_2, which was dried before it was put to reaction, at –78°C. The red suspension was stirred over night and the precipitating solid was subsequently removed by filtration. After storage of a resulting solution for one week at –24°C, red crystals were obtained, which could be identified as the starting material Cp_2TiCl_2.

In the next experiment, iron(II)acetate and $OSe(NH\textit{t}Bu)_2$ in THF were added; after stirring and removing the resulting solid, brownish crystals were obtained, which turned out to be *tert*butylammonium and acetate. In the reactions of methyl lithium and methyl potassium with **16**, no crystals could be obtained. NMR experiments could not clarify which compounds were formed in solution.

In collaboration with Dr. Nina Lock the topic of the seleniumdiimide synthesis was followed. The next experiments with other solvents were carried out by Dr. Nina Lock. In one reaction, selenium tetrachloride and *tert*butylamine were dissolved in dichlormethane (DCM) (Scheme 3.23). The resulting $\textit{t}BuNH_3Cl$ was removed by filtration and the residue was washed with DCM. At this, the whole process of filtration was cooled (–30°C). Half of the solvent was removed *in vacuo* at 0°C and toluene was added.

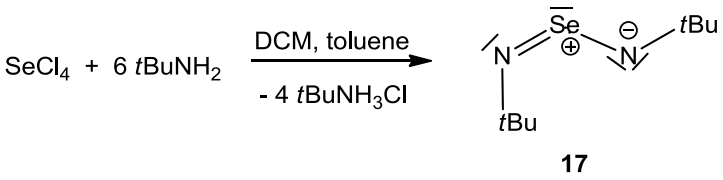

Scheme 3.23: Synthesis of Se(N*t*Bu)$_2$.

After one day storage at –78°C, the resulting solid was dissolved in toluene. After the yellow solution had been stored three months at –78°C, yellow crystals were obtained. Remarkably, the crystals could be analyzed by X-ray structure determination as the non-hydrolyzed species Se(N*t*Bu)$_2$ (**17**), which crystallizes in the triclinic space group $P\bar{1}$ with one molecule in the asymmetric unit (Figure 3.38). The *syn*, *anti* conformation is presented in solid state, which confirms the presented results of *Herberhold et al.*[76] and *Chivers et al.*[79].

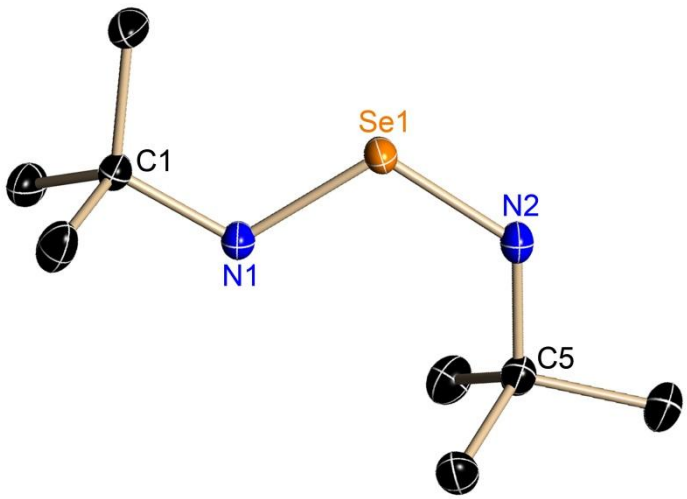

Figure 3.38: Crystal structure of Se(N*t*Bu)$_2$ (**17**). Hydrogen atoms are omitted for clarity. Displacement ellipsoids are at 50 % probability.

The Se1–N1 bond length is 1.7299(10) Å and the Se1–N2 distance is 1.7070(11) Å (Table 3.18). As expected, the selenium-nitrogen bond lengths of **17** are shorter in comparison to the hydrolyzed species **16** and longer in comparison to the homolog S(N*t*Bu)$_2$.[69] Due to the NBO/NRT analysis of the sulfurdiimide, it could be presumed that the Se–N bonds in **17** are also different. The bonding patter may be described with one formal double bond and one polarized bond (Scheme 3.23).[69] The N1–Se1–N2 angle of 113.24(5)° is between the sulfur homolog (117.4(1)°) and **16** (98.420(7)°). Due to the bulkier electron pair at the selenium atom, the angle is smaller in comparison to

$S(NtBu)_2$. The N1–Se1–N2 angle of **16** is smaller than the analog angle in **17** because of the presence of the oxygen atom.

Table 3.18: Selected bond lengths/Å and angles/° of **17**, **16** and $S(Nt Bu)_2$[69].

	17	**16**	$S(Nt Bu)_2$
Se1/S1–N1	1.7299(10)	1.8377(15)	1.5370(4)
Se1/S1–N2	1.7070(11)	1.8246(15)	1.5279(4)
N1–Se1/S1–N2	113.24(5)	98.420(7)	117.4(1)

In different NMR experiments (^1H, ^{13}C, ^{15}N, ^{77}Se) at –80°C signals from compound **17** could be observed in solution. In the ^1H NMR spectrum, a signal at 1.77 ppm represents the proton of the *tert*butyl group of the *E*-$Se(NtBu)_2$ and a signal at 1.12 ppm is identified as belonging to the *tert*butyl group of the *Z*-isomer. In the ^{13}C NMR spectrum, the signals at 65.6 and 28.4 ppm represents the carbons of the *E*-isomer and at 66.0 and 32.5 ppm of the *Z*-$Se(NtBu)_2$. In the ^{15}N NMR spectrum, the signal at 101.9 ppm is identified as belonging to the nitrogen atoms of the *E*-isomer and the signal at –5.71 ppm to the *Z*-isomer. A signal at 1656.1 ppm in the ^{77}Se NMR spectrum is represent the selenium atom. ^1H NMR experiments at different temperatures show that the two signals of the *E*- and *Z*-isomer are shifted. By the increase of temperature, the signals converge. Against the assumption of *Herberhold et al.*,[76] two signals, with a slightly shift, are still present at 30°C.

With this crystal structure of the seleniumdiimide **17**, it could be confirmed that the *syn, anti* conformer is still present in solid states. In further research, the synthesis of the seleniumtriimide, analog to the $S(Nt Bu)_3$[31], and the metalation of the seleniumdiimide should be carried out.

4. Conclusion and outlook

In summary, this thesis is divided into four parts: the synthesis of novel metal complexes of the sulfur-nitrogen ligand, $S(NtBu)_4^{2-}$ (i), exchange of the THF donor molecules in the starting material (**1**) by other donor solvent molecules (ii), the synthesis of new tetrahedrally coordinated sulfur ligands, $S(NR)_4^{2-}$, (iii) and the synthesis of di(*tert*butyl)seleniumdiimide, $Se(NtBu)_2$, (iv).

A series of novel metal complexes of the $S(NtBu)_4^{2-}$ ligand could be synthesized successfully and fully characterized (Figure 4.1). These complexes show that $S(NtBu)_4^{2-}$ can serve as a ligand for transition metals from soft copper(II) to hard zinc(II) cations at opposite sides. Moreover, the first heterobimetallic complexes of this tetrahedrally coordinated sulfur ligand could be presented herein (**5**). Furthermore, the S–N bonds vary only marginally between the different metal cations. The S–N bond distances sum up to 6.37(3) Å, from which can be concluded that the electropositive sulfur responds to the metal-polarized negative charge at the outside of the $[S(NR)_4]^{2-}$ tetrahedron. In all complexes, polarized sulfur-nitrogen bonds with a covalent character and an additively ionic part, which is responsible for the shorter bonding, are present. The metal atoms could be reduced, which should be verified in a future project. Proceeding, the electronic behavior of the copper complex **8** could be probed by EPR analysis to corroborate which electron configuration and splitting is present. Complex **9** could be tested for N_2 and O_2 activation

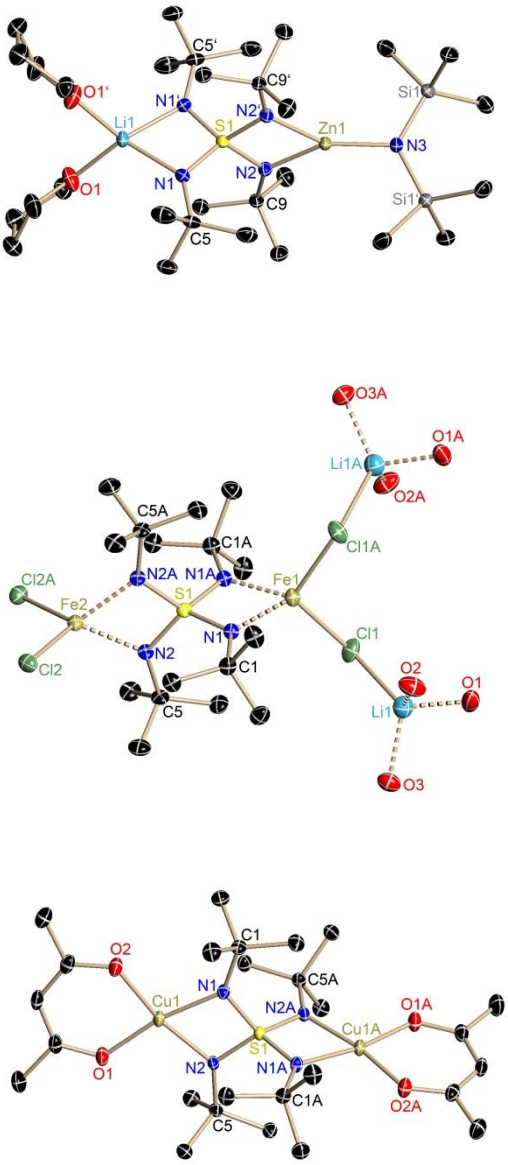

Figure 4.1: Homo- and hetero bimetallic complexes (**5**, **6**, **8**) of the $S(NtBu)_4^{2-}$ ligand.

Moreover, by defined hydrolyses with water, several interesting metal compounds could be obtained (**3**, **4**, **9**). Also, different metal cations could be coordinated in this way, which reflects the high flexibility of this ligand. For these three complexes it could also assumed that polarized sulfur-nitrogen bonds with a covalent character and an additively ionic part are present.

Furthermore, two novel tetrahedrally coordinated sulfur compounds with different coordinated Lewis bases, $[(py)_4Li_2(N\textit{t}Bu)_4S]$ (**11**) and $[(dme)_2Li_2(N\textit{t}Bu)_4S]$ (**12**), could be obtained. These complexes are potential starting materials for further transmetalation reactions.

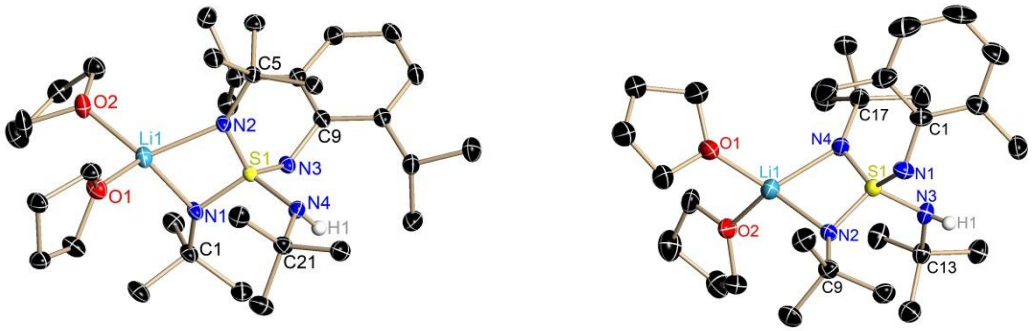

Figure 4.2: Novel lithiated complexes of a sulfur-nitrogen ligand (**14**, **15**).

Additionally, novel asymmetric complexes of a tetrahedrally coordinated sulfur atom with three equal and one variable imido group could be obtained and characterized (Figure 4.2). It could be shown that the variation of the imido group influences the $S(N_4R_3R')^{2-}$ ligand so that one nitrogen atom could be protonated and only the mono lithiated species of this sulfur-nitrogen ligand could be synthesized. The deprotonation of these ligands followed by metalation represents a very advantageous tool for the synthesis of new hetero bimetallic compounds.

Finally, the hydrolyzed di(t*ert*butyl)seleninyldiimide and the di(t*ert*butyl)-seleniumdiimide could be synthesized and characterized (Figure 4.3). The literature known synthesis of $Se(N\textit{t}Bu)_2$[76] always led to a mixture of the desired compound and the hydrolyzed form, $OSe(NH\textit{t}Bu)_2$. The non-hydrolyzed species and the hydrolyzed compound could only be obtained by an optimized reaction pathway.

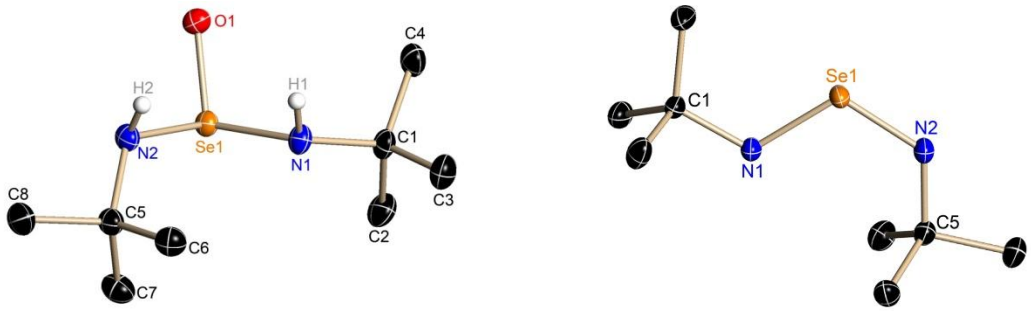

Figure 4.3: Synthesized OSe(NH*t*Bu)$_2$ (**16**) and Se(N*t*Bu)$_2$ (**17**).

The *syn, anti* conformation of the moieties in Se(N*t*Bu)$_2$ (**17**) could be confirmed in solid state. In future, the synthesis of the seleniumtriimide, the metalation and electron-density studies of the Se(N*t*Bu)$_2$ should be carried out to compare it to the chalcogen-nitrogen compounds and to characterize the structural behavior of these complexes.

5. Experimental section

5.1. General procedure

All experiments were performed either under an inert gas atmosphere of purified dry argon with standard *Schlenk* techniques or in an argon box.[126, 127] The glassware was dried at 130°C, assembled hot and was cooled under reduced pressure. All solvents were dried over appropriate alkali metals, distilled and degassed prior to use.

5.2 Spectroscopic and analytic methods

5.2.1. Nuclear magnetic resonance

All samples were prepared and filled into *Schlenk*-NMR tubes inside an argon dry box. The NMR tube was sealed to exclude any impurities. Solvents were dried with potassium. Spectra were recorded at variable temperatures at a *Bruker Avance 300*, or a *Bruker Avance 500* NMR spectrometer. All chemical shifts δ are given in ppm, relative to the residual proton signal of the deuterated solvent. Assignments of the shifts were checked by two-dimensional correlation spectra.

5.2.2. Mass spectrometry

EI-spectra were recorded with a *MAT 95* device (EI-MS: 70 eV). Peaks are given as a mass to charge ratio (*m/z*) of the fragment ions, based on the molecular mass of the isotopes with the highest natural abundance.

5.2.3. Elemental analysis

Elemental analysis was performed as a combustion analysis by the *Analytische Labor des Institutes für Anorganische Chemie* at the Georg-August Universität Göttingen with an *elementar vario EL III* device.

5.2.4. Mößbauer experiments

Mößbauer spectra were recorded with a ^{57}Co source in a Rh matrix using an alternating constant acceleration *Wissel* Mößbauer spectrometer operated in the transmission mode and equipped with a *Janis* closed-cycle helium cryostat. Isomer shifts are given relative to iron metal at ambient temperature (80 K). Simulation of the experimental data was performed with the *Mfit* program.[128]

6. Syntheses

6.1. [Cu(N*t*Bu)Cu(N(SiMe$_3$)$_2$)] (2)

A mixture of $CuCl_2$ (39.5 mg, 0.294 mmol, 2.0 eq) and $Li(N(SiMe_3)_2)$ (60.1 mg, 0.294 mmol, 2.0 eq) in THF (5 mL) was stirred over night at room temperature. $[(thf)_4Li_2(NtBu)_4S]$ (100 mg, 0.147 mmol, 1.0 eq) in THF/water (2 mL/0.5 mL) was added to the green solution and stirred over night. After LiCl was separated by filtration and the dark red solution was stored at –24°C, colorless crystals were obtained after one week.

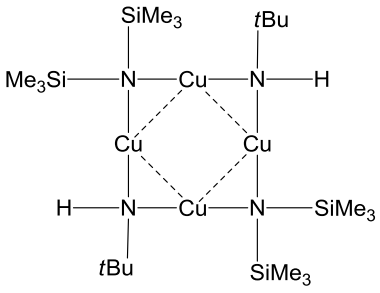

Yield: 48 mg, 0.067 mmol, 46 %

^{1}H–NMR (300.13 MHz, THF–d_8): δ = 3.73 (s, 2 H, N<u>*H*</u>), 1.26 (s, 18 H, NHC<u>*H*$_3$</u>), 0.06 (s, 36 H, SiC<u>*H*$_3$</u>) ppm.

6.2. $[Cu(N\mathit{t}Bu)_2(N(H)\mathit{t}Bu)SO]_2$ (3)

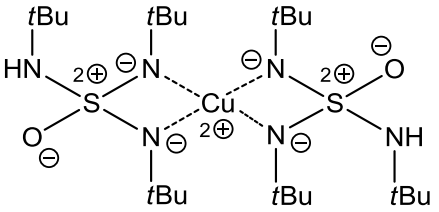

A mixture of $CuCl_2$ (39.5 mg, 0.294 mmol, 2.0 eq) and $Li(N(SiMe_3)_2)$ (60.1 mg, 0.294 mmol, 2.0 eq) in toluene (5 mL) was stirred over night at room temperature. $[(thf)_4Li_2(N\mathit{t}Bu)_4S]$ (100 mg, 0.147 mmol, 1.0 eq) in THF/water (2 mL/0.5 mL) was added to the white solution and stirred over night. After LiCl, Li-HMDS and $\mathit{t}BuNH_2$ were separated by filtration and the yellow solution was stored at –24°C, colorless crystals were obtained after one week.

Yield: 52 mg, 0.088 mmol, 60 %

Elemental analysis (found (calc.) [%]): C 35.38 (48.99), H 6.84 (9.59), N 10.03 (14.28), S 7.11 (10.90). Deviations caused by residual grease $((Me_2SiO)_n)$.

^{1}H–NMR (300.13 MHz, THF–d_8): δ = 5.45 (s, 2 H, N$\underline{H}$), 1.29 (s, 54 H, C$\underline{H_3}$) ppm.

^{13}C{^{1}H}–NMR (75.468 MHz, THF–d_8): δ = 31.4 (18 $\underline{C}H_3$), 29.0 (6 $\underline{C}(CH_3)_3$) ppm.

^{15}N–NMR (30.432 MHz, THF–d_8): δ = –307.9 (2 $\underline{N}$H), –111.8 (4 $\underline{N}$) ppm.

EI-MS m/z [%]: 650.2 ($[Cu\{(N\mathit{t}Bu)_2(N(H)\mathit{t}Bu)SO\}_2+Cu^+]^+$, 6), 207 ($[Cu(NH\mathit{t}Bu)_2]^+$, 12).

6.3. [Zn{(N*t*Bu)$_2$(N(H)*t*Bu)SO}$_2$] (4)

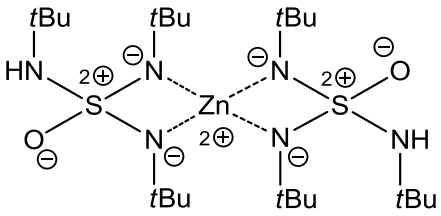

A mixture of $ZnCl_2$ (40.1 mg, 0.294 mmol, 2.0 eq) and $Li(N(SiMe_3)_2)$ (60.1 mg, 0.294 mmol, 2.0 eq) in toluene (5 mL) was stirred over night at room temperature. $[(thf)_4Li_2(NtBu)_4S]$ (100 mg, 0.147 mmol, 1.0 eq) in THF/water (2 mL/0.5 mL) was added to the white solution and stirred over night. After LiCl, Li-HMDS and *t*BuNH$_2$ were separated by filtration and the yellow solution was stored at –24°C, yielding colorless crystals after one week.

Yield: 63 mg, 0.107 mmol, 73 %

Elemental analysis (found (calc.) [%]): C 39.20 (48.84), H 6.78 (9.56), N 10.34 (14.24), S 7.62 (10.86). Deviations caused by residual grease ($(Me_2SiO)_n$).

^{1}H–NMR (300.13 MHz, THF–d_8): δ = 5.55 (s, 2 H, N*H*), 1.30 (s, 54 H, CH_3) ppm.

^{13}C{^{1}H}–NMR (75.468 MHz, THF–d_8): δ = 31.2 (18 $\underline{C}H_3$), 28.8 (6 $\underline{C}(CH_3)_3$) ppm.

^{15}N–NMR (30.432 MHz, THF–d_8): δ = –365.7 (2 $\underline{N}$H), –227.3 (4 $\underline{N}$) ppm.

EI-MS m/z [%]: 500.9 ([OS_2(N*t*Bu)$_4$(NH*t*Bu)]$^+$, 9), 451 ([S(N*t*Bu)$_5$Zn]$^+$, 9), 429 ([O_2S(N*t*Bu)$_3$(NH*t*Bu)Zn]$^+$, 10), 327 ([OS(N*t*Bu)$_2$(NH*t*Bu)Zn]$^+$, 8), 207 ([Zn(N*t*Bu)$_2$]$^+$, 100).

6.4. [(thf)$_2$Li(N(SiMe$_3$)$_2$)Zn(N*t*Bu)$_4$S] (5)

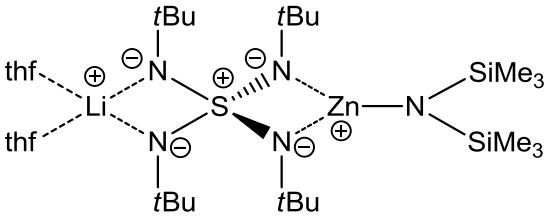

A solution of $ZnCl_2$ (80 mg, 0.591 mmol, 2.0 eq) and Li(N(SiMe$_3$)$_2$) (120 mg, 0.591 mmol, 2.0 eq) in toluene (3 mL) was stirred at room temperature for 4 h. [(thf)$_4$Li$_2$(N*t*Bu)$_4$S] (201 mg, 0.296 mmol, 1.0 eq) in THF (2 mL) was added to the white solution and stirred over night. After lithium chloride was separated by filtration and the brown solution was stored at –24°C for 4 days, colorless crystals were obtained.

Yield: 71 mg, 0.102 mmol, 34 %

Elemental analysis (found (calc.) [%]): C 50.97 (51.96), H 9.34 (10.17), N 9.89 (10.10), S 4.76 (4.62).

^{1}H–NMR (300.13 MHz, THF–d_8): δ = 3.59–3.57 (m, 8 H, O(C$\underline{H}_2$)$_2$), 1.74–1.71 (m, 8 H, O(CH$_2$)$_2$(C$\underline{H}_2$)$_2$), 1.30 (s, 54 H, C$\underline{H}_3$). ppm.

^{7}Li–NMR (116.64 MHz, THF–d_8): δ = 0.18 (s, 1 Li) ppm.

^{13}C{^{1}H}–NMR (75.468 MHz, THF–d_8): δ = 67.5 (4 O($\underline{C}$H$_2$)$_2$, 57.6 (4 $\underline{C}$CH$_3$), 30.4 (18 $\underline{C}$H$_3$), 26.3 (4 O(CH$_2$)$_2$($\underline{C}$H$_2$)$_2$) ppm.

^{15}N–NMR (30.432 MHz, THF–d_8): δ = –355.56 (1 $\underline{N}$), –218.54 (4 $\underline{N}$) ppm.

^{29}Si–NMR (59.627 MHz, THF–d_8): δ = –113.0 (s, 2 Si) ppm.

6.5. [{(thf)$_3$Li}$_2$(FeCl)$_2$(N*t*Bu)$_4$S] (6)

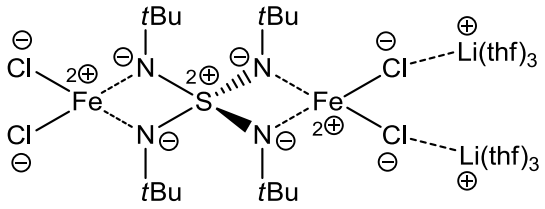

A solution of $FeCl_2$ (37 mg, 0.295 mmol, 2.0 eq) and Li(N(SiMe$_3$)$_2$) (0.81 mg, 0.240 mmol, 1.6 eq) in toluene (2 mL) was stirred for 4 h at room temperature. [(thf)$_4$Li$_2$(N*t*Bu)$_4$*S*] (100 mg, 0.147 mmol, 1.0 eq) in THF (2 mL) was added to the green solution and stirred over night. After the brown solution was stored at –24°C, colorless crystals were obtained after one week.

Yield: 112 mg, 0.120 mmol, 82 %

Elemental analysis (found (calc.) [%]): Due to the low yield and the extreme sensibility of this compound a correct elemental analysis could not be obtained.

^{1}H–NMR (500.13 MHz, THF–d_8): δ = 3.42–3.68 (m, 24 H, OC$\underline{H}_2$) 1.64–1.83 (m, 24H, C$\underline{H}_2$), 1.31 (s, 36 H, C$\underline{H}_3$) ppm.

^{7}Li–NMR (194.37 MHz, THF–d_8): δ = 3.5 (s, Li) ppm.

^{13}C{^{1}H}–NMR (125.758 MHz, THF–d_8): δ = 67.4 (12 O$\underline{C}$H$_3$), 29.8 (12 $\underline{C}$H$_3$), 25.3 (12 OCH$_2\underline{C}$H$_2$) ppm.

Mössbauer: hs-Fe(II) (78.47 %): δ_{exp} = 0.88 mm/s

$|\Delta E_a|$ = 3.63 mm/s

Γ_{FWHM} = 0.58 mm/s

hs-Fe(III) (21.53 %): δ_{exp} = 0.40 mm/s

$|\Delta E_a|$ = 0.95 mm/s

Γ_{FWHM} = 0.58 mm/s (correlated)

6.6. [(acac)$_2$Cu$_2$(N*t*Bu)$_4$S] (8)

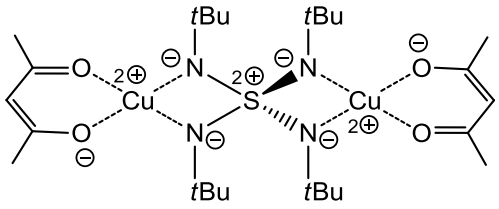

Cu(acac)$_2$ (77 mg, 0.294 mmol, 2.0 eq) and [(thf)$_4$Li$_2$(N*t*Bu)$_4$S] (100 mg, 0.147 mmol, 1.0 eq) were dissolved in THF (10 mL) and stirred over night at room temperature. After lithium acetylacetonate was removed by filtration and the green solution was stored at -24°C for 3 month, colorless crystals were obtained.

Yield: 56 mg, 0.087 mmol, 59 %

Elemental analysis (found (calc.) [%]): C 44.23 (48.65), H 7.47 (7.85), N 6.76 (8.73), S 4.94 (5.00).

This poor elemental analysis is due to the contamination of the sample with approximately 25 % silicon join grease (at 0.09 ppm in the ^{1}H-NMR and at 1.35 ppm in the ^{13}C-NMR for (OSiMe$_2$)$_n$). Due to paramagnetism the NMR signals are very broad.

^{1}H–NMR (400.13 MHz, THF–d_8): δ = 5.72 (s, 36 H, C<u>*H*</u>$_3$), 3.88 (s, 12 H, C<u>*H*</u>$_3$), –16.74 (s, 2 H, C<u>*H*</u>) ppm.

^{15}N–NMR (30.432 MHz, THF–d_8): δ = –269.0 (<u>*N*</u>) ppm.

EI-MS m/z [%]: 640 ([(acac)$_2$Cu$_2$(N*t*Bu)$_4$S]$^+$, 50), 625 ([(acac)$_2$Cu$_2$(N*t*Bu)$_4$S-O]$^+$, 25), 395 ([OCu(N*t*Bu)$_4$S]$^+$, 58), 380 ([Cu(N*t*Bu)$_4$S]$^+$, 30), 336 ([(acac)Cu(N*t*Bu)$_2$S]$^+$,10), 324 ([Cu$_2$(acac)$_2$]$^+$, 100), 304 ([(acac)Cu(N*t*Bu)$_2$]$^+$, 14).

6.7. [(acac)Pd(N*t*Bu)$_2$(N(H)*t*Bu)SO] (9)

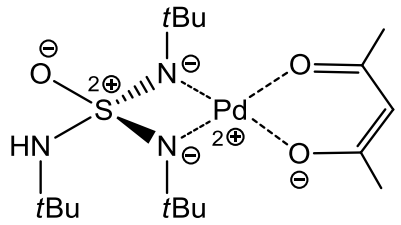

Pd(acac)$_2$ (119 mg, 0.294 mmol, 2.0 eq) and [(thf)$_4$Li$_2$(N*t*Bu)$_4$S] (100 mg, 0.147 mmol, 1.0 eq) in THF/water (11 mL/0.5 mL) was stirred over night. After Li(acac) and *t*BuNH$_2$ were separated by filtration and the brown solution was stored at –24°C, yellow-orange crystals were obtained after 4 weeks.

Yield: 55 mg, 0.118 mmol, 80 %

Elemental analysis (found (calc.) [%]): C 42.56 (43.63), H 7.57 (7.54), N 8.08 (8.98), S 6.73 (6.85).

^{1}H–NMR (300.13 MHz, THF–d_8): δ = 6.42 (s, 1 H, N*H*), 5.31 (s, 1 H, C*H*), 1.84 (s, 6 H, C*H*$_3$), 1.46 (s, 9 H, NHC*H*$_3$), 1.38 (s, 18 H, NC*H*$_3$) ppm.

^{13}C{^{1}H}–NMR (75.468 MHz, THF–d_8): δ = 185.9 (2 *C*CH$_3$), 100.2 (1 *C*H), 56.9(2 N*C*(CH$_3$)$_3$), 54.0 (1 NH*C*(CH$_3$)$_3$), 31.3 (6 NC(*C*H$_3$)$_3$), 30.7 (3 NHC(*C*H$_3$)$_3$), 25.6 (2 *C*H$_3$) ppm.

^{15}N–NMR (30.432 MHz, THF–d_8): δ = –312.5 (2 *N*), –246.4 (1 *N*H) ppm.

EI-MS m/z [%]: 467 ([(acac)Pd(N*t*Bu)$_2$(N(H)*t*Bu)SO]$^+$, 50), 452 ([(acac)Pd-(N*t*Bu)$_2$(N(H)*t*Bu)SH]$^+$, 100), 396 ([(acac)Pd(N*t*Bu)(N(H)*t*Bu)SO]$^+$, 58), 395 ([(acac)Pd(N*t*Bu)$_2$SO]$^+$, 44), 262 ([(N*t*Bu)$_2$(N(H)*t*Bu)SO]$^+$, 22), 205 ([Pd(acac)]$^+$, 12).

6.8. $[(py)_4Li_2(NtBu)_4S]$ (11)

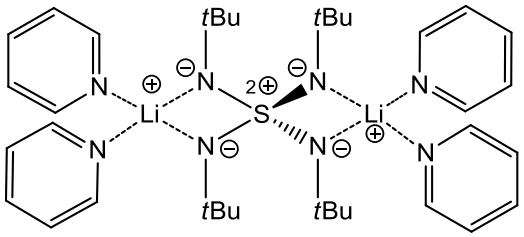

To the cooled suspension (–78°C) of 1.476 M *n*BuLi (2.70 mL, 4 mmol, 2.0 eq) *t*BuNH$_2$ (0.42 mL, 4 mmol, 2.0 eq) was added dropwise. After one hour stirring S(NtBu)$_3$ (490 mg, 2 mmol, 1.0 eq) dissolved in distillated, dried pyridine (5 mL) was added to the white reaction mixture. The brown solution was stirred over night at rt. After two days at rt colorless crystals could be obtained.

Yield: 705 mg, 1.091 mmol, 55 %

Elemental analysis (found (calc.) [%]): C 58.80 (66.85), H 7.57 (8.73), N 15.47(17.32), S 6.82 (4.96)

^{1}H–NMR (300.13 MHz, THF–d_8): δ = 8.54–8.52 (m, 8 H, NC<u>*H*</u>), 7.68–7.62 (m, 4 H, N(CH)$_2$C<u>*H*</u>), 7.27–7.22 (m, 8 H, NCHC<u>*H*</u>), 1.38 (s, 36 H, C<u>*H*$_3$</u>) ppm.

^{7}Li–NMR (116.64 MHz, THF–d_8): δ = 1.1 (s, Li) ppm.

^{13}C{^{1}H}–NMR (75.468 MHz, THF–d_8): δ = 150.6 (8 N<u>*C*</u>H), 136.1 (4 N(CH)$_2$<u>*C*</u>H), 124.2 (8 NCH<u>*C*</u>H), 51.3 (2 <u>*C*</u>CH$_3$), 34.2 (12 <u>*C*</u>H$_3$) ppm.

^{15}N–NMR (30.432 MHz, THF–d_8): δ = –358.7 (4 <u>*N*</u>), –263.8 (4 <u>*N*</u>*t*Bu) ppm.

6.9. [(dme)$_2$Li$_2$(N*t*Bu)$_4$S] (12)

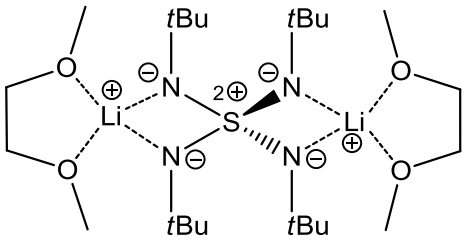

To a cooled suspension (–78°C) of 1.476 M *n*BuLi (2.70 mL, 4 mmol, 2.0 eq) *t*BuNH$_2$ (0.42 mL, 4 mmol, 2.0 eq) was added dropwise. After one hour stirring S(NtBu)$_3$ (490 mg, 2 mmol, 1.0 eq) in distillated, dried 1,2-dimethoxyethan (5 mL) was added to the white reaction mixture. The brown solution was stirred over night at rt. After two days at rt colorless crystals could be obtained.

Yield: 688 mg, 1.35 mmol, 68 %

Elemental analysis (found (calc.) [%]): C 53.65 (56.45), H 9.30 (11.05), N 10.57 (10.97), S 6.27 (6.28).

^{1}H–NMR (300.13 MHz, THF–d_8): δ = 3.43 (s, 8 H, C<u>*H*</u>$_2$), 3.27 (s, 12 H, OC<u>*H*</u>$_3$), 1.38 (s, 36H, C<u>*H*</u>$_3$) ppm.

^{7}Li–NMR (116.64 MHz, THF–d_8): δ = 0.8 (s, Li) ppm.

^{13}C{^{1}H}–NMR (75.468 MHz, THF–d_8): δ = 72.7 (4 O<u>*C*</u>H$_2$), 58.8 (4 O<u>*C*</u>H$_3$), 51.4 (4 <u>*C*</u>CH$_3$), 34.3 (12 <u>*C*</u>H$_3$) ppm.

^{15}N–NMR (30.432 MHz, THF–d_8): δ = –260.8 (4 <u>*N*</u>) ppm.

EI-MS m/z [%]: 421.3 ([(dme)Li$_2$(NH*t*Bu)(N*t*Bu)$_3$S]$^+$, 20).

6.10.[(thf)$_2$Li(N*t*Bu)$_2$(NH*t*Bu)S(Ndipp)] (14)

To a cooled suspension of 1.66 M *n*BuLi (2.41 mL, 4 mmol, 2.0 eq) distillated diisopropylaniline (0.75 mL, 4 mmol, 2.0 eq) was added. The white suspension was stirred 30 min at rt. Then S(NtBu)$_3$ (490 mg, 2 mmol, 1.0 eq) in THF (6 mL) was added dropwise and was stirred over night at rt. After half of the solvent was removed *in vacuo* the brown solution was stored at –24°C, yielding brown crystals after 5 weeks.

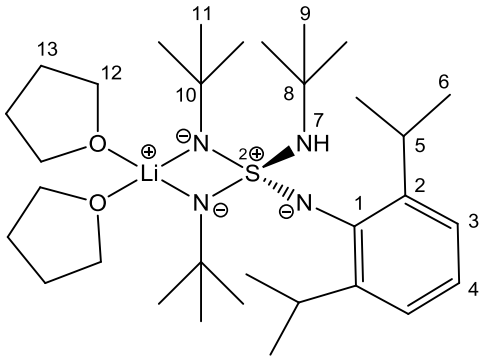

Yield: 502mg, 0.876 mmol, 44 %

Elemental analysis (found (calc.) [%]): C 65.33 (67.09), H 9.45 (10.73), N 8.64 (9.78), S 5.13 (5.60).

^{1}H–NMR (300.13 MHz, THF–d_8): δ = 7.25 (s, 1 H, N$\underline{H}^7$), 6.85–6.83 (m, 1 H, C$\underline{H}^4$), 6.53–6.51 (m, 2 H, C$\underline{H}^3$), 3.59–3.57 (m, 8 H, C$\underline{H}_2{}^{12}$), 2.96–2.93 (m, 2 H, CH^5), 1.74–1.71 (m, 8 H, C$\underline{H}_2{}^{13}$), 1.31 (s, 18 H, C$\underline{H}_3{}^{11}$), 1.22 (s, 9 H, C$\underline{H}_3{}^9$), 1.16 (s, 12 H, C$\underline{H}_3{}^6$) ppm.

^{7}Li–NMR (116.64 MHz, THF–d_8): δ = –1.2(s, Li) ppm.

^{13}C{^{1}H}–NMR (75.468 MHz, THF–d_8): δ = 140.2 (1 $\underline{C}^1$), 132.1 (2 $\underline{C}^2$), 122.6 (2 $\underline{C}^3$), 118.2 (2 $\underline{C}^4$), 67.4 (4 $\underline{C}^{12}$), 58.1 (1 $\underline{C}^8$), 34.0 (2 $\underline{C}^{10}$), 30.1 (6 $\underline{C}^{11}$), 27.9 (3 $\underline{C}^9$), 26.3 (2 $\underline{C}^5$), 25.2 (4 $\underline{C}^{13}$), 22.4 (4 $\underline{C}^6$) ppm.

^{15}N–NMR (30.432 MHz, THF–d_8): δ = –251.0 (1 $\underline{N}$), –220.3 (3 $\underline{N}$H/Li) ppm.

EI-MS m/z [%]: 350.4 ([(N*t*Bu)(NH*t*Bu)S(Ndipp)]$^+$, 20), 336.3 ([(*t*Bu)(NH*t*Bu)S(Ndipp)]$^+$, 34).

6.11. [(thf)$_2$Li(N*t*Bu)$_2$(NH*t*Bu)S(Ndmp)] (15)

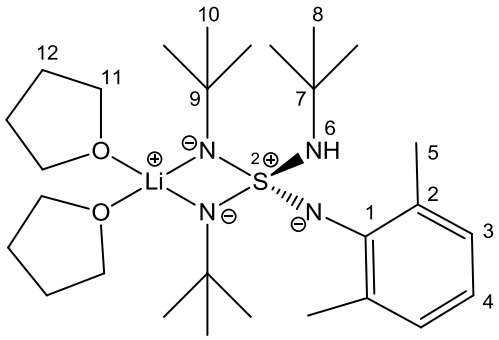

To a cooled suspension of 1.66 M *n*BuLi (2.41 mL, 4 mmol, 2.0 eq) distillated dimethylaniline (0.75 mL, 4 mmol, 2.0 eq) in THF (6 mL) was added. The white-yellow suspension was stirred 30 min at rt. Then S(NtBu)$_3$ (490 mg, 2 mmol, 1.0 eq) in THF (6 mL) was added dropwise and stirred over night at rt. After half of the solvent was removed *in vacuo* the brown solution was stored at –24°C, yielding brown crystals after 5 weeks.

Yield: 420 mg, 0.813 mmol, 41 %

Elemental analysis (found (calc.) [%]): C 65.08 (65.08), H 8.72 (10.34), N 10.10 (10.84), S 6.16 (6.21)

^{1}H–NMR (300.13 MHz, THF–d_8): δ = 7.19 (s, 1 H, N$\underline{H}^6$), 6.69–6.67 (m, 1 H, C$\underline{H}^4$), 6.10–6.07 (m, 2 H, C$\underline{H}^3$), 3.60–3.56 (m, 8 H, C$\underline{H}_2{}^{11}$), 1.75–1.72 (m, 8 H, C$\underline{H}_2{}^{12}$), 1.36 (s, 9 H, C$\underline{H}_3{}^8$), 1.31 (s, 6 H, C$\underline{H}_3{}^5$), 1.18 (s, 18 H, C$\underline{H}_3{}^{10}$) ppm.

^{7}Li–NMR (116.64 MHz, THF–d_8): δ = 1.0(s, Li) ppm.

^{13}C{^{1}H}–NMR (75.468 MHz, THF–d_8): δ = 142.6 (1 $\underline{C}^1$), 128.2 (2 $\underline{C}^2$), 126.5 (2 $\underline{C}^3$), 113.8 (1 $\underline{C}^4$), 67.5 (4 $\underline{C}^{11}$), 52.1 (1 $\underline{C}^7$), 51.2 (2 $\underline{C}^9$), 33.0 (9 $\underline{C}^{8,10}$), 29.8 (2 $\underline{C}^5$), 25.3 (4 $\underline{C}^{12}$) ppm.

^{15}N–NMR (30.432 MHz, THF–d_8): δ = –259.0 (2 $\underline{N}$Li), –254.3 (1 $\underline{N}$H), –218.5 (1 $\underline{N}$) ppm.

6.12. $OSe(NHtBu)_2$ (16)

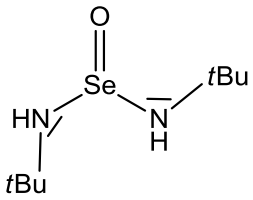

To a cooled (–78°C) white suspension of $SeCl_4$ (2.21 g, 10 mmol, 1.0 eq) in 50 mL Et_2O tBuNH$_2$ (6.20 mL, 60 mmol, 6.0 eq) was added dropwise. After the shining yellow suspension was stirred 45 min at –78°C, the reaction mixture was heated up to rt and stirred for another 30 min. The resulting tBuNH$_3$Cl was removed by filtration and the residue was washed by Et_2O (3 x 10 mL). Thereby the filtration was cooled (–30°C). This filtration was repeated to remove the whole solid. After the yellow solution was stored at –24°C, yellow crystals could obtained after one day.

Yield: 660 mg, 2.78 mmol, 27.8 %

$OSe(NHtBu)_2$: (*E*)-$Se(NtBu)_2$: (*Z*)-$Se(NtBu)_2$ (2.5 eq : 1.0 eq : 1.0 eq)

Elemental analysis (found (calc.) [%]): C 29.45 (40.51), H 5.80 (7.65), N 6.62 (11.81). Deviations caused by residual $Se(NtBu)_2$ and $SeCl_4$.

^{1}H–NMR (500.13 MHz, toluene–d_8): δ = 5.17 (s, 2 H, NH), 1.74 (s, 18 H, C$\underline{H}_3$(*E*-Isomer)), 1.24 (s, 18 H, C$\underline{H}_3$), 1.28 (s, 18 H, C$\underline{H}_3$(*Z*-Isomer)) ppm.

^{13}C{^{1}H}–NMR (125.758 MHz, toluene–d_8): δ = 66.6 (1 $\underline{C}$(CH$_3$)$_3$ (*Z*-Isomer)), 65.3 (1 $\underline{C}$(CH$_3$)$_3$ (*E*-Isomer)), 53.5 (1 $\underline{C}$(CH$_3$)$_3$), 33.0 (1 $\underline{C}$H$_3$ (*Z*-Isomer)), 31.6 (1 $\underline{C}$H$_3$), 28.8 (1 $\underline{C}$H$_3$ (*E*-Isomer)) ppm.

6.13. $Se(NtBu)_2$ (17)

done by Dr. Nina Lock

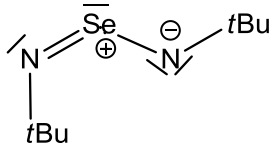

To a cooled (–78°C) white suspension of $SeCl_4$ (2.21 g, 10 mmol, 1.0 eq) in 50 mL DCM tBuNH$_2$ (6.20 mL, 60 mmol, 6.0 eq) was added dropwise. After the shining yellow suspension was stirred 45 min at –78°C and 30 min at 0°C, the reaction mixture, the resulting tBuNH$_3$Cl was removed by filtration and the residue was washed by DCM (3 x 10 mL). Thereby the filtration was cooled (–30°C). Half of the solvent was removed *in vacuo* at 0°C and toluene was added. After the yellow solution was stored at –78°C, yellow crystals could obtained after three month.

Yield: 312 mg, 1.412 mmol, 14.1 %

Elemental analysis (found (calc.) [%]):C 43.36 (43.44), H 8.45 (8.20), N 11.44 (12.66).

^{1}H–NMR (400.130 MHz, toluene–d_8): δ = 1.77 (s, 18 H, C$\underline{H}_3$ (*E*-Isomer)), 1.12 (s, 18 H, C$\underline{H}_3$ (*Z*-Isomer)) ppm.

^{13}C{^{1}H}–NMR (100.613 MHz, toluene–d_8): δ = 66.0 (1 $\underline{C}$(CH$_3$)$_3$ (*Z*-Isomer)), 65.6 (1 $\underline{C}$(CH$_3$)$_3$ (*E*-Isomer)), 32.5 (1 $\underline{C}$H$_3$ (*Z*-Isomer)), 28.4 (1 $\underline{C}$H$_3$ (*E*-Isomer)) ppm.

^{15}N–NMR (40.560 MHz, toluene –d_8): δ = –5.71 (2 $\underline{N}$ (*Z*-Isomer)), 101.9 (2 $\underline{N}$ (*E*-Isomer)) ppm.

^{77}Se–NMR (76.311 MHz, toluene –d_8): δ = 1656.1 ppm.

7. Crystallographic section

7.1. Crystal application

The crystal selection was carried out on a moveable table that is equipped with a vacuum line including a high vacuum sliding vane rotary pump, an argon gas supply, a polarisation microscope equipped with an X-TEMP2 crystal cooling device.[129, 130] Air and moisture sensitive crystals were taken directly from Schlenk flasks. Crystal selection and manipulation was carried out under the microscope in a drop of perfluorinated polyether oil.[131] The X-TEMP2 device was used to cool the glass object slide during crystal manipulation. Suitable crystals were selected using the polarisation filter of the microscope. The crystals were mounted in a very small amount of the perfluorinated polyether on the tip of a glass fiber or in a MiTeGen Kryoloop. The sample was very quickly placed in the cold gas stream of the sample cooling device of the diffractometer.

7.2. Data collection and processing

All compounds were measured on a *Bruker D8 Goniometer* platform, equipped with an *APEX II CCD* X-ray detector. The compounds were measured using either an *Incoatec* microfocus source with mirror optics[132] or on a rotating anode turbo X-ray source. Both are equipped with an *APEX II CCD* detector, mounted on a three-circle *D8 goniometer*, and mirrors as monochromator optics, which supplies very intense and brilliant MoK_α radiation ($\lambda = 0.71073$ Å). All crystals were centered optically using a video camera after being placed on the diffractometer.

Data collection was controlled by the *APEX2* package.[133] A test run (matrix scan) was recorded prior to each experiment to check the crystal quality, to get a rough estimate of the cell parameters, and to determine the optimum exposure time. All scans of the data collections were performed in an ω-scan mode with a step-width of 0.3° or 0.5° at fixed ϕ-angles.

The determination of the unit cells and orientation matrices was performed with the tools supplied in the *APEX2* package.[133] The collected frames were integrated with *SAINT*[134] using the 3d profiling method described by *Kabsch*.[135] All data sets were

corrected for absorption and scaled using *SADABS*[136] or *TWINABS*.[137] *SADABS* and *TWINABS* refine an empirical model function by symmetry-equivalent reflections.

7.3. Structure solution and refinement

The structures were solved with direct methods or Patterson superposition procedure using *SHELXS*.[138] Data were merged according to the determined symmetry with *SHELXL*.[138] All refinements were performed on F^2 with *SHELXL*. If not stated otherwise, the hydrogen atoms of the compounds were refined isotropically on calculated positions using a riding model. The positions were geometrically optimized and the U_{iso} were constrained to 1.2 U_{eq} of the pivot atom or 1.5 U_{eq} of the methyl carbon atom. The position of certain hydrogen atoms (*e. g*. OH groups) were found with difference *Fourier* analysis of the rest electron density. If not stated otherwise, the hydrogen bond lengths were restrained to a sensible value and the U_{iso} were constrained as mentioned above. In all refinements the function $M(p_i, k)$ (Eq. 7-1) was minimized using the weights w_H defined in Eq. 7-2.

Eq. 7-1. $$M(p_i, k) = \sum_H w_H [k|F_{obs}(H)|^2 - |F_{calc}(H)|^2]^2 = \min$$

Eq. 7-2. $$w_H^{-1} = \sigma_H^2 F_{obs}^2 + (g1 \cdot P)^2 + g2 \cdot P \quad \text{with} \quad P = \left(\frac{F_{obs}^2 + 2F_{calc}^2}{3}\right)$$

The results of the refinements were verified by comparison of the calculated and the observed structure factors. Commonly used criteria are the residuals $R1$ (Eq. 7-3) and $wR2$ (Eq. 7-4). The $wR2$ is more significant, because the model is refined against F^2.

Eq. 7-3. $$R1 = \frac{\sum_H (|F_{obs}| - |F_{calc}|)}{\sum_H |F_{obs}|}$$

Eq. 7-4. $$wR2 = \frac{\sum_H w_H (|F_{obs}|^2 - |F_{calc}|^2)^2}{\sum_H w_H |F_{obs}|^4}$$

Additionally, the goodness of fit (GoF, S), a figure or merit showing the relation between deviation of F_{calc} from F_{obs} and the over-determination of refined parameters is calculated (Eq. 7-5).

Eq. 7-5. $$S = \sqrt{\frac{\sum(w_H(F_{obs}^2 - F_{calc}^2)^2)}{(n-p)}}$$

The residual densities from difference *Fourier* analysis should be low. Due to the model restrictions the residuals are normally found in the bonding regions. Higher residuals for heavy scatterers are acceptable as they arise mainly from absorption effects and *Fourier* truncation errors due to the limited recorded resolution range. The highest peak and deepest hole from difference *Fourier* analysis are listed in the crystallographic tables.

Additionally, the orientation, size, and ellipticity of the ADPs show the quality of the model. Ideally, the ADPs should be oriented perpendicular to the bonds, be equal in size, and show little ellipticity. All graphics were generated and plotted with the *XShell* program at the 50 % probability level.

All hydrogen atoms bonded to sp^2 (sp^3) carbon atoms were assigned ideal positions and refined using a riding model with U_{iso} constrained to 1.2 (1.5) times the U_{eq} value of the parent carbon atom. Hydrogen atoms bound to heteroatoms were located on the electron density map and refined using distance restraints. This is necessary because of the low electronegativity of hydrogen. Thus, its electron density is usually delocalised in direction of the heteroatom and only pseudo hydrogen positions can be found.

7.4. Treatment of disorder

Structures containing disordered fragments were refined using constraints and restraints. The geometries of chemically equivalent but crystallographically independent fragments can be fitted to each other by distance restraints. Especially the 1,2 distances (bond lengths) and 1,3 distances (bond angles) are set to be equal within their effective standard deviations. This is helpful for refining disordered positions as the averaging of equivalent fragments implements chemical information and stabilizes the refinement.

7.5. Crystallographic details

7.5.1. [Cu(N*t*Bu)Cu(N(SiMe$_3$)$_2$)] (2)

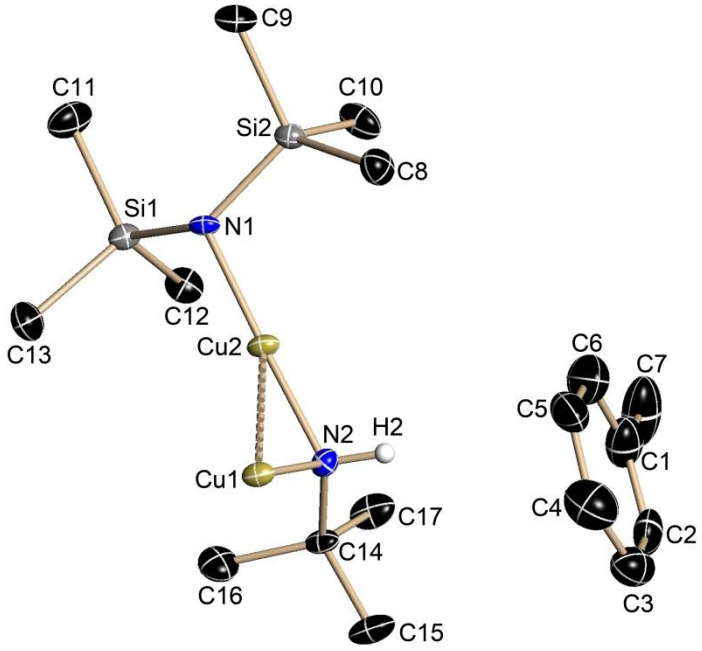

Figure 7.1: Asymmetric unit of [Cu(N*t*Bu)Cu(N(SiMe$_3$)$_2$] (**2**). The anisotropic displacement parameters are depicted at the 50 % probability level. Hydrogen atom H2 was found in the Fourier difference map and refined freely. The other hydrogen atoms are omitted for clarity. The toluene was refined using SIMU and RIGU.

Table 7.1: Crystallographic data of [Cu(N*t*Bu)Cu(N(SiMe$_3$)$_2$ (**2**).

Identification code	sad_a	Z	2
Empirical formula	$C_{27}H_{64}N_4Si_4Cu_4$	ρ_c [Mgm^{-3}]	1.348
Formula weight [g/mol]	811.34	μ [mm^{-1}]	2.240
Temperature [K]	100(2)	F (000)	852
Wavelength [Å]	0.71073	θ-range [°]	1.998-26.016
Crystal system	Monoclinic	Reflections collected	11563
Space group	$P2_1/n$	Completeness to Θmax	99.6 %
a [Å]	8.695(2)	Independent reflections	3918[R(int) = 0.0302]
b [Å]	19.060(2)	Restraints/parameters	118/221
c [Å]	12.319(2)	GooF	1.019
α [°]	90	$R1/wR2$ (I>2σ(I))	0.0363/0.0841
β [°]	101.74(2)	$R1/wR2$ (all data)	0.0541/0.0917
γ [°]	90	Diff. peak and hole [eÅ^{-3}]	2.048/-0.299
V [Å^3]	1998.9(6)	Max./min. transmission	0.4302/0.3815

7.5.2. [Cu{(N*t*Bu)$_2$(N(H)*t*Bu)SO}$_2$] (3)

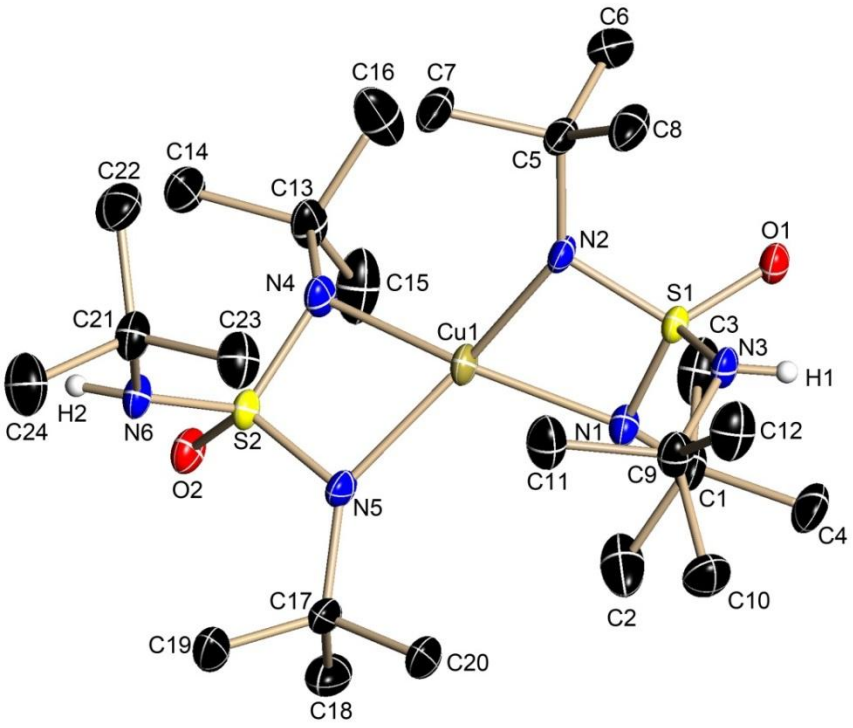

Figure 7.2: Asymmetric unit of [Cu{(N*t*Bu)$_2$(N(H)*t*Bu)SO}$_2$] (**3**). The anisotropic displacement parameters are depicted at the 50 % probability level. Hydrogen atoms H1 and H2 were found in the Fourier difference map and refined freely. The other hydrogen atoms are omitted for clarity.

Table 7.2: Crystallographic data of [Cu{(N*t*Bu)$_2$(N(H)*t*Bu)SO}$_2$] (**3**).

Identification code	sad_a	Z	1
Empirical formula	$C_{24}H_{56}CuN_6O_2S_2$	ρ_c [Mgm^{-3}]	1.265
Formula weight [g/mol]	588.40	μ [mm^{-1}]	0.872
Temperature [K]	100(2)	F (000)	638
Wavelength [Å]	0.71073	θ-range [°]	2.053-28.338
Crystal system	Triclinic	Reflections collected	3192
Space group	$P\bar{1}$	Completeness to Θmax	100.0 %
a [Å]	9.383(6)	Independent reflections	7714 [R(int) = 0.0348]]
b [Å]	9.488(6)	Restraints/parameters	0/342
c [Å]	20.145(13)	GooF	1.051
α [°]	94.44(2)	$R1/wR2$ (I>2σ(I))	0.0481/0.1168
β [°]	95.56(2)	$R1/wR2$ (all data)	0.0590/0.1216
γ [°]	119.03(10)	Diff. peak and hole [eÅ^{-3}]	1.460/-0.642
V [Å^3]	1544.65(17)	Max./min. transmission	0.6494/0.7457

7.5.3. [Zn{(N*t*Bu)$_2$(N(H)*t*Bu)SO}$_2$] (4)

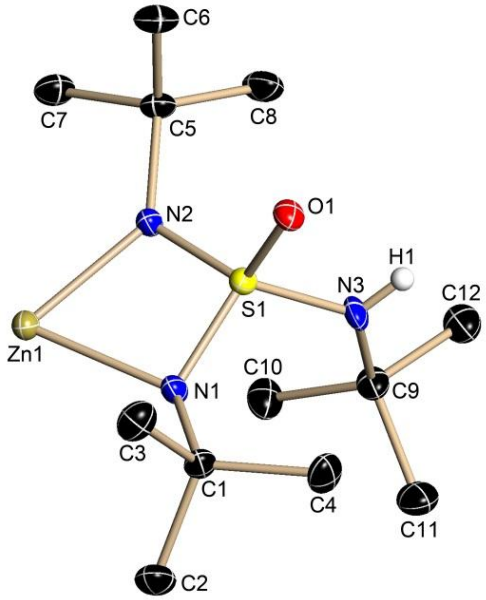

Figure 7.3: Asymmetric unit of [Zn{(N*t*Bu)$_2$(N(H)*t*Bu)SO}$_2$] (**4**). The anisotropic displacement parameters are depicted at the 50 % probability level. Hydrogen atom H1 was found in the Fourier difference map and refined freely. The other hydrogen atoms are omitted for clarity.

Table 7.3: Crystallographic data of [Zn{(N*t*Bu)$_2$(N(H)*t*Bu)SO}$_2$] (**4**).

Identification code	sad_a	Z	4
Empirical formula	$C_{24}H_{56}N_6O_2S_2Zn$	ρ_c [Mgm^{-3}]	1.271
Formula weight [g/mol]	590.23	μ [mm^{-1}]	0.962
Temperature [K]	100(2)	F (000)	1280
Wavelength [Å]	0.71073	θ-range [°]	2.253-25.676
Crystal system	Orthorhombic	Reflections collected	27418
Space group	*Pccn*	Completeness to Θmax	100.0 %
a [Å]	10.877(16)	Independent reflections	2933 [R(int) = 0.0676]
b [Å]	15.680(2)	Restraints/parameters	50/172
c [Å]	18.080(3)	GooF	1.046
α [°]	90	$R1/wR2$ (I>2σ(I))	0.0351/0.0701
β [°]	90	$R1/wR2$ (all data)	0.0556/0.0760
γ [°]	90	Diff. peak and hole [eÅ^{-3}]	0.331/-0.310
V [Å^3]	3083.5(8)	Max./min. transmission	0.6656/0.7455

7.5.4. [(thf)$_2$Li(N(SiMe$_3$)$_2$)Zn(N*t*Bu)$_4$S] (5)

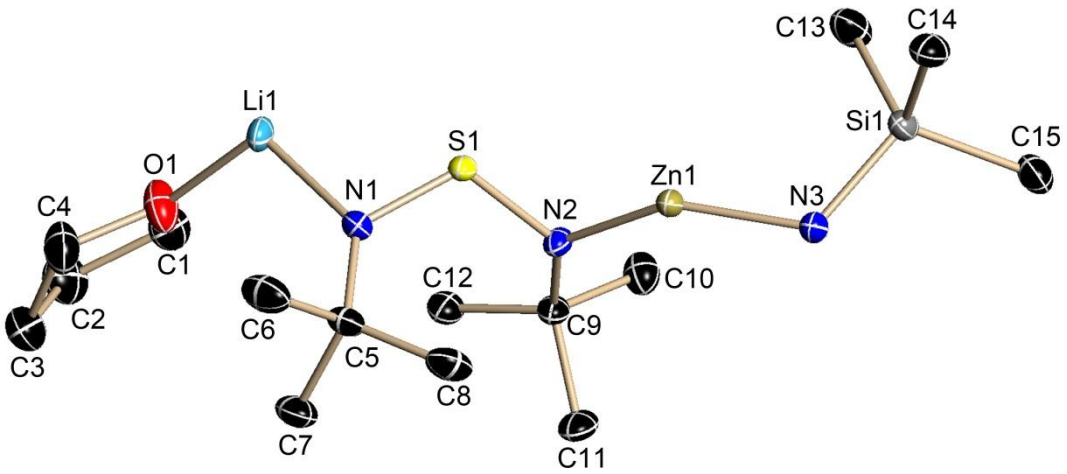

Figure 7.4: Asymmetric unit of [(thf)$_2$Li(N(SiMe$_3$)$_2$)Zn(N*t*Bu)$_4$S] (**5**). The anisotropic displacement parameters are depicted at the 50 % probability level. The hydrogen atoms are omitted for clarity.

Table 7.4: Crystallographic data of [(thf)$_2$Li(N(SiMe$_3$)$_2$)Zn(N*t*Bu)$_4$S] (**5**).

Identification code	sad_a	Z	4
Empirical formula	$C_{30}H_{70}Li\ N_5O2SSi_2Zn$	ρ_c [Mgm^{-3}]	1.160
Formula weight [g/mol]	693.46	μ [mm^{-1}]	0.762
Temperature [K]	100(2)	F (000)	1512
Wavelength [Å]	0.71073	θ-range [°]	1.947-26.015
Crystal system	Monoclinic	Reflections collected	38879
Space group	$C2/c$	Completeness to Θmax	99.8 %
a [Å]	15.507(3)	Independent reflections	3909[R(int) = 0.0773]
b [Å]	15.390(3)	Restraints/parameters	0/202
c [Å]	18.081(3)	GooF	1.230
α [°]	90	$R1/wR2$ (I>2σ(I))	0.0318/0.0792
β [°]	113.090(10)	$R1/wR2$ (all data)	0.0387/0.0814
γ [°]	90	Diff. peak and hole [eÅ^{-3}]	0.373/-0.292
V [Å^3]	3969.4(13)	Max./min. transmission	0.7454/0.6890

7.5.5. [{(thf)$_3$Li}$_2$(FeCl)$_2$(N*t*Bu)$_4$*S*] (6)

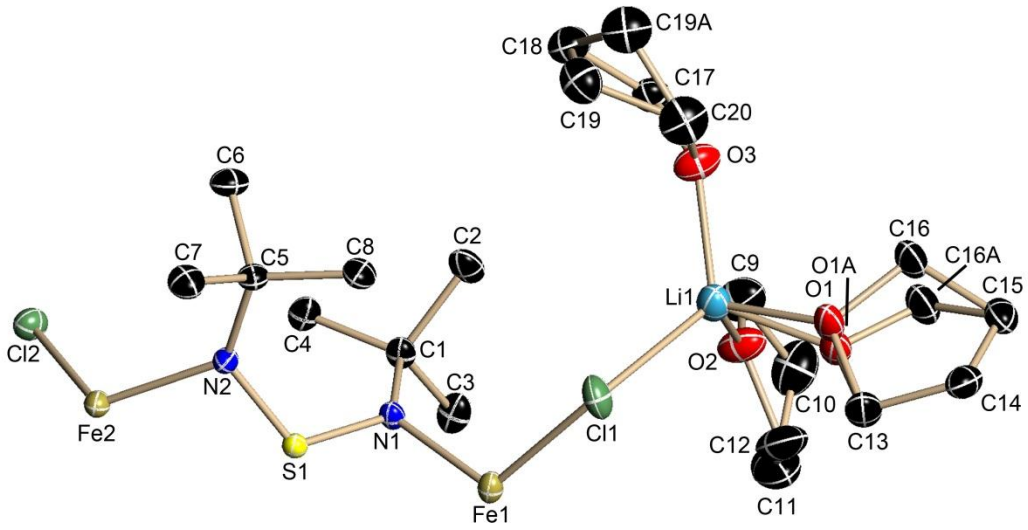

Figure 7.5: Asymmetric unit of [(thf)$_3$Li(FeCl)$_2$(N*t*Bu)$_4$*S*] (**6**). The anisotropic displacement parameters are depicted at the 50 % probability level. The hydrogen atoms are omitted for clarity. The THF molecules are disordered in a ratio of 94:6 (O1:O1A) and 86:14 (C19:C19A). They are refined using SIMU.

Table 7.5: Crystallographic data of[(thf)$_3$Li(FeCl)$_2$(N*t*Bu)$_4$*S*] (**6**).

Identification code	twin4_a	Z	4
Empirical formula	$C_{40}H_{84}Cl_4Fe_2Li_2N_4O_6S$	ρ_c [Mgm^{-3}]	1.291
Formula weight [g/mol]	1016.55	μ [mm^{-1}]	0.843
Temperature [K]	100(2)	F (000)	2168
Wavelength [Å]	0.71073	θ-range [°]	1.775-27.514
Crystal system	Monoclinic	Reflections collected	4388
Space group	C2/c	Completeness to Θmax	100.0 %
a [Å]	21.48(10)	Independent reflections	5997[R(int)=0.0496]
b [Å]	14.48(10)	Restraints/parameters	442/309
c [Å]	19.2(2)	GooF	1.075
α [°]	90	$R1/wR2$ (I>2σ(I))	0.0411/0.0709
β [°]	118.93(10)	$R1/wR2$ (all data)	0.0630/0.0766
γ [°]	90	Diff. peak and hole [eÅ^{-3}]	0.745552/0.615933
V [Å^3]	5229(70)	Max./min. transmission	0.615933/0.745552

7.5.6. $[Li_4(acac)_4(thf)]$ (7)

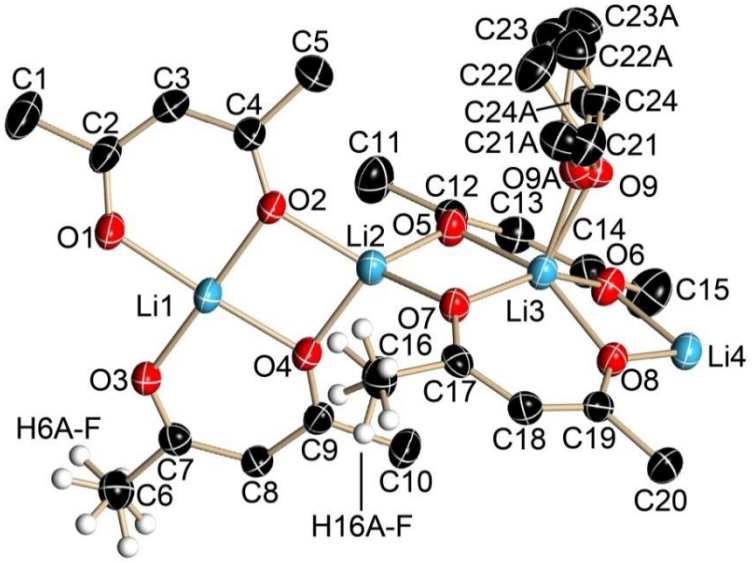

Figure 7.6: Asymmetric unit of $[Li_4(acac)_4(thf)]$ (**7**). The anisotropic displacement parameters are depicted at the 50 % probability level. The hydrogen atoms are omitted for clarity. The THF group is disordered in a ratio of 70:30 (O9:O9A). The hydrogen of the methyl groups C16 and C6 are refined with HFIX 127.

Table 7.6: Crystallographic data of $[Li_4(acac)_4(thf)]$ (**7**).

Identification code	p21n	Z	2
Empirical formula	$C_{48}H_{72}Li_8O_{16}$	ρ_c [Mgm^{-3}]	1.155
Formula weight [g/mol]	992.57	μ [mm^{-1}]	0.084
Temperature [K]	100(2)	F (000)	1056
Wavelength [Å]	0.71073	θ-range [°]	1.904-25.089
Crystal system	Monoclinic	Reflections collected	18616
Space group	$P2_1/n$	Completeness to Θmax	97.5 %
a [Å]	10.927(3)	Independent reflections	5033 [R(int)=0.0819]
b [Å]	21.030(6)	Restraints/parameters	553/389
c [Å]	12.456(3)	GooF	0.990
α [°]	90	$R1/wR2$ (I>2σ(I))	0.0537/0.1133
β [°]	94.250(6)	$R1/wR2$ (all data)	0.1187/0.1426
γ [°]	90	Diff. peak and hole [eÅ^{-3}]	0.208/-0.181
V [Å^3]	2854.3(13)	Max./min. transmission	0.6953/0.7452

7.5.7. $[(acac)_2Cu_2(NtBu)_4S]$ (8)

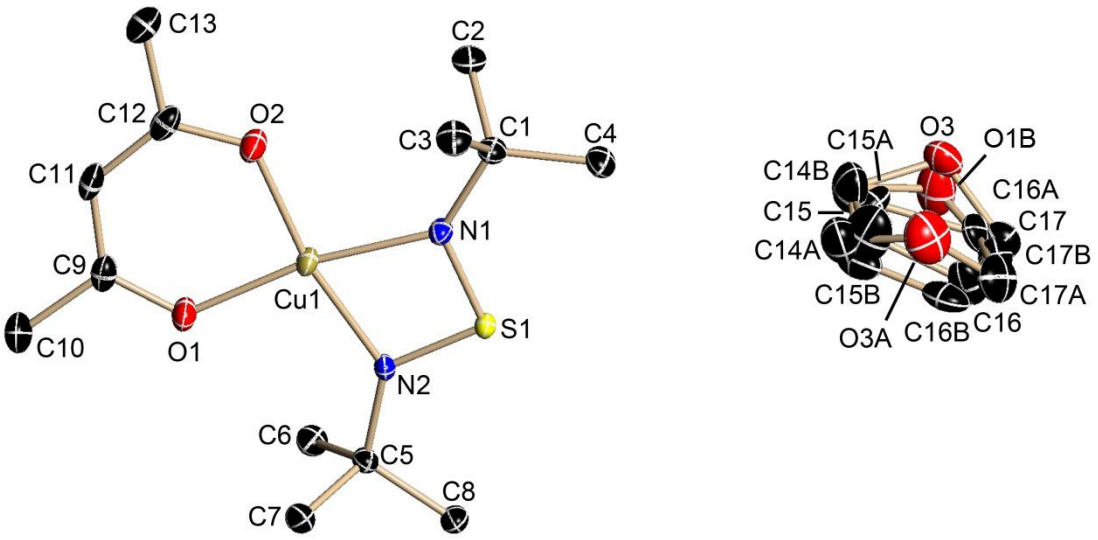

Figure 7.7: Asymmetric unit of $[(acac)_2Cu_2(NtBu)_4S]$ (**8**). The anisotropic displacement parameters are depicted at the 50 % probability level. The hydrogen atoms are omitted for clarity. The THF is disordered in a ratio of 70:20:10 (O3:O1B:O3A) and are refined using SIMU and DELU.

Table 7.7: Crystallographic data of $[(acac)_2Cu_2(NtBu)_4S]$ (**8**).

Identification code	rh	Z	2
Empirical formula	$C_{17}H_{33}CuN_2O_3S_{0.5}$	ρ_c [Mgm^{-3}]	1.326
Formula weight [g/mol]	786.04	μ [mm^{-1}]	1.178
Temperature [K]	100(2)	F (000)	840
Wavelength [Å]	0.71073	θ-range [°]	1.958-26.371
Crystal system	monoclinic	Reflections collected	26841
Space group	$P2/n$	Completeness to Θmax	100.0 %
a [Å]	12.546(10)	Independent reflections	4036[R(int)=0.0350]
b [Å]	9.281(10)	Restraints/parameters	464/311
c [Å]	16.950(10)	GooF	1.042
α [°]	90	$R1/wR2$ (I>2σ(I))	0.0268/0.0633
β [°]	93.85(10)	$R1/wR2$ (all data)	0.0365/0.0665
γ [°]	90	Diff. peak and hole [eÅ^{-3}]	0.422/-0.257
V [Å^3]	1969.2(3)	Max./min. transmission	0.6887/0.7455

7.5.8. [(acac)Pd(N*t*Bu)$_2$(N(H)*t*Bu)SO] (9)

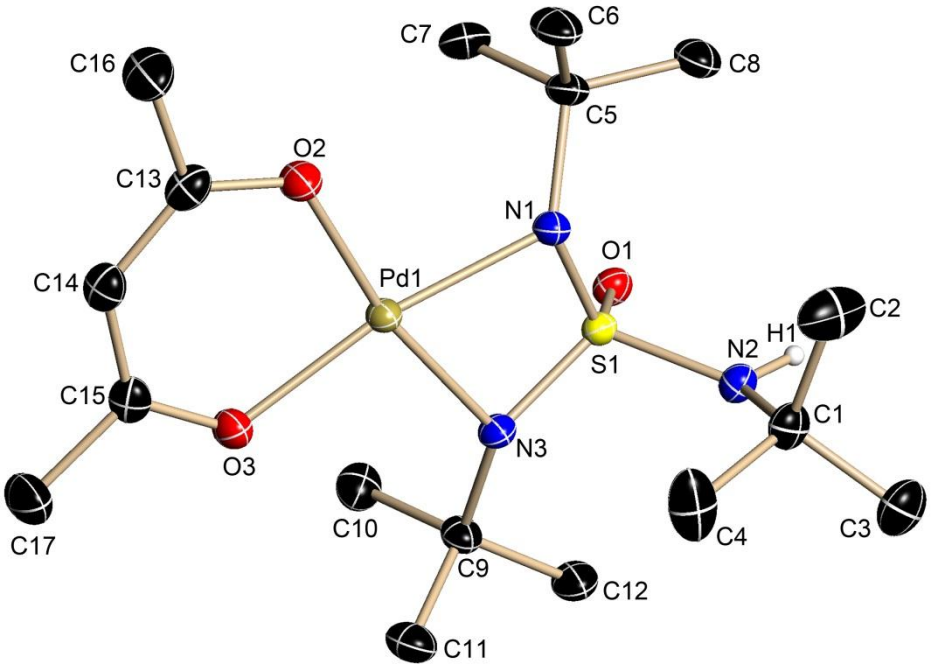

Figure 7.8: Asymmetric unit of [(acac)Pd(N*t*Bu)$_2$(N(H)*t*Bu)SO] (**9**). The anisotropic displacement parameters are depicted at the 50 % probability level. Hydrogen atom H1 was found in the Fourier difference map and refined using DFIX. The other hydrogen atoms are omitted for clarity. The crystal is a twin (BASF 0.14).

Table 7.8: Crystallographic data of [(acac)Pd(N*t*Bu)$_2$(N(H)*t*Bu)SO] (**9**).

Identification code	p21c_a	Z	1
Empirical formula	$C_{68}H_{140}N_{12}O_{12}Pd_4S_4$	ρ_c [Mgm^{-3}]	1.418
Formula weight [g/mol]	1871.75	μ [mm^{-1}]	0.961
Temperature [K]	100(2)	F (000)	976
Wavelength [Å]	0.71073	θ-range [°]	1.469-25.731
Crystal system	Monoclinic	Reflections collected	18198
Space group	$P2_1/c$	Completeness to Θmax	99.9 %
a [Å]	9.808(7)	Independent reflections	4170 [R(int) = 0.0311]
b [Å]	27.732(15)	Restraints/parameters	74/241
c [Å]	9.086 (5)	GooF	1.075
α [°]	90	$R1/wR2$ (I>2σ(I))	0.0217/0.0522
β [°]	117.52(10)	$R1/wR2$ (all data)	0.0247/0.0532
γ [°]	90	Diff. peak and hole [eÅ^{-3}]	0.398/-0.386
V [Å^3]	5229(70)	Max./min. transmission	0.6500/0.7455

7.5.9. [MeZn(NH$_2$*t*Bu)Br]$_3$ (10)

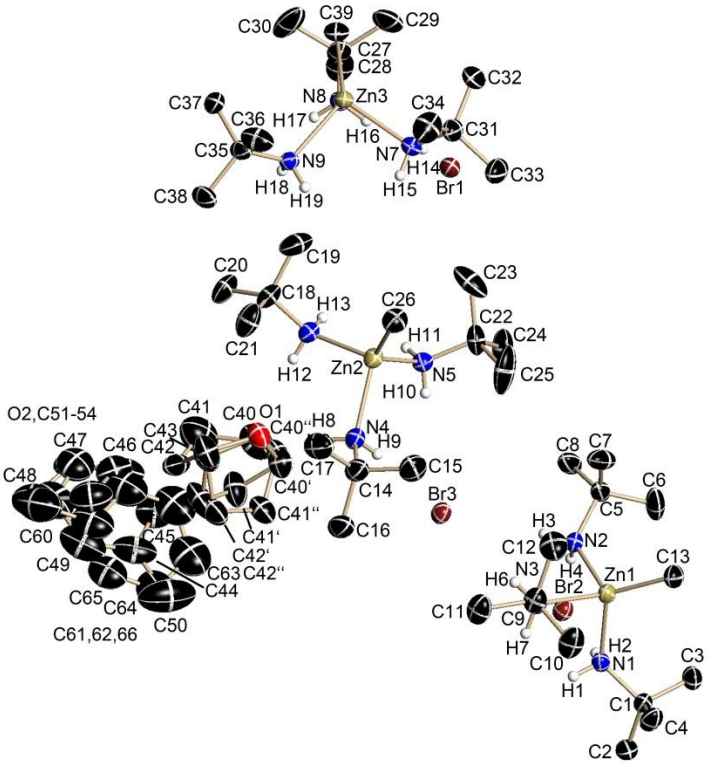

Figure 7.9: Asymmetric unit of [MeZn(NH$_2$*t*Bu)Br]$_3$ (**10**). The anisotropic displacement parameters are depicted at the 50 % probability level. The hydrogen atoms are omitted for clarity. The toluene and THF molecule are disordered in a ratio of 0.59:0.18:0.23. The other THF molecule is disordered in a ratio of 0.75:0.25. They are refined using RIGU, SIMU, SADI and FLAT.

Table 7.9: Crystallographic data of [MeZn(NH$_2$*t*Bu)Br]$_3$ (**10**).

Identification code	sad_a	Z	12
Empirical formula	$C_{16.44}H_{41.33}BrN_3O_{0.41}Zn$	ρ_c [Mgm^{-3}]	1.229
Formula weight [g/mol]	432.97	μ [mm^{-1}]	2.761
Temperature [K]	100(2)	F (000)	2751
Wavelength [Å]	0.71073	θ-range [°]	1.316-26.453
Crystal system	Monoclinic	Reflections collected	182642
Space group	$P2_1/c$	Completeness to Θmax	100.0 %
a [Å]	15.8069(9)	Independent reflections	14432 [R(int) = 0.0505]
b [Å]	17.9389(11)	Restraints/parameters	1112/845
c [Å]	25.2841(14)	GooF	1.051
α [°]	90	$R1/wR2$ (I>2σ(I))	0.0278/0.0699
β [°]	101.757(2)	$R1/wR2$ (all data)	0.0376/0.0757
γ [°]	90	Diff. peak and hole [eÅ^{-3}]	1.591/-0.508
V [Å^3]	7019.1(7)	Max./min. transmission	0.3337/0.4296

7.5.10. [(thf)$_2$Li(N*t*Bu)$_2$(NH*t*Bu)S(Ndipp)] (14)

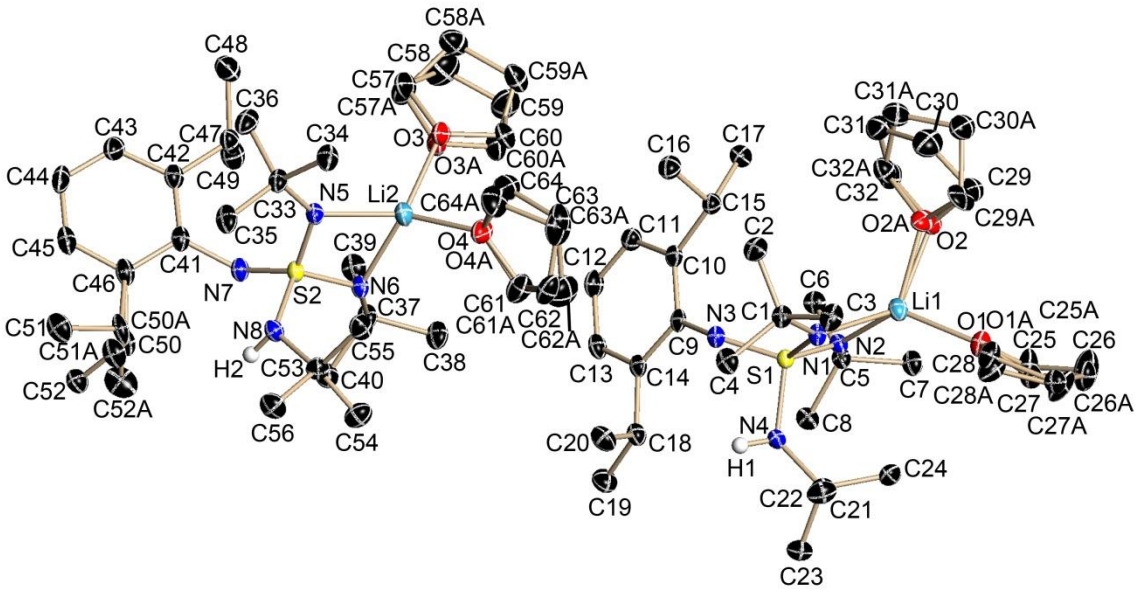

Figure 7.10: Asymmetric unit of [(thf)$_2$Li(N*t*Bu)$_2$(NH*t*Bu)S(Ndipp)] (**14**). The anisotropic displacement parameters are depicted at the 50 % probability level. Hydrogen atoms H1 and H2 were found in the Fourier difference map and refined using SADI. The other hydrogen atoms are omitted for clarity. The THF molecules are disordered in a ratio of 61:39 (O1:O1A), 90:10 (O2:O2A), 86:14 (O3A:O3B) and 64:36 (O4:O4A). The isopropyl group is disordered in a ratio of 94:6 (C50:C50A). They are refined using RIGU, SIMU and EADP.

Table 7.10: Crystallographic data of [(thf)$_2$Li(N*t*Bu)$_2$(NH*t*Bu)S(Ndipp)] (**14**).

Identification code	final	Z	8
Empirical formula	$C_{32}H_{61}LiN_4O_2S$	ρ_c [Mgm^{-3}]	1.112
Formula weight [g/mol]	572.84	μ [mm^{-1}]	0.127
Temperature [K]	100(2)	F (000)	2528
Wavelength [Å]	0.71073	θ-range [°]	1.034-25.681
Crystal system	Monoclinic	Reflections collected	98063
Space group	$P2_1/c$	Completeness to Θmax	97.9 %
a [Å]	19.690(2)	Independent reflections	12693 [R(int) = 0.0582]
b [Å]	10.395(2)	Restraints/parameters	1118/948
c [Å]	33.429(2)	GooF	1.020
α [°]	90	$R1/wR2$ (I>2σ(I))	0.0398/0.0934
β [°]	90.690(10)	$R1/wR2$ (all data)	0.0611/0.1014
γ [°]	90	Diff. peak and hole [eÅ^{-3}]	0.367/-0.502
V [Å^3]	6841.7(15)	Max./min. transmission	0.6763/0.7454

7.5.11. [(thf)$_2$Li(N*t*Bu)$_2$(NH*t*Bu)S(Ndmp)] (15)

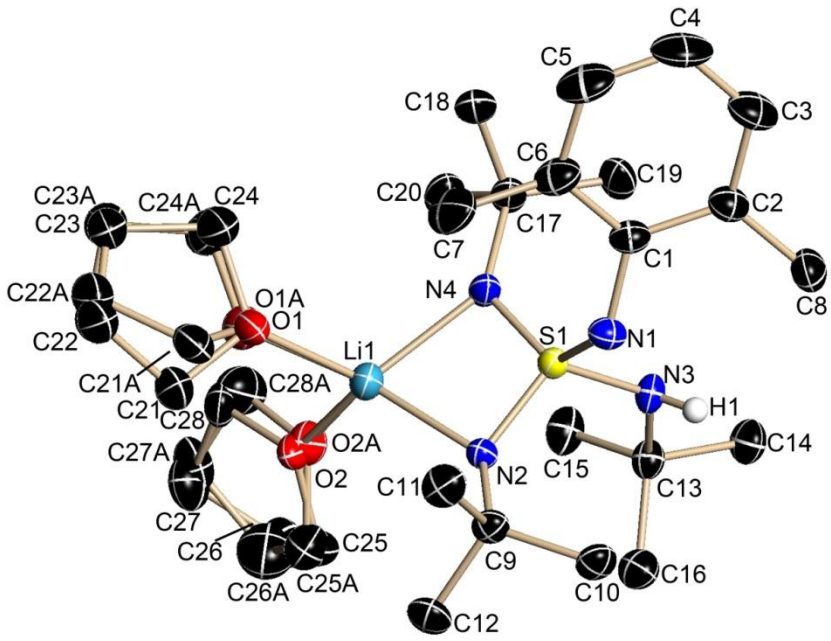

Figure 7.11: Asymmetric unit of [(thf)$_2$Li(N*t*Bu)$_2$(NH*t*Bu)S(Ndmp)] (**15**). The anisotropic displacement parameters are depicted at the 50 % probability level. Hydrogen atom H1 was found in the Fourier difference map and refined freely. The other hydrogen atoms are omitted for clarity. The THF molecules are disordered in a ratio of 70:30 (O1:O1A) and 60:40 (O2:O2C). They are refined using RIGU, DELU and SIMU.

Table 7.11: Crystallographic data of [(thf)$_2$Li(N*t*Bu)$_2$(NH*t*Bu)S(Ndmp)] (**15**).

Identification code	sad_a	Z	4
Empirical formula	$C_{28}H_{53}LiN_4O_2S$	ρ_c [Mgm^{-3}]	1.119
Formula weight [g/mol]	516.74	μ [mm^{-1}]	0.135
Temperature [K]	100(2)	F (000)	1136
Wavelength [Å]	0.71073	θ-range [°]	1.749-26.372
Crystal system	Monoclinic	Reflections collected	72436
Space group	$P2_1/c$	Completeness to Θmax	100 %
a [Å]	10.643(2)	Independent reflections	6260 [R(int) = 0.0330]
b [Å]	14.223(3)	Restraints/parameters	336/434
c [Å]	20.531(4)	GooF	1.187
α [°]	90	$R1/wR2$ (I>2σ(I))	0.0583/0.1286
β [°]	99.190(10)	$R1/wR2$ (all data)	0.0608/0.1298
γ [°]	90	Diff. peak and hole [eÅ^{-3}]	0.707/-0.359
V [Å^3]	3068.0(11)	Max./min. transmission	0.6927/0.7455

7.5.12. OSe(NH*t*Bu)$_2$ (16)

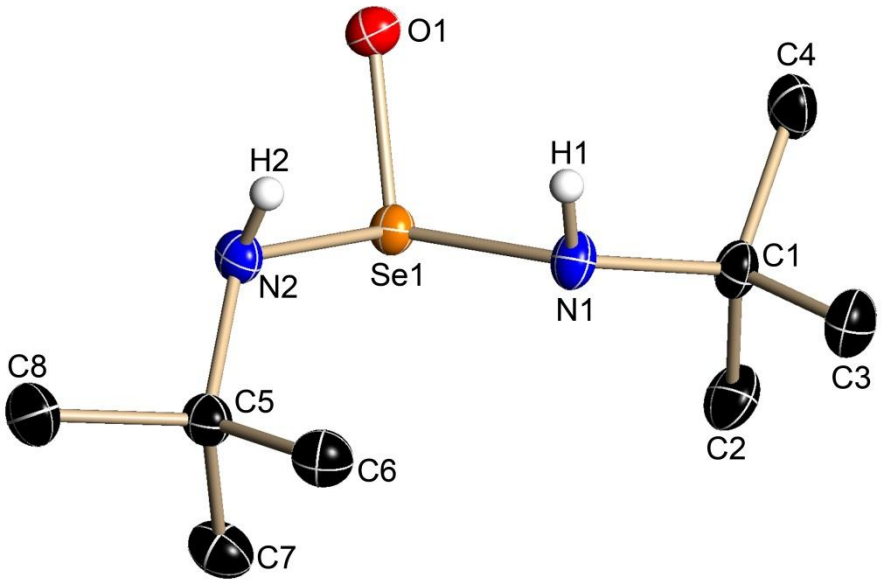

Figure 7.12: Asymmetric unit of OSe(NH*t*Bu)$_2$ (**16**). Hydrogen atoms H1 and H2 were found in the Fourier difference map. The other hydrogen atoms are omitted for clarity. The anisotropic displacement parameters are depicted at the 50 % probability level. The hydrogen atoms are omitted for clarity.

Table 7.12: Crystallographic data of OSe(NH*t*Bu)$_2$ (**16**).

Identification code	sad_a	Z	2
Empirical formula	$C_4H_{10}NO_{0.5}Se_{0.5}$	ρ_c [Mgm^{-3}]	1.393
Formula weight [g/mol]	119.61	μ [mm^{-1}]	3.256
Temperature [K]	100(2)	F (000)	248
Wavelength [Å]	0.71073	θ-range [°]	2.08-26.36
Crystal system	Triclinic	Reflections collected	3.256
Space group	$P\bar{1}$	Completeness to Θmax	99.9 %
a [Å]	6.1212(3)	Independent reflections	2328 [R(int) = 0.0292]
b [Å]	9.5376(5)	Restraints/parameters	28/124
c [Å]	10.251(5)	GooF	1.130
α [°]	107.111(2)	$R1/wR2$ (I>2σ(I))	0.0204/0.0524
β [°]	90.262(2)	$R1/wR2$ (all data)	0.0228/0.0530
γ [°]	93.994(2)	Diff. peak and hole [eÅ^{-3}]	0.653/-0.552
V [Å^3]	570.39(5)	Max./min. transmission	0.6010/0.7461

7.5.13. Se(N*t*Bu)$_2$ (17)

measured by Dr. Nina Lock

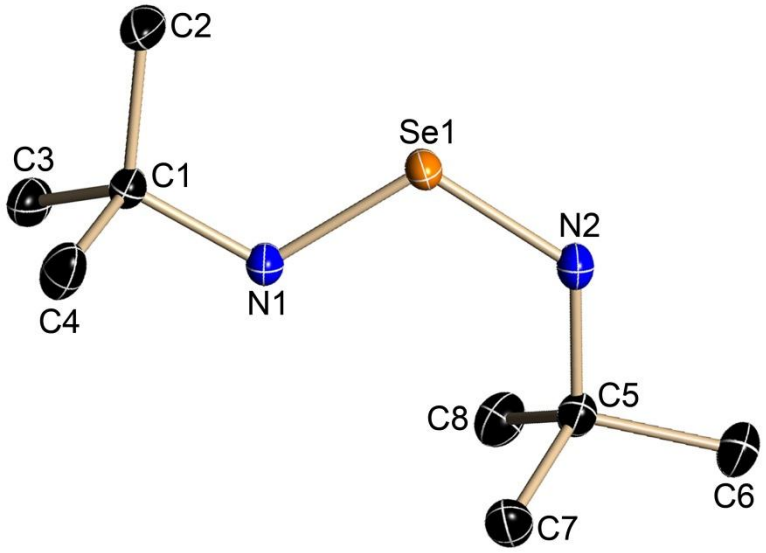

Figure 7.13: Asymmetric unit of Se(N*t*Bu)$_2$ (**17**). The anisotropic displacement parameters are depicted at the 50 % probability level. The hydrogen atoms are omitted for clarity.

Table 7.13: Crystallographic data of Se(N*t*Bu)$_2$ (**17**).

Identification code	p1_a	Z	2
Empirical formula	$C_8H_{18}N_2Se$	ρ_c [Mgm^{-3}]	1.368
Formula weight [g/mol]	221.20	μ [mm^{-1}]	3.445
Temperature [K]	100(2)	F (000)	228
Wavelength [Å]	0.71073	θ-range [°]	2.136-26.354
Crystal system	Triclinic	Reflections collected	24412
Space group	$P\bar{1}$	Completeness to Θmax	100.0 %
a [Å]	6.046(2)	Independent reflections	2208 [R(int) = 0.0206]
b [Å]	9.355(2)	Restraints/parameters	25/106
c [Å]	10.039(2)	GooF	1.137
α [°]	71.72(2)	$R1/wR2$ (I>2σ(I))	0.0128/0.0345
β [°]	88.65(2)	$R1/wR2$ (all data)	0.0133/0.0347
γ [°]	85.05(2)	Diff. peak and hole [eÅ^{-3}]	0.351/-0.172
V [Å^3]	537.1(2)	Max./min. transmission	0.6994/0.8622

7.6. Crystallographic cooperations

7.6.1. Structures measured for Prinson Samuel

work group Prof. Dr. Dr. h.c. mult. H. W. Roesky

7.6.1.1. LGeFNiPr2R

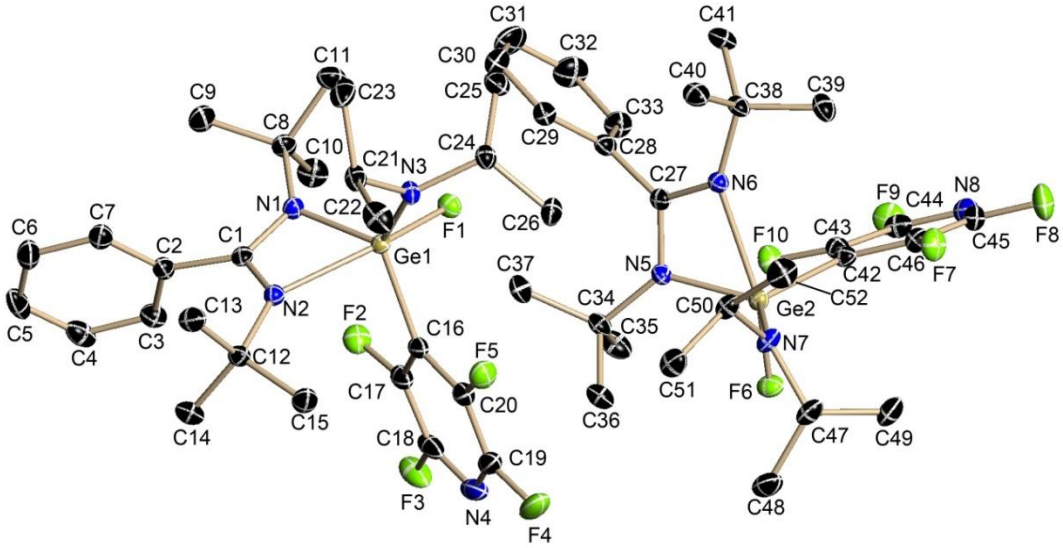

Figure 7.14: Asymmetric unit of LGeFNiPr2R. The anisotropic displacement parameters are depicted at the 50 % probability level. The hydrogen atoms are omitted for clarity.

Table 7.14: Crystallographic data of LGeFNiPr2R.

Identification code	sad_a	Z	8
Empirical formula	$C_{26}H_{37}F_5GeN_4$	ρ_c [Mgm^{-3}]	1419
Formula weight [g/mol]	573.18	μ [mm^{-1}]	1.198
Temperature [K]	100(2)	F (000)	2384
Wavelength [Å]	0.71073	θ-range [°]	1.458/7.523
Crystal system	Monoclinic	Reflections collected	98347
Space group	$P2_1/n$	Completeness to Θmax	100.0 %
a [Å]	15.122 (8)	Independent reflections	12312 [R(int) = 0.0364]
b [Å]	19.248(10)	Restraints/parameters	0/669
c [Å]	19.887(10)	GooF	1.033
α [°]	90	$R1/wR2$ (I>2σ(I))	0.0247/0.0576
β [°]	112.05(2)	$R1/wR2$ (all data)	0.0299/0.0593
γ [°]	90	Diff. peak and hole [eÅ^{-3}]	0.375/-0.273
V [Å^3]	5365.4(5)	Max./min. transmission	0.6977/0.7456

7.6.1.2. LSitBu2Ad

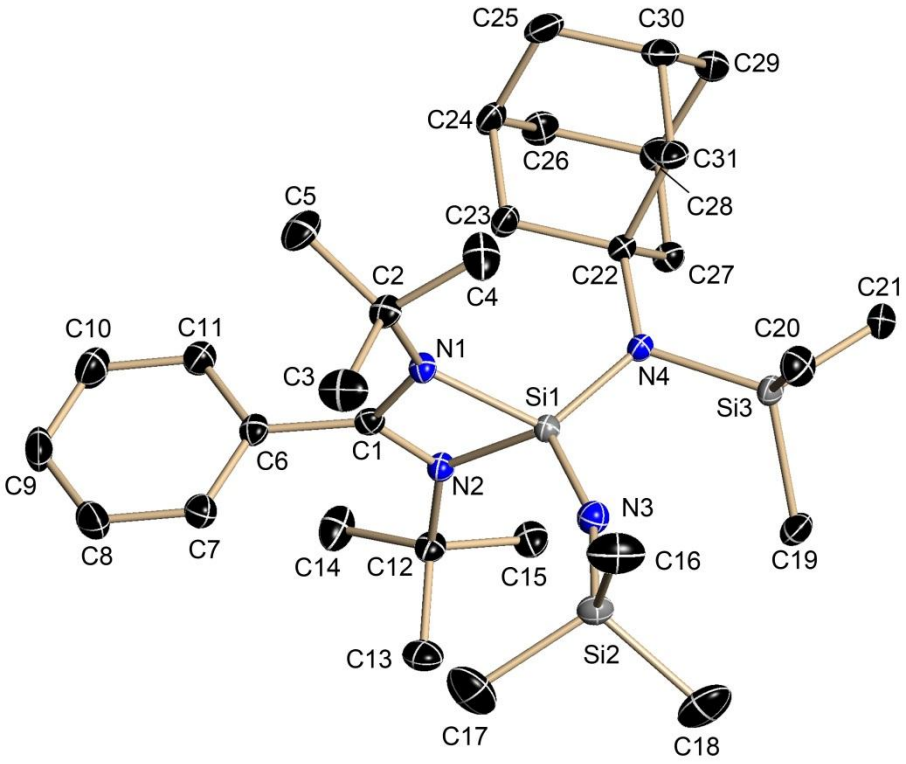

Figure 7.15: Asymmetric unit of LSitBu2Ad. The anisotropic displacement parameters are depicted at the 50 % probability level. The hydrogen atoms are omitted for clarity.

Table 7.15: Crystallographic data of LSitBu2Ad.

Identification code	sad_a	Z	2
Empirical formula	$C_{31}H_{56}N_4Si_3$	ρ_c [Mgm^{-3}]	1.121
Formula weight [g/mol]	569.07	μ [mm^{-1}]	0.166
Temperature [K]	100(2)	F (000)	624
Wavelength [Å]	0.71073	θ-range [°]	1.10-26.73
Crystal system	Triclinic	Reflections collected	13997
Space group	$P\bar{1}$	Completeness to Θmax	99.4 %
a [Å]	9.875(2)	Independent reflections	2933 [R(int) = 0.0676]
b [Å]	9.906(2)	Restraints/parameters	0/355
c [Å]	19.285(2)	GooF	1.038
α [°]	91.21(2)	$R1/wR2$ (I>2σ(I))	0.0379/0.0928
β [°]	104.27(2)	$R1/wR2$ (all data)	0.0478/0.0985
γ [°]	111.65(2)	Diff. peak and hole [eÅ^{-3}]	0.472/-0.252
V [Å^3]	1686.1(5)	Max./min. transmission	0.9836/ 0.9675

7.6.1.3. LSitBu3

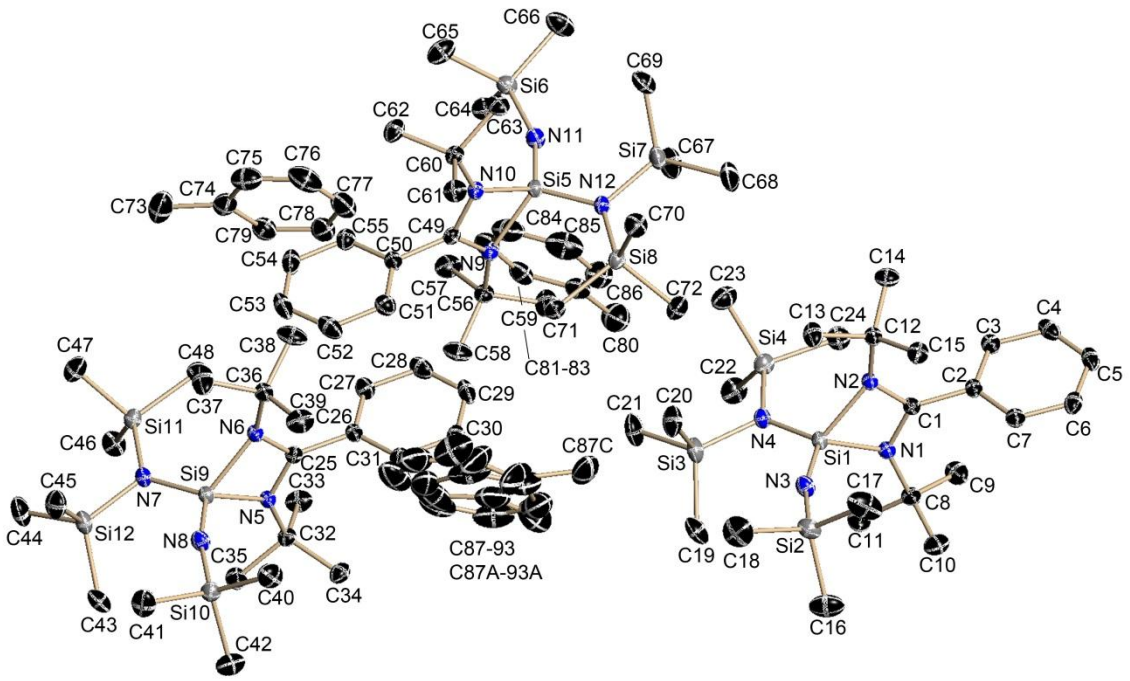

Figure 7.16: Asymmetric unit of LSitBu3. The anisotropic displacement parameters are depicted at the 50 % probability level. The hydrogen atoms are omitted for clarity. The toluene is disordered in a ratio of 49:51 (C87:C87A) and refined using SIMU, DELU and FLAT.

Table 7.16: Crystallographic data of LSitBu3.

Identification code	p-1_a	Z	2
Empirical formula	$C_{93}H_{174}N_{12}Si_{12}$	ρ_c [Mgm^{-3}]	1.086
Formula weight [g/mol]	1797.52	μ [mm^{-1}]	0.187
Temperature [K]	100(2)	F (000)	1968
Wavelength [Å]	0.71073	θ-range [°]	1.26-26.04
Crystal system	Triclinic	Reflections collected	109840
Space group	$P\bar{1}$	Completeness to Θmax	99.5 %
a [Å]	13.269(2)	Independent reflections	21603 [R(int) = 0.0357]
b [Å]	16.300(2)	Restraints/parameters	415/1177
c [Å]	25.856(3)	GooF	1.043
α [°]	87.86(2)	$R1/wR2$ (I>2σ(I))	0.0368/0.0953
β [°]	82.51(2)	$R1/wR2$ (all data)	0.0490/0.1004
γ [°]	82.79(2)	Diff. peak and hole [eÅ^{-3}]	0.404/-0.264
V [Å^3]	5499.4(12)	Max./min. transmission	0.7453/0.6905

7.6.1.4. JMPPSMn

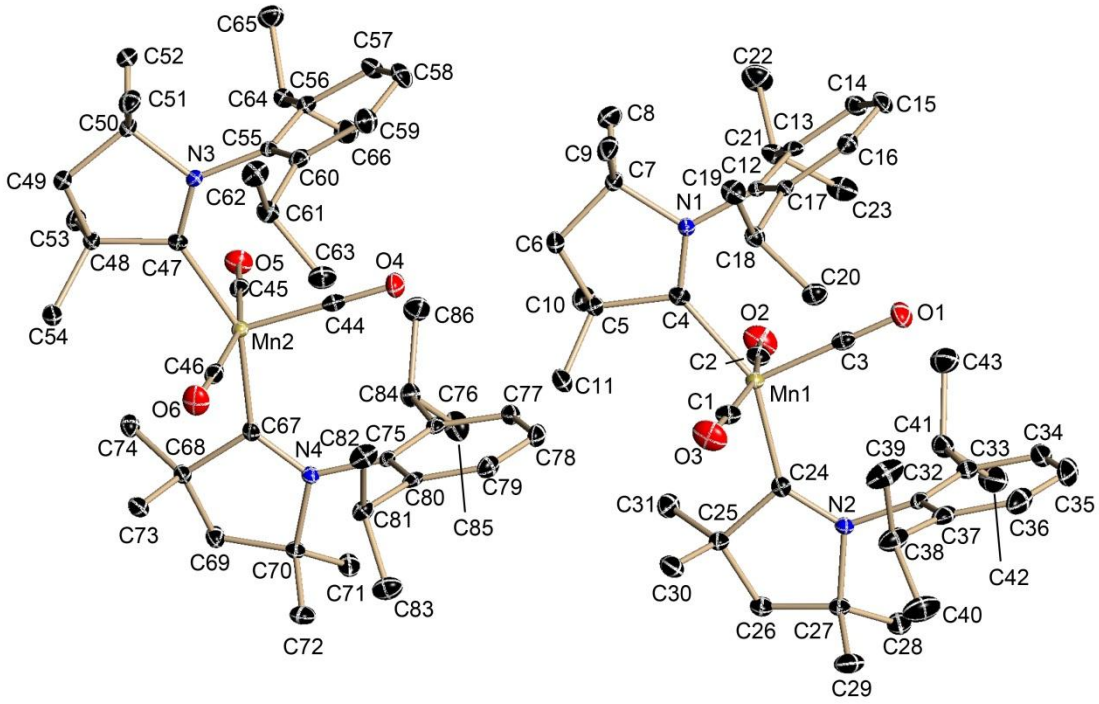

Figure 7.17: Asymmetric unit of JMPPSMn. The anisotropic displacement parameters are depicted at the 50 % probability level. The hydrogen atoms are omitted for clarity.

Table 7.17: Crystallographic data of JMPPSMn.

Identification code	sad_a	Z	2
Empirical formula	$C_{86}H_{124}Mn_2N_4O_6$	ρ_c [Mgm^{-3}]	1.271
Formula weight [g/mol]	1419.76	μ [mm^{-1}]	0.962
Temperature [K]	100(2)	F (000)	1280
Wavelength [Å]	0.71073	θ-range [°]	2.253-25.676
Crystal system	Triclinic	Reflections collected	27418
Space group	$P\bar{1}$	Completeness to Θmax	100.0 %
a [Å]	10.877(16)	Independent reflections	2933 [R(int) = 0.0676]
b [Å]	15.680(2)	Restraints/parameters	50/172
c [Å]	18.080(3)	GooF	1.046
α [°]	90	$R1/wR2$ (I>2σ(I))	0.0351/0.0701
β [°]	90	$R1/wR2$ (all data)	0.0556/0.0760
γ [°]	90	Diff. peak and hole [eÅ^{-3}]	0.331/-0.310
V [Å^3]	3083.5(8)	Max./min. transmission	0.6656/0.7455

7.6.1.5. LH2N3

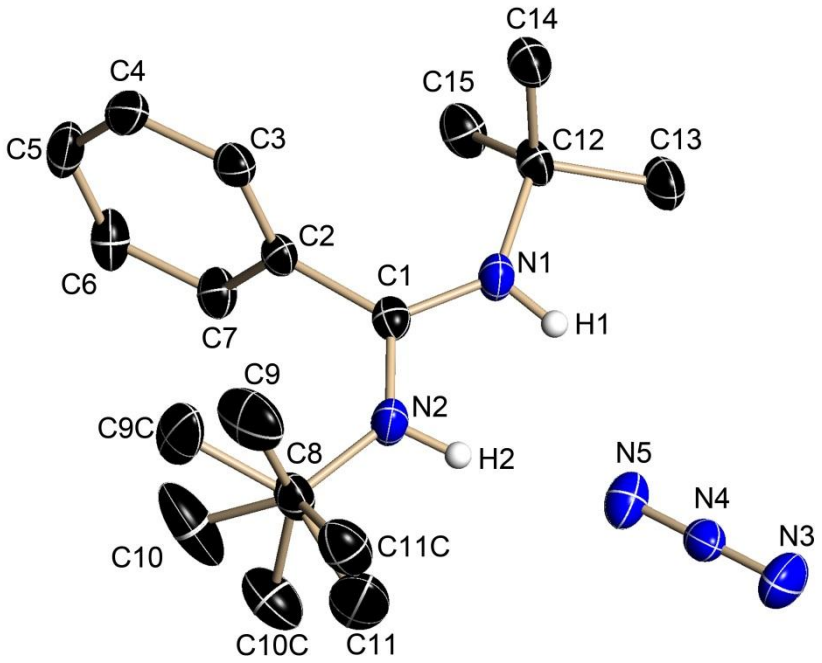

Figure 7.18: Asymmetric unit of LH2N3. The anisotropic displacement parameters are depicted at the 50 % probability level. Hydrogen atoms H1 and H2 were found in the Fourier difference map and refined using SADI. The other hydrogen atoms are omitted for clarity The *tert*butyl group (C8-C11) is disordered in a ratio of 77:23 (C9C:C9) and refined using EADP and DELU.

Table 7.18: Crystallographic data of LH2N3.

Identification code	rh	Z	4
Empirical formula	$C_{15}H_{25}N_5$	ρ_c [Mgm^{-3}]	1.134
Formula weight [g/mol]	275.40	μ [mm^{-1}]	0.071
Temperature [K]	100(2)	F (000)	600
Wavelength [Å]	0.71073	θ-range [°]	2.25-25.33
Crystal system	Monoclinic	Reflections collected	16508
Space group	$P2_1/n$	Completeness to Θmax	99.4 %
a [Å]	12.083(3)	Independent reflections	2921 [R(int) = 0.0289]
b [Å]	8.975(2)	Restraints/parameters	122/203
c [Å]	14.912(4)	GooF	1.065
α [°]	90	$R1/wR2$ (I>2σ(I))	0.0408/0.1035
β [°]	94.17(2)	$R1/wR2$ (all data)	0.0538/0.1099
γ [°]	90	Diff. peak and hole [eÅ^{-3}]	0.198/-0.149
V [Å^3]	1612.8(7)	Max./min. transmission	0.9943/0.9929

7.6.1.6. LSnF

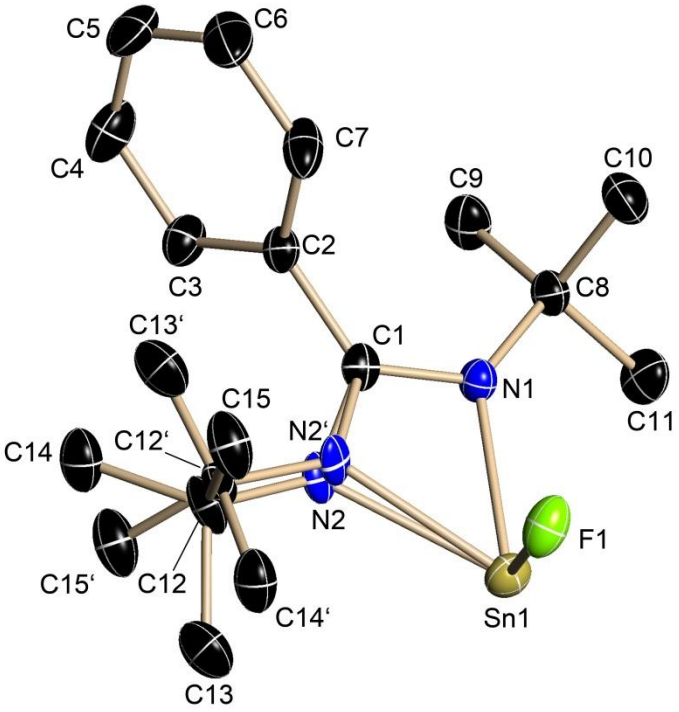

Figure 7.19: Asymmetric unit of LSnF. The anisotropic displacement parameters are depicted at the 50 % probability level. The hydrogen atoms are omitted for clarity. The *tert*butylimido group is disordered in a ratio of 60:40 (N2:N') and refined using EADP, DELU and SIMU.

Table 7.19: Crystallographic data of LSnF.

Identification code	sad	Z	2
Empirical formula	$C_{30}H_{46}F_2N_4Sn_2$	ρ_c [Mgm^{-3}]	1.506
Formula weight [g/mol]	738.09	μ [mm^{-1}]	1.570
Temperature [K]	100(2)	F (000)	744
Wavelength [Å]	0.71073	θ-range [°]	2.035-26.788
Crystal system	Monoclinic	Reflections collected	40528
Space group	$P2_1/c$	Completeness to Θmax	100.0 %
a [Å]	10.149(3)	Independent reflections	3475 [R(int) = 0.0284]
b [Å]	9.614(2)	Restraints/parameters	107/209
c [Å]	16.921(2)	GooF	1.087
α [°]	90	$R1/wR2$ (I>2σ(I))	0.0180/0.0409
β [°]	99.62(2)	$R1/wR2$ (all data)	0.0205/0.0422
γ [°]	90	Diff. peak and hole [eÅ^{-3}]	0.511/-0.392
V [Å^3]	1627.8(6)	Max./min. transmission	0.7454/0.6847

7.6.2. Structures measured for Dr. Rajendra Ghadwal

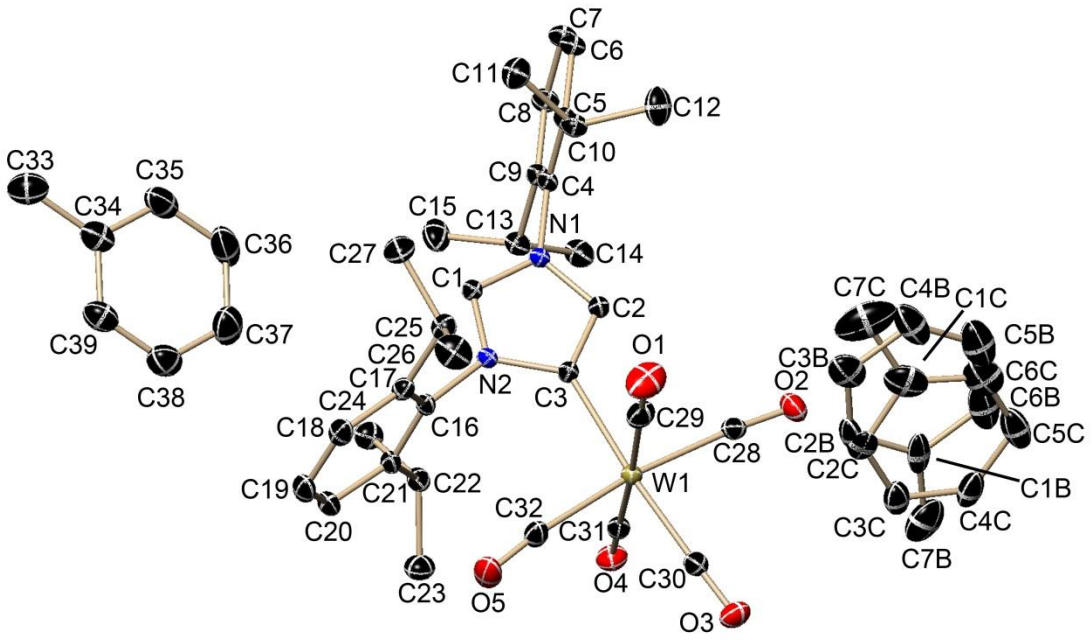

Figure 7.20: Asymmetric unit of raj71. The anisotropic displacement parameters are depicted at the 50 % probability level. The hydrogen atoms are omitted for clarity. The toluene is on a superposition, disordered in a ratio of 26:24 (C1C:C1B) and refined using DELU, SIMU and RIGU.

Table 7.20: Crystallographic data of raj71.

Identification code	rh	Z	2
Empirical formula	$C_{42.5}H_{48}N_2O_5W$	ρ_c [Mgm^{-3}]	1.456
Formula weight [g/mol]	850.68	μ [mm^{-1}]	3.023
Temperature [K]	100(2)	F (000)	862
Wavelength [Å]	0.71073	θ-range [°]	1.602-33.443
Crystal system	Triclinic	Reflections collected	60979
Space group	$P\bar{1}$	Completeness to Θmax	100.0 %
a [Å]	12.193(2)	Independent reflections	13473 [R(int) = 0.0244]
b [Å]	13.362(2)	Restraints/parameters	636/562
c [Å]	14.396(3)	GooF	1.053
α [°]	105.95(2)	$R1/wR2$ (I>2σ(I))	0.0211/0.0486
β [°]	105.95(2)	$R1/wR2$ (all data)	0.0240/0.0494
γ [°]	105.95(2)	Diff. peak and hole [eÅ^{-3}]	2.332/-1.096
V [Å^3]	1939.8(7)	Max./min. transmission	0.9092/0.7995

8. Abbreviations

Å	ÅNGSTROM
acac	acetylacetonate
Ad	adamantyl
ADP	anisotropic displacement parameters
Ar	2,6-dimethylphenyl
Bu	butyl
CCDC	Cambridge Crystallographic Data Center
Cp	cyclopentadienyl
COD	cycloocta-1,5-diene
Cy	cyclohexyl
DCM	dichloromethane
DFT	discrete fourier transformation
dipp	2,6-diisopropylphenyl
DME	1,2-dimethoxyethane
dmp	2,6-dimethylphenyl
EI-MS	electron impact mass spectrometry
EPR	Electron Paramagnetic Resonance
eq.	equivalents
Et	ethyl
et al.	*et alii*; and others
GooF	goodness of fit
HMDS	hexamethyldisilazane (Bis(trimethylsilyl)amine)
I	iso
K-Selectride	potassium tri-*sec*-butylhydroborate
L	liquid
M	molar
Me	methyl
Mes	mesityl
min.	minimal
mnt	(*Z*)-1,2-dicyanoethene-1,2-bis(thiolate)
m/z	mass/electron number
N	normal
naph	1-naphthaline
NBO/NRT	natural bonding orbital/natural resonance theory
NMR	nuclear magnetic resonance
nosyl	*o*-nitrobenzenesulfonyl
Ph	phenyl

Pm	picometer
Ppm	parts per million
Pr	propyl
Rt	room temperature
t, tert	tertiary
THF	tetrahydrofuran
TMEDA	tetramethylethylenediamine
TMS	trimethylsilyl
Tosyl	*p*-toluenesulfonyl
TPP	triphenylphosphane
VSCC	valence shell charge concentration

9. References

[1] D. Stalke, *Chem. Commun.* **2012**, *48*, 9559.

[2] I. Langmuir, *J. Am. Chem. Soc.* **1919**, *41*, 1543.

[3] F. Pauer, D. Stalke, *J. Organomet. Chem.* **1991**, *418*, 127.

[4] P. Hope, L. A. Wiles, *J. Chem. Soc.* **1965**, 5386.

[5] O. J. Scherer, R. Schmitt, *J. Organomet. Chem.* **1969**, *16*, P11.

[6] O. Scherer, R. Wies, *Z. Naturforsch.* **1970**, *B25*, 1486.

[7] J. Kuyper, P. C. Keijzer, K. Vrieze, *J. Organomet. Chem.* **1976**, *116*, 1.

[8] J. Kuyper, K. Vrieze, *J. Chem. Soc., Chem. Commun.* **1976**, 64.

[9] D. Hänssgen, W. Roelle, *J. Organomet. Chem.* **1973**, *63*, 269.

[10] F. T. Edelmann, F. Knösel, F. Pauer, D. Stalke, W. Bauer, *J. Organomet. Chem.* **1992**, *438*, 1.

[11] S. Freitag, W. Kolodziejski, F. Pauer, D. Stalke, *J. Chem. Soc., Dalton Trans.* **1993**, 3479.

[12] H. W. Roesky, A. Grünhagen, F. T. Edelmann, M. Noltemeyer, *Z. Naturforsch.* **1989**, *B44*, 1365.

[13] J. W. Bats, H. Fuess, M. Diehl, H. W. Roesky, *Inorg. Chem.* **1978**, *17*, 3031.

[14] H. W. Roesky, B. Mainz, M. Noltemeyer, *Z. Naturforsch.* **1990**, *B45*, 53.

[15] F. Knösel, M. Noltemeyer, F. T. Edelmann, *Z. Naturforsch.* **1989**, *B44*, 1171.

[16] R. Fleischer, S. Freitag, F. Pauer, D. Stalke, *Angew. Chem. Int. Ed. Engl.* **1996**, *35*, 204; *Angew. Chem.* **1996**, *108*, 208.

[17] R. Fleischer, D. Stalke, *J. Organomet. Chem.* **1998**, *550*, 173.

[18] R. Fleischer, D. Stalke, *Coord. Chem. Rev.* **1998**, *176*, 431.

[19] R. Mews, O. Glemser, *Inorg. Chem.* **1972**, *11*, 2521.

[20] G. Kresze, W. Wucherpfennig, *Angew. Chem. Int. Ed. Engl.* **1967**, *6*, 149; *Angew. Chem.* **1967**, *79*, 109.

[21] R. Fleischer, B. Walfort, A. Gbureck, P. Scholz, W. Kiefer, D. Stalke, *Chem. Eur. J.* **1998**, *4*, 2266.

[22] R. Fleischer, A. Rothenberger, D. Stalke, *Angew. Chem. Int. Ed. Engl.* **1997**, *36*, 1105; *Angew. Chem.* **1997**, *109*, 1140.

[23] R. Cramer, D. D. Coffman, *J. Org. Chem.* **1961**, *26*, 4010.

[24] A. J. Morris, C. H. L. Kennard, J. R. Hall, G. Smith, *Inorg. Chim. Acta* **1982**, *62*, 247.

[25] S. E. Kabir, M. Ruf, H. Vahrenkamp, *J. Organomet. Chem.* **1996**, *512*, 261.

[26] D. Ilge, D. S. Wright, D. Stalke, *Chem. Eur. J.* **1998**, *4*, 2275.

[27] R. Fleischer, D. Stalke, *Organometallics* **1998**, *17*, 832.

[28] O. Glemser, J. Wegener, *Angew. Chem. Int. Ed. Engl.* **1970**, *9*, 309; *Angew. Chem.* **1970**, *82*, 324.

[29] O. Glemser, S. Pohl, F.-M. Tesky, R. Mews, *Angew. Chem. Int. Ed. Engl.* **1977**, *16*, 789; *Angew. Chem.* **1977**, *89*, 829.

[30] W. Lidy, W. Sundermeyer, W. Verbeek, *Z. Anorg. Allg. Chem.* **1974**, *406*, 228.

[31] R. Fleischer, S. Freitag, D. Stalke, *J. Chem. Soc., Dalton Trans.* **1998**, 193.

[32] R. Appel, B. Ross, *Angew. Chem. Int. Ed. Engl.* **1968**, *7*, 546; *Angew. Chem.* **1968**, *80*, 561.

[33] H. Folkerts, W. Hiller, M. Herker, S. F. Vyboishchikov, G. Frenking, K. Dehnicke, *Angew. Chem. Int. Ed. Engl.* **1995**, *34*, 1362; *Angew. Chem.* **1995**, *107*, 1469.

[34] J. Matussek, *Diplomarbeit*, Göttingen, **2010**.

[35] E. Carl, *Diplomarbeit*, Göttingen, **2010**.

[36] F. A. Cotton, G. Wilkinson, C. A. Murillo, M. Bochmann, in *Advanced inorganic chemistry, Vol. 6*, John Wiley & Sons, Inc., New York, **1999**.

[37] A. A. Danopoulos, G. Wilkinson, B. Hussain, M. B. Hursthouse, *J. Chem. Soc., Chem. Commun.* **1989**, 896.

[38] A. A. Danopoulos, C. J. Longley, G. Wilkinson, B. Hussain, M. B. Hursthouse, *Polyhedron* **1989**, *8*, 2657.

[39] A. A. Danopoulos, G. Wilkinson, M. B. Hursthouse, B. Hussain, *Polyhedron* **1989**, *8*, 2947.

[40] A. A. Danopoulos, G. Wilkinson, *Polyhedron* **1990**, *9*, 1009.

[41] A. A. Danopoulos, W.-H. Leung, G. Wilkinson, B. Hussain-Bates, M. B. Hursthouse, *Polyhedron* **1990**, *9*, 2625.

[42] A. A. Danopoulos, G. Wilkinson, B. Hussain-Bates, M. B. Hursthouse, *J. Chem. Soc., Dalton Trans.* **1990**, 2753.

[43] A. A. Danopoulos, G. Wilkinson, T. K. N. Sweet, M. B. Hursthouse, *J. Chem. Soc., Dalton Trans.* **1994**, 1037.

[44] T. Kitazume, J. n. M. Shreeve, *Inorg. Chem.* **1977**, *16*, 2040.

[45] H. W. Roesky, K. Ambrosius, *Z. Naturforsch.* **1978**, *33B*, 759.

[46] H.-J. Koch, H. W. Roesky, S. Besser, R. Herbst-Irmer, *Chem. Ber.* **1993**, *126*, 571.

[47] T. Chivers, X. Gao, M. Parvez, *Angew. Chem. Int. Ed. Engl.* **1995**, *34*, 2549; *Angew. Chem.* **1995**, *107*, 2756.

[48] B. Wrackmeyer, E. V. Klimkina, W. Milius, *Z. Anorg. Allg. Chem.* **2006**, *632*, 2331.

[49] P. R. Raithby, C. A. Russell, A. Steiner, D. S. Wright, *Angew. Chem. Int. Ed. Engl.* **1997**, *36*, 649; *Angew. Chem.* **1997**, *109*, 670.

[50] D. N. Woodruff, E. J. L. McInnes, D. O. Sells, R. E. P. Winpenny, R. A. Layfield, *Inorg. Chem.* **2012**, *51*, 9104.

[51] J. K. Brask, T. Chivers, M. Parvez, *Inorg. Chem.* **2000**, *39*, 2505.

[52] J. K. Brask, T. Chivers, *Angew. Chem. Int. Ed. Engl.* **2001**, *40*, 3960; *Angew. Chem.* **2001**, *113*, 4082.

[53] F. M. Tesky, R. Mews, O. Glemser, *Z. Anorg. Allg. Chem.* **1979**, *452*, 103.

[54] K. Okuma, H. Tareuchi, H. Ohta, H. Matsuyama, *Bull. Chem. Soc. Jpn.* **1991**, *64*, 315.

[55] B. Walfort, D. Stalke, *Angew. Chem. Int. Ed. Engl.* **2001**, *40*, 3846; *Angew. Chem.* **2001**, *113*, 3965.

[56] J. Wessel, U. Behrens, E. Lork, T. Borrmann, W.-D. Stohrer, R. Mews, *Inorg. Chem.* **2002**, *41*, 4715.

[57] W. Kutzelnigg, *Angew. Chem. Int. Ed. Engl.* **1984**, *23*, 272; *Angew. Chem*. **1984**, *96*, 262.

[58] A. E. Reed, F. Weinhold, *J. Am. Chem. Soc.* **1986**, *108*, 3586.

[59] A. E. Reed, P. v. R. Schleyer, *J. Am. Chem. Soc.* **1990**, *112*, 1434.

[60] J. A. Dobado, H. Martínez-Garzía, J. M. Molina, M. R. Sundberg, *J. Am. Chem. Soc.* **1998**, *120*, 8461.

[61] D. W. J. Cruickshank, *J. Mol. Struct.* **1985**, *130*, 177.

[62] D. W. J. Cruickshank, M. Eisenstein, *J. Mol. Struct.* **1985**, *130*, 143.

[63] T. Stefan, R. Janoschek, *J. Mol. Model.* **2000**, *6*, 282.

[64] J. Cioslowski, P. R. Surján, *J. Mol. Struct.* **1992**, *255*, 9.

[65] J. Cioslowski, S. T. Mixon, *Inorg. Chem.* **1993**, *32*, 3209.

[66] B. Walfort, A. P. Leedham, C. R. Russell, D. Stalke, *Inorg. Chem.* **2001**, *40*, 5668.

[67] D. Leusser, B. Walfort, D. Stalke, *Angew. Chem. Int. Ed.* **2002**, *41*, 2079; *Angew. Chem.* **2002**, *41*, 2183.

[68] J. Henn, D. Ilge, D. Leusser, D. Stalke, B. Engels, *J. Phys. Chem. A* **2004**, *108*, 9442.

[69] D. Leusser, J. Henn, N. Kocher, B. Engels, D. Stalke, *J. Am. Chem. Soc.* **2004**, *126*, 1781.

[70] R. F. W. Bader, in *Atoms in Molecules*, Oxford University Press, New York, **1990**.

[71] D. B. Chesnut, *J. Phys. Chem. A* **2003**, *107*, 4307.

[72] R. E. Rundle, *J. Am. Chem. Soc.* **1947**, *69*, 1327.

[73] E. D. Glendening, J. K. Badenhoop, A. E. Reed, J. E. Carpenter, F. Weinhold*, Vol. NBO 4.M*, Theoretical Chemistry Institute, University of Wisconsin, Madison, WI, **1999**.

[74] M. S. Schmøkel, S. Cenedese, J. Overgaard, M. R. V. Jørgensen, Y.-S. Chen, C. Gatti, D. Stalke, B. B. Iversen, *Inorg. Chem.* **2012**, *51*, 8607.

[75] K. B. Sharpless, T. Hori, L. K. Truesdale, C. O. Dietrich, *J. Am. Chem. Soc.* **1976**, *98*, 269.

[76] M. Herberhold, W. Jellen, *Z. Naturforsch.* **1986**, *41b*, 144.

[77] B. Wrackmeyer, B. Distler, S. Gerstmann, M. Herberhold, *Z. Naturforsch.* **1993**, *48b*, 1307.

[78] M. Bruncko, T.-A. V. Khuong, K. B. Sharpless, *Angew. Chem. Int. Ed. Engl.* **1996**, *35*, 454; *Angew. Chem.* **1996**, *108*, 453.

[79] N. Sandblom, T. Ziegler, T. Chivers, *Inorg. Chem.* **1998**, *37*, 354.

[80] T. Maaninen, T. Chivers, R. Laitinen, G. Schatte, M. Nissinen, *Inorg. Chem.* **2000**, *39*, 5341.

[81] T. Maaninen, R. Laitinen, T. Chivers, *Chem. Commun.* **2002**, 1812.

[82] H. M. Tuononen, R. J. Suontamo, J. U. Valkonen, R. S. Laitinen, T. Chivers, *Inorg. Chem.* **2003**, *42*, 2447.

[83] N. M. Boag, S. Clapham, *Acta Crystallogr., Sect. E* **2005**, *61*, 2172.

[84] Z. Fu, T. Chivers, *Can. J. Chem.* **2007**, *85*, 358.

[85] M. Krieger, S. Schlecht, K. Harms, K. Dehnicke, *Z. Anorg. Allg. Chem.* **1998**, *624*, 1565.

[86] P. Reiß, D. Fenske, *Z. Anorg. Allg. Chem.* **2000**, *626*, 1317.

[87] G. Gilli, P. Gilli, in *The Nature of the Hydrogen Bonds*, Oxford University Press, Oxford (England), **2009**.

[88] R. D. Shannon, *Acta Crystallogr.* **1976**, *A32*, 751.

[89] A. R. Pray, *Inorg. Synth.* **1957**, *5*, 153.

[90] D. F. Shriver, M. A. Drezdzon, 2nd ed., John Wiley & Sons. Inc., **1986**.

[91] N. Agrawal, A. Singh, *Ind. J. Chem., Sect. A* **2007**, *46*, 1938.

[92] U. Siemeling, U. Vorfeld, B. Neumann, H.-G. Stammler, *Inorg. Chem.* **2000**, *39*, 5159.

[93] A. J. Blake, N. L. Gillibrand, G. J. Moxey, D. L. Kays, *Inorg. Chem.* **2009**, *48*, 10837.

[94] V. V. Sliznev, N. Vogt, J. Vogt, *J. Mol. Struct.* **2006**, *780–781*, 247.

[95] M. V. Bennett, S. Stoian, E. L. Bominaar, E. Münck, R. H. Holm, *J. Am. Chem. Soc.* **2005**, *127*, 12378.

[96] M. V. Bennett, R. H. Holm, *Angew. Chem. Int. Ed.* **2006**, *45*, 5613; *Angew. Chem.* **2006**, *118*, 5741.

[97] R. E. Cowley, J. r. m. Elhaïk, N. A. Eckert, W. W. Brennessel, E. Bill, P. L. Holland, *J. Am. Chem. Soc.* **2008**, *130*, 6074.

[98] N. Muresan, C. C. Lu, M. Ghosh, J. C. Peters, M. Abe, L. M. Henling, T. Weyhermöller, E. Bill, K. Wieghardt, *Inorg. Chem.* **2008**, *47*, 4579.

[99] S. Meyer, S. Demeshko, S. Dechert, F. Meyer, *Inorg. Chim. Acta* **2010**, *363*, 3088.

[100] S. Sproules, K. Wieghardt, *Coord. Chem. Rev.* **2010**, *254*, 1358.

[101] S. Meyer, C. M. Orben, S. Demeshko, S. Dechert, F. Meyer, *Organometallics* **2011**, *30*, 6692.

[102] H. Andres, E. L. Bominaar, J. M. Smith, N. A. Eckert, P. L. Holland, E. Münck, *J. Am. Chem. Soc.* **2002**, *124*, 3012.

[103] H. Beinert, R. H. Holm, E. Münck, *Science* **1997**, *277*, 653.

[104] J. P. Fackler, T. Moyer, J. A. Costamagna, R. Latorre, J. Granifo, *Inorg. Chem.* **1987**, *26*, 836.

[105] M. M. Rodriguez, E. Bill, W. W. Brennessel, P. L. Holland, *Science* **2011**, *334*, 780.

[106] M. F. Pilz, C. Limberg, S. Demeshko, F. Meyer, B. Ziemer, *Dalton Trans.* **2008**, 1917.

[107] G. Shoham, D. W. Christianson, R. A. Bartsch, G. S. Heo, U. Olsher, W. N. Lipscomb, *J. Am. Chem. Soc.* **1984**, *106*, 1280.

[108] D. D. Bray, N. F. Bray, *Inorg. Chim. Acta* **1986**, *111*, L39.

[109] M. M. Olmstead, P. P. Power, G. Sigel, *Inorg. Chem.* **1986**, *25*, 1027.

[110] N. A. Khanjin, F. M. Menger, *J. Org. Chem.* **1997**, *62*, 8923.

[111] M. G. Davidson, P. R. Raithby, A. L. Johnson, P. D. Bolton, *Eur. J. Inorg. Chem.* **2003**, 3445.

[112] W. A. Henderson, N. R. Brooks, W. W. Brennessel, V. G. Young, *Chem. Mater.* **2003**, *15*, 4679.

[113] D. V. Sevenard, O. Kazakova, E. Lork, T. Dülcks, D. L. Chizhov, G.-V. Röschenthaler, *J. Mol. Struct.* **2007**, *846*, 87.

[114] H. A. Jahn, E. Teller, *Math. Phys. Sciences A* **1937**, *161*, 220.

[115] M. A. Hitchman, *Comm. Inorg. Chem.* **1994**, *15*, 197.

[116] M. A. Halcrow, *Chem. Soc. Rev.* **2013**, *42*, 1784.

[117] M. Atanasov, B. Delley, D. Reinen, *Z. Anorg. Allg. Chem.* **2010**, *636*, 1740.

[118] K. Heinze, A. Reinhart, *Inorg. Chem.* **2006**, *45*, 2695.

[119] K. Izod, J. C. Steward, W. Clegg, R. W. Harrington, *Dalton Trans.* **2007**, 257.

[120] A. Armstrong, T. Chivers, M. Parvez, R. T. Boeré, *Angew. Chem. Int. Ed.* **2004**, *43*, 502; *Angew. Chem.* **2004**, *116*, 508.

[121] A. Armstrong, T. Chivers, M. Parvez, G. Schatte, R. T. Boeré, *Inorg. Chem.* **2004**, *43*, 3453.

[122] J. F. Bickley, M. C. Copsey, J. C. Jeffery, A. P. Leedham, C. A. Russell, D. Stalke, A. Steiner, T. Stey, S. Zacchini, *Dalton Trans.* **2004**, 989.

[123] S. D. Robertson, T. Chivers, J. Konu, *J. Organomet. Chem.* **2007**, *692*, 4327.

[124] L. M. Atagi, D. M. Hoffman, D. C. Smith, *Inorg. Chem.* **1993**, *32*, 5084.

[125] A. Maaninen, T. Chivers, M. Parvez, J. Pietikäinen, R. S. Laitinen, *Inorg. Chem.* **1999**, *38*, 4093.

[126] W. Schlenk, A. Thal, *Ber. Dtsch. Chem. Ges.* **1913**, *46*, 2840.

[127] W. Schlenk, J. Appenrodt, A. Michael, A. Thal, *Ber. Dtsch. Chem. Ges.* **1914**, *47*, 473.

[128] E. Bill, in *Mfit*, Max-Planck Institute for Chemical Energy Conversion, Mülheim/Ruhr, Germany.

[129] D. Stalke, *Chem. Soc. Rev.* **1998**, *27*, 171.

[130] T. Kottke, D. Stalke, *J. Appl. Crystallogr.* **1993**, *26*, 615.

[131] H. Hope, *Acta Crystallogr.* **1988**, *B44*, 22.

[132] T. Schulz, K. Meindl, D. Leusser, D. Stern, J. Graf, C. Michaelsen, M. Ruf, G. M. Sheldrick, D. Stalke, *J. Appl. Crystallogr.* **2009**, *42*, 885.

[133] in *Bruker AXS Inst. Inc.*, WI, USA, Madison, **2011**.

[134] in *Bruker AXS Inst. Inc.*, WI, USA, Madison, **2009**.

[135] W. Kabsch, *J. Appl. Crystallogr.* **1988**, *21*, 916.

[136] G. M. Sheldrick, in *SADABS 2008/2*, Göttingen, **2008**.

[137] G. M. Sheldrick, in *TWINABS v1.05 in Bruker APEX v2.1-0* (Ed.: Bruker AXS Inst. Inc.), WI, USA, Madison, **2005**.

[138] G. M. Sheldrick, *Acta Crystallogr., Section A* **2008**, *64*, 112.

Danksagung

Als erstes möchte ich mich bei Prof. Stalke für die interessante Themenstellung, die mir überlassenen Freiheiten und das damit verbundene Vertrauen danken. Sein anhaltender Glaube an mein Thema hat mir den Mut gegeben bis zum Ende durchzuhalten.

Prof. Ackermann möchte ich für die Übernahme des Korreferats und für die damit verbundene Arbeit und Zeit danken.

Ein großer Dank geht an meine tollen Korrekturleser Nils F. G. Wittenberg, Ann-Christin Pöppler, Hilke Wolf, Christian Maaß, David R. Dauer, Nina Lock, Elena Carl, Regine Herbst-Irmer und Torben Böhnisch.

Vielen Dank an Heike Tappe dafür, dass sie im Hintergrund alles regelt; Martin Schlote für seine Hilfe beim Organisieren von Chemikalien und Geräten; der NMR-Abteilung für Ratschläge und Messen meiner Proben; Christoph Schnegelsberg für die Hilfe beim Messen des ESI-MS; dem Analytischen Labor für das Messen der Elementar Analysen und Serhiy Demeshko für die große Mühe meine Proben mittels Mößbauer Spektroskopie zu untersuchen.

Mein Dank gilt auch den Maschinenschraubern, Hilke Wolf, Lennard Krause, Felix Engelhard und Peter Stollberg, die in unzähligen Stunden die Maschinen immer wieder zum Laufen gebracht haben und ohne die die ganzen Messungen nicht möglich gewesen wären.

Einen großen Dank auch an Regine Herbst-Irmer für ihre Hilfe, Korrekturen und Ratschläge beim Verfeinern und Messen der Kristalle. Was würde der Arbeitskreis ohne dich machen?!

Vielen Dank auch an meine drei AC-F Praktikanten Oliver Mitevski, Alexander Rabe und Jan Schwellenbach, die mich im Labor unterstützt und auf neue Ideen gebracht haben.

Als nächstes möchte ich mich beim ganzen AK Stalke für die schönen letzten Jahre während der Diplom- und Promotionszeit bedanken. Ihr seid ein super Arbeitskreis, mit dem man so manches erleben kann und einen immer wieder zum Lachen bringt.

Insbesondere sei meinen Laborkolleginnen Elena Carl, mit der sich die „Leiden“ des Diploms und der Promotion viel leichter erleben lassen und Nina Lock, die mit ihrer

frischen, aufbauenden Art ein stinkendes Selenthema erträglicher machen lässt, gedankt.

Felix Engelhart und Martin Dzemski möchte ich für die Hilfe bei Computerproblemen danken.

Lennard Krause danke ich für die schnelle Hilfe bei 3Lamda Problemen.

Ann-Christin Pöppler danke ich für die wunderschönen letzten acht Jahre; angefangen auf der Mathe-Party, über gemeinsames Weinen zwischen Umkleideschränken bis hin zu vielen tollen Momenten.

Zugleich möchte ich mich auch bei Christian Maaß für die schönen acht Jahr danken, insbesondere natürlich für das Bereitstellen von Lösungen im AC-0 Praktikum und das Löschen der Brände in meinem Abzug.

Vielen lieben Dank auch meinem ganzen Semester für die tolle Zeit. Das Freitags-Mensen war gerade beim Schreiben und dem verbundenem Stress immer eine gute Ablenkung. Der Sportplatz/Sportabzeichen-Gruppe vielen Dank für die schönen Stunden in der Sonne. Bei Lea Büttner und Sandra Meese möchte ich mich herzlich für die lustigen Abende und das gemeinsame Schwitzen beim „Schnittenhopsen“ und ABC-Hüpfen bedanken. Torben Böhnisch möchte ich für die schöne Zeit des Zusammenwohnens danken.

Vielen, vielen lieben Dank an meine Eltern und Sonja, die mir emotional den Rücken gestärkt haben und immer an mich geglaubt haben. Ich hab euch lieb!

Und zu guter Letzt möchte ich mich bei Nils für die letzten eineinhalb Jahre bedanken, in denen er immer für mich da war. Mit dem ich tolle Zeiten erlebt habe und der mich immer motiviert und unterstützt hat.

Curriculum vitae